Prediction of Concentrations of Reactive Nitrogen Species in Aqueous Solutions and Cells

by

ChangHoon Lim

B.S. Chemical Engineering (2000)

Seoul National University, Seoul, Republic of Korea

Submitted to the Department of Chemical Engineering

in Partial Fulfillment of the Requirements of the Degree of

DOCTOR OF PHILOSOPHY IN CHEMICAL ENGINEERING

at the

MASSACHUSETTS INSTITUTE OF TECHNOLOGY

September, 2011

Signature of Author .....

Department of Chemical Engineering

Aug 24, 2011

Certified by.....

William M. Deen

Carbon P. Dubbs Professor of Chemical Engineering

Thesis Supervisor

Accepted by.....

William M. Deen

Carbon P. Dubbs Professor of Chemical Engineering

Chairman, Committee for Graduate Students

Prediction of Concentrations of Reactive Nitrogen Species in Aqueous Solutions and Cells

by

ChangHoon Lim

Submitted to the Department of Chemical Engineering on Aug 24, 2011
in Partial Fulfillment of the Requirements of the Degree of
Doctor of Philosophy in Chemical Engineering

Abstract

Reactive nitrogen species (RNS) derived from nitric oxide (NO) have been implicated in cancer and other diseases, but their intracellular concentrations are largely unknown. To estimate them under steady-state conditions representative of inflamed tissues, a kinetic model was developed that included the effects of cellular antioxidants, amino acids, proteins, and lipids. For an NO concentration of 1 μM, total peroxynitrite (Per, the sum of $ONOO^-$ and ONOOH), nitrogen dioxide (NO_2), and nitrous anhydride (N_2O_3) were calculated to have concentrations in the nM, pM, and fM ranges, respectively. The concentrations of NO_2 and N_2O_3 were predicted to decrease markedly with increases in glutathione (GSH) levels, due to the scavenging of each by GSH. Although lipids accelerate the oxidation of NO by O_2 (because of the high solubility of each in hydrophobic media), lipid-phase reactions were calculated to have little effect on NO_2 or N_2O_3 concentrations. The major sources of intracellular NO_2 were found to be the reaction of Per with metals and with CO_2, whereas the major sinks were its reactions with GSH and ascorbate (AH^-). The radical-scavenging ability of GSH and AH^- caused 3-nitrotyrosine to be the only tyrosine derivative predicted to be formed at a significant rate. The major GSH reaction product was S-nitrosoglutathione. Analytical (algebraic) expressions were derived for the concentrations of the key reactive intermediates, allowing the calculations to be extended readily.

To investigate the mutagenic and toxic effects of NO on cells, methods are needed to expose them to constant, physiological levels of NO for hours to days. One way to do this is to co-culture target cells with activated macrophages, which can synthesize NO at constant rates for long periods. A novel method, developed in the laboratory of Professor G. N. Wogan at MIT, involves the use of Transwell™ permeable supports (Corning), in which a porous membrane separates two chambers in a culture dish. Target cells and macrophages are placed on the top and bottom of the insert, respectively. Although the two cell types are in close diffusional contact, the target cells can be recovered separately for viability and mutation assays. To infer the NO concentration at the level of the cells from measured rates of formation of nitrite (NO_2^-), a reaction-diffusion model was developed to calculate NO and O_2 concentrations as a function of height in the medium. In this system the oxidation of NO to NO_2^- competes with the diffusional loss of NO to the incubator gas. It was shown that a one-dimensional, steady-state formulation is justified. The key factors affecting NO and O_2 concentrations are the total rate of respiratory O_2 consumption by the cells and their net rate of NO generation. Because the overall rate of the multi-step NO oxidation is second order in NO, the fractional loss of NO from the system by diffusion increases as the NO concentration is reduced. Also, the fractional loss of NO is increased if cellular O_2 consumption is elevated. The cellular NO concentration was predicted to be nearly proportional to the square root of the NO_2^- formation rate. Thus, in experiments in the

Wogan laboratory in which NMA (an inhibitor of NO synthase) was added to the culture medium, reducing NO_2^- formation by 90%, the cellular NO concentration was calculated to decrease only by about two-thirds (from 1.1 μM to 0.36 μM). To facilitate the use of the reaction-diffusion model by other laboratories, a graphical method was developed to allow cellular NO concentrations to be estimated from measured rates of NO_2^- accumulation.

The controlled delivery of NO_2 into aqueous solutions, in the absence of NO, would be useful in investigating its rates of reaction with biological molecules and in isolating its effects on cells from those of other RNS. Two possible NO_2 delivery methods were investigated theoretically. One was the direct contact of NO_2 gas mixtures with stirred aqueous solutions, and the other was diffusion of NO_2 through gas-permeable tubing (such as polydimethylsiloxane, PDMS) into such solutions. In gases and in water, NO_2 dimerizes reversibly to form dinitrogen tetroxide (N_2O_4), which reacts rapidly with water to produce nitrite and nitrate. Thus, it was necessary to describe the coupled reaction and diffusion of NO_2 and N_2O_4 in each kind of system. Microscopic models were developed to describe spatial variations in concentrations near the gas-liquid interface, or within the tubing wall and immediately adjacent liquid. These were used to predict parameter values (such as mass transfer coefficients) in macroscopic models designed to describe bulk aqueous concentrations. Because the direct measurement of NO_2 and N_2O_4 concentrations at the low levels desired for biological experiments is impractical, the combined models are needed to estimate bulk NO_2 and N_2O_4 concentrations from measurable quantities such as rates of NO_2^- accumulation. For direct gas-liquid contacting, the utility of a quasi-equilibrium approximation (QEA) was examined. This assumes that the NO_2 and N_2O_4 concentrations are related as for dimerization equilibrium. At relatively high NO_2 concentrations in the delivery gas, the results from the QEA and exact equations were in excellent agreement. As the NO_2 level was reduced, the QEA eventually fails, because NO_2 increasingly resembles an unreactive species as its concentration approaches zero. However, the QEA was found to be quite accurate throughout the practical range of concentrations (0.001% to 1% NO_2 gas), the relative error in total fluxes not exceeding 6%. The results show that it is desirable to use as low an NO_2 concentration as is analytically feasible (such as 0.001% NO_2 gas). This minimizes both the concentration of N_2O_4 and the effects of concentration nonuniformities in the aqueous boundary layer. For NO_2 delivery through gas-permeable tubing such as PDMS, the modeling was more complicated and the results more uncertain. The main complication was due to the presence of a concentration boundary layer within the membrane next to the liquid, which required that the governing equations be rescaled for that region. The major source of uncertainty is the unknown solubility of N_2O_4 in PDMS. However, as the gas concentration was lowered, the results became insensitive to this parameter. For 1% NO_2 gas, the estimated bulk NO_2 concentrations were 7.1 μM for the direct gas contact and 0.35 μM for the gas-permeable tubing. For 0.001% NO_2 gas, the estimated NO_2 concentrations were 0.45 μM for the direct gas contact and 0.14 μM for the gas-permeable tubing. For both methods, the times to reach steady state were predicted to be quite fast, at most 10 seconds.

Acknowledgements

I would like to express my sincere appreciation for my thesis advisor, Professor William M. Deen. His penetrating insight and advice have been invaluable, and I have learned a lot from him throughout the entire my doctoral student period. I am also thankful for the important feedback through questions, and advice from Prof. K. Dane Wittrup and Prof. Peter. C. Dedon.

It was happy and a good atmosphere working with my lab members: Ian Zacharia, Panadda Dechadilok, Kristin Mattern, Gaurav Bhalla, Melanie Chin, and Brian Skinn. I thank them for their help and shared time during my study. Also thank Minyoung Kim, Laura Trudel and Prof. Gerald. N. Wogan for collaborating works.

Last, I would like to show my thanks and love to my family. Especially, my wife, JinHui Ryu, did devotion to raising three kids-Jimmy, Isaac, and Victoria during my study. Without my wife and kids, I cannot proceed on this stage. Also, thank my all friends for their friendship, support, and shared time.

This work was supported by NIH/NCI grant 2P01CA26731.

Table of Contents

List of Figures

List of Tables

Chapter 1

Background

1.1 Nitric Oxide Chemistry and Biology

Nitric oxide (NO) is a colorless gas with an unpaired electron delocalized over the molecule. It reacts readily with O_2 to form nitrate (NO_3^-) and nitrite (NO_2^-), and this reaction is called NO autoxidation (Conner and Grisham, 1995). During the NO autoxidation, nitrogen dioxide (NO_2) and nitrous anhydride (N_2O_3) are also produced. The rapid reaction of NO with superoxide (O_2^-) forms peroxynitrite ($ONOO^-$) (Tamir and Tannenbaum, 1996). The discovery of NO as an endogenously-generated molecule was the result of several independent avenues of research. Research throughout the 80s eventually determined that NO is generated from the guanidine nitrogen of L-arginine, by an enzyme called NO synthase (NOS) (Moncada et al., 1989). Endothelial cells have constitutive NOS (cNOS), which produces a basal level of NO that diffuses into vascular smooth muscles to induce relaxation (Waldman and Murad, 1988). On the other hand, macrophages and neutrophils have inducible NOS (iNOS) that produces NO upon induction by proinflammatory cytokines and certain bacterial products (Nathan and Hibbs, 1991). NO also functions as a signaling molecule involved in the gastrointestinal system, hepatic function, cardiovascular system, lung physiology, and central nervous system (Conner and Grisham, 1995). However, NO and its derivatives (NO_2, N_2O_3, peroxynitite etc.) display cytotoxic and mutagenic properties at high concentrations, which suggest a causative role for NO in the pathophysiology of diseases associated with chronic inflammation, such as cancer (deRojas-Walker et al., 1995; Lewis et al., 1995; Tamir and Tannenbaum, 1996). In other words, sustained high local rates of NO generation may result in a significant health risk.

1.2 Nitrogen Dioxide Chemistry and Biology

Nitrogen dioxide (NO_2) is a well-known toxic species and a strongly oxidizing radical. As a common atmospheric pollutant, NO_2 is commonly believed to be related to the development of lung cancer and heart disease in smokers. NO_2 can be endogenously-generated via several pathways. As mentioned above, NO_2 can be produced directly from NO autoxidation. Also, NO_2 can be formed from the decomposition of peroxynitrous acid (ONOOH) (Hodges and Ingold, 1999), the decomposition of nitrosoperoxycarbonate ($ONOOCO_2^-$) (Goldstein and Czapski, 1998; Hodges and Ingold, 1999) and so on. The other peroxynitrite-related pathways are discussed in Chapter 2. Nitrite (NO_2^-) can be oxidized to NO_2 under physiological conditions by reactions catalyzed by a variety of enzymes in the presence of hydrogen peroxide. Those enzymes include myeloperoxidase (Eiserich et al., 1998), copper-zinc superoxide dismutase (Singh et al., 1998), horseradish peroxidase, lactoperoxidase (van der Vliet et al., 1997) etc. In solutions and in the gas phase, NO_2 exists in equilibrium with its dimer, dinitrogen tetroxide (N_2O_4). Once formed, N_2O_4 decays in water to produce nitrite and nitrate. Since the dimerization rate varies as the square of the NO_2 concentration, NO_2 should be the major species under physiological conditions. The more detailed NO_2 chemistry is presented in Chapter 2.

NO_2 exposure causes peroxidation of lipids, mutagenicity in bacterial test systems and formation of carcinogenic nitrosamines by reaction with secondary amines (Cross et al., 1997). As suggested by its reactions with alkenes in nonaqueous solutions, it is highly likely that NO_2 causes membrane damage and cell death (Pryor and Lightsay, 1981; Pryor et al., 1982). Also, it was shown that NO_2 selectively oxidizes tyrosine and cysteine residues in peptides, and this leads to the loss of activity of enzymes (Prutz et al., 1985). Recombination of protein-tyrosyl

radicals with NO_2 produces nitrated proteins that have been detected in injured tissues and cells from diverse pathologies (Ischiropoulos, 1998).

1.3 Nitric Oxide Delivery Methods and Co-Culture Delivery System

To better characterize the cytotoxic and mutagenic properties of NO, methods are needed to achieve constant, physiological levels of NO in cell cultures. Several methods for NO delivery to biological solutions have been developed so far. Both addition of NO-saturated aqueous solutions (Liu et al., 1998; Thomas et al., 2001) and release from NO donor compounds (Estevez et al., 1999; Gasco et al., 1996) were not suited for long-term, constant levels of NO exposure to cell cultures. However, NO delivery by gas permeation through membranes such as Silastic tubing (Lewis and Deen, 1994; Wang and Deen, 2003) can achieve steady state NO concentrations indefinitely (up to at least 72h).

1.3.1 Improvement of NO Delivery Methods

NO delivery by diffusion through Silastic tubing works well for exposing cells, but its usefulness in kinetic studies has been limited by the high NO_2 and N_2O_3 concentrations that occur in a thin (~1 μm) region next to the tubing (Wang and Deen, 2003). It is well known that autoxidation of NO is significantly increased in hydrophobic media (Liu et al., 1998) because of the higher solubility of NO and O_2 in these environments. Hence, it is likely that the high NO_2 and N_2O_3 concentrations in the boundary layer next to the NO delivery tubing come from the enhanced NO and O_2 concentrations inside the Silastic membrane. Thus, suppressing NO oxidation in the membrane should eliminate the "hot spot". A model was developed that predicts that replacing the Silastic tubing with porous hydrophobic tubing (such as PTFE) will do this. This concept was implemented in the laboratory by Brian Skinn in the Deen group and

successfully eliminates the "hot spot" (Skinn et al., 2011). Although not described in this thesis, my modeling contributed to the new delivery system design.

1.3.2 Co-Culture Delivery System

Several methods for NO delivery to biological solutions have been developed so far. Among those, co-culture of target cells and macrophages is one of the methods suited for long-term, constant levels of NO exposure to cell cultures. Transwell^{TM} permeable supports (Corning, NY), consist of 100 mm culture dishes each containing a 75 mm diameter insert having a polycarbonate membrane with 0.4 μm pores that separates two chambers. Target cells are placed on the top of a porous membrane and macrophages adhered to the bottom side. This system allows free exchange of fluids but no direct contact between macrophages and the target cells, and also enables the separation between these two types of cells, even when both are adherent. In addition, target cells can be recovered separately for viability and mutation assays. The separation between two cell types might be better to mimic in vivo biological inflammation than the NO delivery by gas permeation through membranes.

1.4 Controlled Nitrogen Dioxide Delivery to Biological Solutions

To better characterize the toxicological and mutagenic effects of NO_2, methods are needed to deliver NO_2 at constant rates over relatively long periods of time (i.e., from several hours to days). The other great advantage of NO_2 delivery reactor is that it is possible to eliminate the effects of other NO derivatives such as nitrous anhydride (N_2O_3) and peroxynitrite and isolate the effect of NO_2 only. Most previous studies of NO_2 transport into aqueous solutions have dealt with the absorption of NO_2 and N_2O_4 gases in the context of nitric acid manufacture

(Kameoka and Pigford, 1977, Thomas and Vanderschuren, 1999). There appear to have been no attempts to deliver NO_2 to cell cultures or other biological solutions.

1.5 Intracellular Concentration of Reactive Nitrogen Species

Nalwaya and Deen (2003) developed a reaction-diffusion model to calculate steady state concentrations of NO and $ONOO^-$ in cells exposed to external sources of NO and/or $ONOO^-$, based on estimated rates of O_2^- production in the cytosol and mitochondria. For this purpose, the only important reactions were the formation of $ONOO^-$ from NO and O_2^-, the decomposition of ONOOH and $ONOO^-$ (the latter catalyzed by CO_2), and the scavenging of O_2^- by superoxide dismutase. It was shown that rates of diffusion are fast enough to cause the intracellular concentrations of NO, O_2, and CO_2 to each closely approximate those in the adjacent extracellular fluid. In other words, for a given cell, the concentrations of these dissolved gases may be viewed as being imposed by the surroundings. Other reactive nitrogen species, such as NO_2 and N_2O_3, were not considered.

More recently, Lancaster (2006) proposed a much more comprehensive model of intracellular chemistry related to NO, including oxidation, nitrosation, and nitration pathways. Among the 51 reactions considered were several involving glutathione, which is a major intracellular antioxidant, and tyrosine, which has derivatives that have been used as biomarkers. Although this pioneering model contained enough chemical detail to predict intracellular concentrations of reactive nitrogen species, such concentration estimates were not reported. Also, the model was formulated to describe time-dependent responses to the sudden introduction of key reactants. That is, cells were modeled as transient batch reactors. While such a formulation may be appropriate for simulating certain in vitro experiments, the time scale for inflammatory

processes is such that the various chemical species will be at steady state, with rates of formation and consumption in continuous balance.

1.5 Objectives

The first objective of this thesis was to develop a mathematical model to predict the intracellular concentrations of NO_2, N_2O_3 and related radicals. To estimate them under steady-state conditions representative of inflamed tissues, a kinetic model was developed that included the effects of cellular antioxidants, amino acids, proteins, and lipids. As described in Chapter 2, two-phase reaction analysis of the whole nitric oxide chemistry was performed. Emphasis was placed on the analytical form of the results with algebraic expressions which are no need for any numerical software.

The second objective was to predict NO concentrations in the novel co-culture system mentioned above. Chapter 3 presents a reaction-diffusion model that describes the effects of cellular NO generation and O_2 consumption on cellular NO concentrations in this system.

The third objective was to investigate theoretically two possible approaches for controlled NO_2 delivery to biological solutions. One is the delivery of NO_2 gas directly into the liquid solution, and the other is the permeation of NO_2 gas through PDMS (polydimethylsiloxane) tubing which follows the previous NO reactor (Wang and Deen, 2003). Chapter 4 presents microscopic and macroscopic models that describe delivery either by gas-liquid contacting or by diffusion of NO_2 through gas-permeable tubing.

The results of Chapter 2 have been published (Lim et al., 2008) and those of Chapter 3 are in a manuscript that is in preparation. Also, the NO delivery improvement work was recently published (Skinn et al., 2011).

Chapter 2

Kinetic Analysis of Intracellular Concentrations of Reactive Nitrogen Species

2.1 Introduction

The objective of the present work was to develop a model for intracellular nitrogen oxide chemistry which combines a reasonably comprehensive set of reactions with a steady-state formulation designed to simulate what occurs in vivo. The chemical system considered by Lancaster (2006) was extended by including additional antioxidants, additional amino acids, and certain lipid-phase reactions. As will be shown, radical scavenging by ascorbate, in particular, has important effects on the concentrations of several species of interest. Concerning lipid-phase chemistry, it has been reported that oxidation of NO by O_2 is greatly accelerated in hydrophobic media by the relatively high solubilities of NO and O_2 (Liu et al., 1998; Moller et al., 2007). Also, the reaction of NO_2 with polyunsaturated fatty acids in membranes (Prutz et al., 1985) might be an important sink for reactive nitrogen species, a possibility which is automatically neglected if only aqueous reactions are included. Concentrations of the reactive nitrogen species and related radicals are estimated, and the biological implications of the results are discussed.

2.2 Model Development

2.2.1 Overview

This section begins with a description of the chemical pathways that are included in the kinetic model. The physical assumptions are then identified and the general form of the mass

balance equations is presented. Following that are derivations of the concentration expressions for specific species. Those derivations are grouped according to what is needed algebraically to proceed to subsequent steps: $ONOO^-$ and carbonate and hydroxyl radicals are considered first; then, NO_2 and N_2O_3; and finally, glutathione and tyrosine derivatives.

2.2.2 Reactions

Figure 2.1 summarizes the nitrogen oxide reactions that were included in modeling the aqueous phase, arranged so as to emphasize the central role of NO_2. As shown, NO_2 may be formed from the reaction of NO with O_2, the decomposition of N_2O_3, the decomposition of peroxynitrous acid (ONOOH), the reaction of $ONOO^-$ with transition metal centers or selenium-containing proteins (denoted collectively as M^{n+}), and the decomposition of nitrosoperoxycarbonate ($ONOOCO_2^-$). The consumption of NO_2 is via its reactions with NO (to form N_2O_3), antioxidants, and amino acids, all of which lead eventually to nitrite (NO_2^-). The antioxidants considered were glutathione (GSH), ascorbate (AH^-), and urate (UH_2^-); the amino acids were cysteine (Cys), tyrosine (Tyr), and tryptophan (Trp), each of which is known to be reactive with NO_2 (Kikugawa and Okamoto, 1994). As indicated by the bold arrows, and as shown later, cytosolic NO_2 appears to be derived mainly from peroxynitrite, and consumed mainly by GSH and AH^-.

The nitrogen oxide chemistry considered in the lipid phase was largely a subset of that shown in Figure 2.1. The central process there was the autoxidation sequence leading from NO and O_2 to NO_2 and N_2O_3. The one new pathway in the lipid part of the model was the consumption of NO_2 by its reaction with polyunsaturated fatty acids. Ions were assumed to be

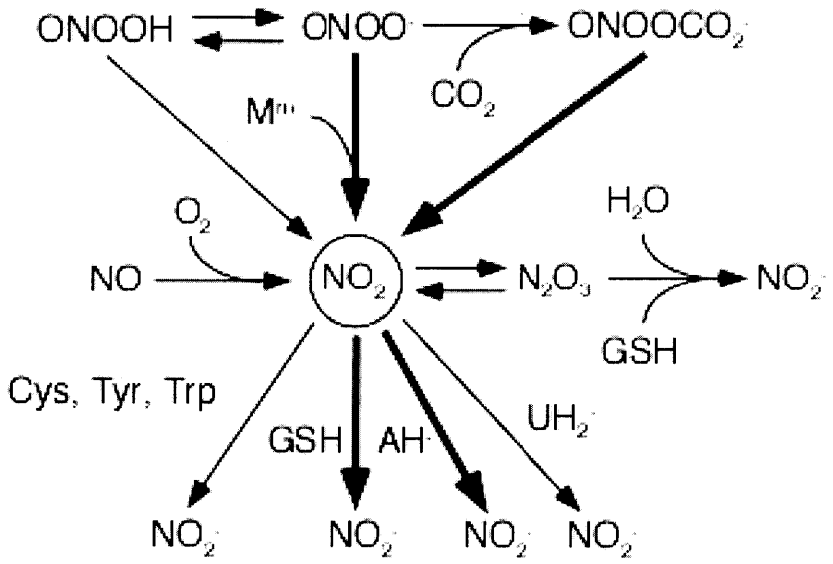

Figure 2.1. Nitrogen oxide chemistry, emphasizing reactions that produce or consume NO_2. The more important sources and sinks are denoted by thicker arrows. NO_2 is derived mainly from peroxynitrite and consumed mainly by antioxidants.

completely excluded from the lipid phase, so that no reactions involving charged species were considered there.

Figure 2.2 provides another view of nitrogen oxide chemistry, focusing now on peroxynitrite. Peroxynitrite ion is formed from the rapid reaction of NO with O_2^-, and is in near-equilibrium with ONOOH. The three pathways that lead from $ONOO^-$ to NO_2 have been mentioned already. Additional reactions yield NO_2^-, including $ONOO^-$ with GSH and ONOOH with proteins. Another feature in Figure 2.2 that was not shown in Figure 2.1 is that the decomposition of $ONOOCO_2^-$ and ONOOH each yield nitrate (NO_3^-) as a stable end product, in addition to the reactive product NO_2.

The glutathione chemistry that was considered is shown in Figure 2.3. Of particular importance is that GSH reacts with each of the trace nitrogen oxides, yielding glutathionyl radical (GS·) from NO_2, S-nitrosoglutathione (GSNO) from N_2O_3, and glutathione sulfenic acid (GSOH) from $ONOO^-$. Other intermediates or products include glutathione sulfinyl radical (GSO·), glutathione peroxysulfenyl radical (GSOO·), glutathione disulfide (GSSG), and the disulfide anion ($GSSG^-$).

Tyrosine nitration chemistry is depicted in Figure 2.4. Tyrosyl radical (Tyr·) is produced by the one-electron oxidation of Tyr by radicals such as GS·, CO_3^- , and NO_2. Tyrosyl radical reacts with NO, NO_2 and itself, to form 3-nitrosotyrosine (Tyr-NO), 3-nitrotyrosine (NO_2-Tyr), and 3,3-dityrosine (diTyr), respectively. It is scavenged by antioxidants, especially AH^-, resulting in the recovery of Tyr.

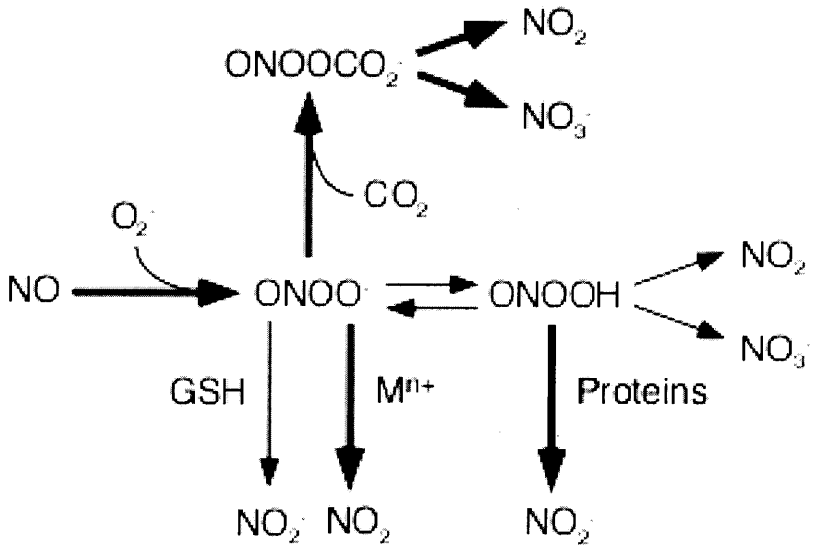

Figure 2.2. Nitrogen oxide chemistry, emphasizing reactions that produce or consume peroxynitrite. The more important reactions are denoted by thicker arrows.

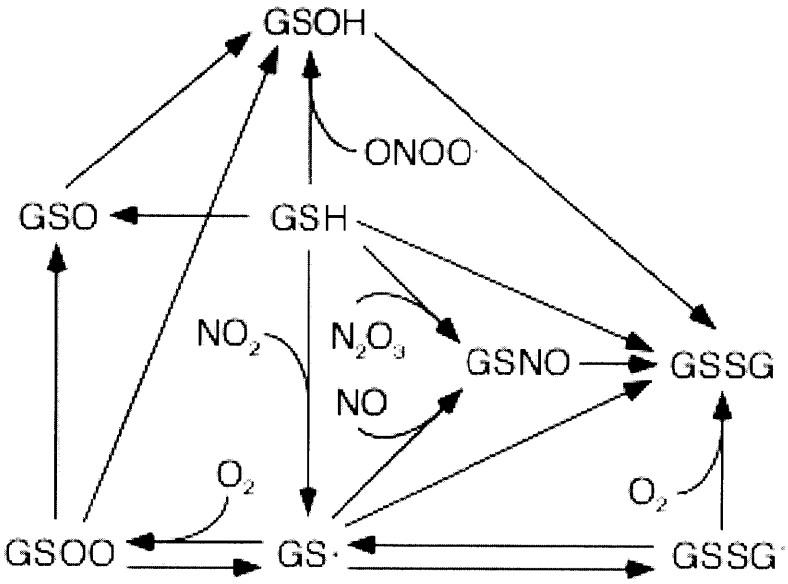

Figure 2.3. Glutathione reactions that involve nitrogen oxides or oxygen.

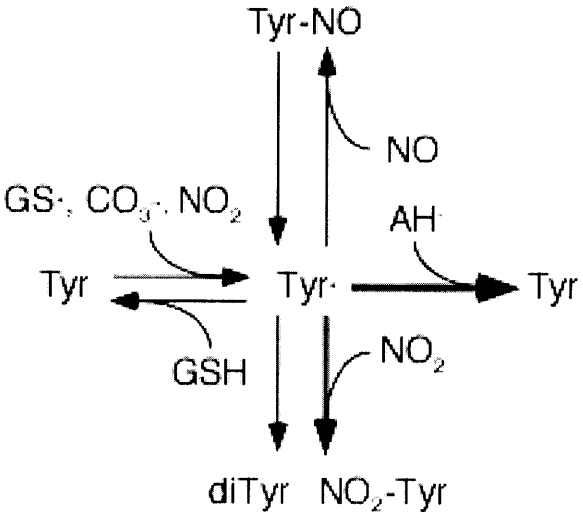

Figure 2.4. Reactions that lead to nitration or nitrosation of tyrosine. The more important reactions are denoted by thicker arrows.

For clarity, certain minor reactions included in the model were omitted from Figures 2.1-2.4. The full set of 66 reactions (excluding acid-base dissociations) is shown in Table 1. Also shown are the rate constants and literature sources. The rate constant for the hydrolysis of N_2O_3 (k_3) includes the catalytic effects of HCO_3^- but neglects the effects of phosphate. Each rate constant in the lipid phase was assumed to be the same as in water. There is evidence that this is true for the reaction of NO with O_2 (Liu et al., 1998; Moller et al., 2007), although for the other reactions this assumption is untested.

2.2.3 Mass Balance Equations

Based on our previous finding that intracellular concentrations of key species vary by only small amounts from the center to the periphery of a cell (Nalwaya and Deen, 2003), we did not attempt to model spatial variations. Although we estimated that concentrations of O_2^- and total peroxynitrite ($ONOO^-$ plus ONOOH) are about 3 and 8 times higher, respectively, in mitochondria than in cytosol (Nalwaya and Deen, 2003), for simplicity we chose here not to make such distinctions. That is, all intracellular aqueous compartments were lumped together. However, a distinction was made between aqueous and lipid concentrations.

All species were assumed to have time-independent concentrations. The species considered fell into three categories: (i) major dissolved gases (NO, O_2, CO_2); (ii) biomolecular targets, including antioxidants, amino acids, and O_2^-; and (iii) reactive intermediates. The concentrations for groups (i) and (ii) were specified directly, based on the literature. Those for group (iii) constituted the unknowns in the set of governing equations. Radicals and other reactive intermediates tend to be present at such low concentrations that their ability to escape a cell is very limited. That is, permeation across the plasma membrane will tend to be slow

Table 2.1. Reactions and rate constants.

#	Reaction	Rate Constant	Reference
1	$2NO + O_2 \xrightarrow{k_1} 2NO_2$	$k_1 = 2.4\times10^6\, M^{-2}s^{-1}$	Lewis and Deen, 1994
2	$NO + NO_2 \underset{k_{-2}}{\overset{k_2}{\rightleftarrows}} N_2O_3$	$k_2 = 1.1\times10^9\, M^{-1}s^{-1}$ $k_{-2} = 8.4\times10^4\, s^{-1}$	Schwartz, 1983 Ross et al., 1998
3	$N_2O_3 + H_2O \xrightarrow{k_3} 2NO_2^- + 2H^+$	$k_3 = 2.6\times10^3\, s^{-1}$	Goldstein et al.,2000
4	$NO_2 + GSH \xrightarrow{k_4} NO_2^- + GS\cdot + H^+$	$k_4 = 2.0\times10^7\, M^{-1}s^{-1}$	Ford et al., 2002
5	$GS\cdot + NO \xrightarrow{k_5} GSNO$	$k_5 = 1.0\times10^9\, M^{-1}s^{-1}$	Kirsch et al., 2001
6	$GS\cdot + GS\cdot \xrightarrow{k_6} GSSG$	$k_6 = 7.5\times10^8\, M^{-1}s^{-1}$	Hoffman and Hayon, 1973
7	$GS\cdot + O_2 \underset{k_{-7}}{\overset{k_7}{\rightleftarrows}} GSOO\cdot$	$k_7 = 2\times10^9\, M^{-1}s^{-1}$ $k_{-7} = 6.2\times10^5\, s^{-1}$	Wardman and von Sonntag, 1995 Wardman and von Sonntag, 1995
8	$GS\cdot + GS^- \underset{k_{-8}}{\overset{k_8}{\rightleftarrows}} GSSG^-$	$k_8 = 6\times10^8\, M^{-1}s^{-1}$ $k_{-8} = 1.6\times10^5\, s^{-1}$	Wardman and von Sonntag, 1995 Wardman and von Sonntag, 1995
9	$GSSG^- + O_2 \xrightarrow{k_9} GSSG + O_2^-$	$k_9 = 5\times10^9\, M^{-1}s^{-1}$	Wardman and von Sonntag, 1995
10	$GS\cdot + GSNO \xrightarrow{k_{10}} GSSG + NO$	$k_{10} = 1.7\times10^9\, M^{-1}s^{-1}$	Wood et al., 1996
11	$GSNO + GSH \xrightarrow{k_{11}} GSSG + NH_3 + N_2O + NO_2^- + NO$	$k_{11} = 5.5\times10^{-3}\, M^{-1}s^{-1}$	Shin and George,2001
12	$2GSNO + O_2^- \xrightarrow{k_{12}} GSSG + 2NO_2^-$	$k_{12} = 6\times10^8\, M^{-2}s^{-1}$	Jourd'heuil et

			al.,1998
13	$GSOO\cdot + GSNO \xrightarrow{k_{13}} GSSG + O_2 + NO$	$k_{13} = 3.8\times10^8\, M^{-1}s^{-1}$	Wood et al., 1996
14	$GSOO\cdot + NO_2 \underset{k_{-14}}{\overset{k_{14}}{\rightleftarrows}} GSOONO_2$	$k_{14} = 1\times10^9\, M^{-1}s^{-1}$ $k_{-14} = 0.75 s^{-1}$	Goldstein et al, 2004 Goldstein et al, 2004
15	$GSOO\cdot + GSOO\cdot \xrightarrow{k_{15}} xO_2^- + products$	$k_{15} = 4\times10^8\, M^{-1}s^{-1}$, $x = 0.56$	Goldstein et al, 2004
16	$GSOO\cdot + NO \xrightarrow{k_{16}} GSOONO$	$k_{16} = 3\times10^9\, M^{-1}s^{-1}$	Goldstein et al, 2004
17	$GSOO\cdot + GSH \xrightarrow{k_{17}} GSO\cdot + GSOH$	$k_{17} = 2\times10^6\, M^{-1}s^{-1}$	Wardman, 1998
18	$N_2O_3 + GSH \xrightarrow{k_{18}} NO_2^- + GSNO\cdot + H^+$	$k_{18} = 6.6\times10^7\, M^{-1}s^{-1}$	Keshive et al., 1996
19	$ONOO^- + GSH \xrightarrow{k_{19}} NO_2^- + GSOH$	$k_{19} = 6.6\times10^2\, M^{-1}s^{-1}$	Bonini and Augusto, 2001
20	$CO_3^- + GSH \xrightarrow{k_{20}} HCO_3^- + GS\cdot$	$k_{20} = 5.3\times10^6\, M^{-1}s^{-1}$ (pH=7.0)	Chen and Hoffman, 1973
21	$O_2^- + GSH + H^+ \xrightarrow{k_{21}} GS\cdot + H_2O_2$	$k_{21} = 200 M^{-1}s^{-1}$	Jones et al., 2003
22	$GSOH + GSH \xrightarrow{k_{22}} GSSG + H_2O$	$k_{22} = 720 M^{-1}s^{-1}$	Luo et al., 2005
23	$Tyr\cdot + GSH \underset{k_{-23}}{\overset{k_{23}}{\rightleftarrows}} GS\cdot + Tyr$	$k_{23} = 3.5\times10^5\, M^{-1}s^{-1}$ $k_{-23} = 3.5\times10^5\, M^{-1}s^{-1}$	Quijano et al., 2005 Quijano et al., 2005
24	$GSO\cdot + GSH \xrightarrow{k_{24}} GSOH + GS\cdot$	$k_{24} = 1\times10^5\, M^{-1}s^{-1}$	Wardman, 1998
25	$ONOO^- + CO_2 \xrightarrow{k_{25}} NO_2 + CO_3^-$	$k_{25} = 1\times10^4\, M^{-1}s^{-1}$	Lymar and Hurst, 1995

	$ONOO^- + CO_2 \xrightarrow{k_{25'}} NO_3^- + CO_2$	$k_{25'} = 2\times10^4 M^{-1}s^{-1}$	Lymar and Hurst, 1995
26	$CO_3^- + O_2^- + H^+ \xrightarrow{k_{26}} HCO_3^- + O_2$	$k_{26} = 4\times10^8 M^{-1}s^{-1}$	Behar et al., 1970
27	$CO_3^- + NO + OH^- \xrightarrow{k_{27}} HCO_3^- + NO_2^-$	$k_{27} = 3.5\times10^9 M^{-1}s^{-1}$	Czapski et al., 1994
28	$CO_3^- + Tyr \xrightarrow{k_{28}} HCO_3^- + Tyr\cdot$	$k_{28} = 4.5\times10^7 M^{-1}s^{-1}$	Goldstein et al.,2000
29	$NO_2 + Tyr \xrightarrow{k_{29}} NO_2^- + Tyr\cdot$	$k_{29} = 3.2\times10^5 M^{-1}s^{-1}$ (pH=7.5)	Prutz et al., 1985
30	$Tyr\cdot + NO \underset{k_{-30}}{\overset{k_{30}}{\rightleftarrows}} Tyr - NO$	$k_{30} = 1\times10^9 M^{-1}s^{-1}$ $k_{-30} = 1\times10^3 s^{-1}$	Goldstein et al.,2000 Goldstein et al.,2000
31	$Tyr - NO \xrightarrow{k_{31}} products$	$k_{31} = 0.5s^{-1}$	Goldstein et al.,2000
32	$O_2^- + Tyr\cdot \xrightarrow{k_{32}} products$	$k_{32} = 1.5\times10^9 M^{-1}s^{-1}$	Goldstein et al.,2000
33	$\cdot OH + Tyr \xrightarrow{k_{33}}$ $0.5Tyr(OH)\cdot + 0.05Tyr\cdot + products$	$k_{33} = 1.4\times10^{10} M^{-1}s^{-1}$	Solar et al., 1984
34	$Tyr(OH)\cdot \xrightarrow{k_{34}} Tyr\cdot + H_2O$	$k_{34} = 1.8\times10^4 s^{-1}$	Solar et al., 1984
35	$Tyr(OH)\cdot + Tyr(OH)\cdot \xrightarrow{k_{35}}$ $TyrOH + products$	$k_{35} = 3\times10^8 M^{-1}s^{-1}$	Solar et al., 1984
36	$Tyr\cdot + Tyr\cdot \xrightarrow{k_{36}} diTyr$	$k_{36} = 4.0\times10^7 M^{-1}s^{-1}$	Hodges et al., 2000
37	$NO_2 + Tyr\cdot \xrightarrow{k_{37}} products$	$k_{37} = 1.7\times10^9 M^{-1}s^{-1}$	Goldstein et al.,2000
38	$NO_2 + Tyr\cdot \xrightarrow{k_{38}} NO_2 - Tyr$	$k_{38} = 1.3\times10^9 M^{-1}s^{-1}$	Goldstein et al.,2000
39	$ONOO^- + H^+ \xrightarrow{k_{39}} NO_2 + \cdot OH$	$k_{39} = 0.06s^{-1}(pH = 7.4)$	Bonini and Augusto, 2001

	$ONOO^- + H^+ \xrightarrow{k_{39'}} NO_3^- + \cdot H^+$	$k_{39'} = 0.14 s^{-1} (pH = 7.4)$	Bonini and Augusto, 2001
40	$\cdot OH + NO \xrightarrow{k_{40}} HNO_2$	$k_{40} = 1 \times 10^{10} M^{-1} s^{-1}$	Goldstein and Czapski, 2000
41	$\cdot OH + O_2^- \xrightarrow{k_{41}} O_2 + OH^-$	$k_{41} = 1 \times 10^{10} M^{-1} s^{-1}$	Jourd'heuil et al., 2001
42	$\cdot OH + ONOO^- \xrightarrow{k_{42}} H^+ + O_2^- + NO_2^-$	$k_{42} = 4.8 \times 10^9 M^{-1} s^{-1}$	Santos et al., 2000
43	$\cdot OH + NO_2^- \xrightarrow{k_{43}} NO_2 + OH^-$	$k_{43} = 5.3 \times 10^9 M^{-1} s^{-1}$	Goldstein and Czapski, 2000
44	$\cdot OH + CO_3^{2-} \xrightarrow{k_{44}} CO_3^- + OH^-$	$k_{44} = 3.0 \times 10^8 M^{-1} s^{-1}$	Buxton and Elliot, 1986
45	$\cdot OH + HCO_3^- \xrightarrow{k_{45}} H_2O + CO_3^-$	$k_{45} = 8.5 \times 10^6 M^{-1} s^{-1}$	Buxton and Elliot, 1986
46	$\cdot OH + GSH \xrightarrow{k_{46}} GS\cdot + H_2O$	$k_{46} = 1.4 \times 10^{10} M^{-1} s^{-1}$	Ross et al., 1998
47	$\cdot OH + AH^- \xrightarrow{k_{47}} A^- \cdot + H_2O$	$k_{47} = 3.3 \times 10^9 M^{-1} s^{-1}$	Ross et al., 1998
48	$\cdot OH + UH_2^- \xrightarrow{k_{48}} UH\cdot^- + H_2O$	$k_{48} = 7.2 \times 10^9 M^{-1} s^{-1}$ (pH=6-7)	Ross et al., 1998
49	$\cdot OH + Trp \xrightarrow{k_{49}} Trp - OH$	$k_{49} = 1.3 \times 10^{10} M^{-1} s^{-1}$	Ross et al., 1998
50	$\cdot OH + CysSH \xrightarrow{k_{50}} CysS\cdot + H_2O$	$k_{50} = 4.7 \times 10^{10} M^{-1} s^{-1}$ (pH=7.0)	Ross et al., 1998
51	$CO_3^- + Trp \xrightarrow{k_{51}} HCO_3^- + Trp\cdot$	$k_{51} = 7.0 \times 10^8 M^{-1} s^{-1}$ (pH=7.0)	Chen and Hoffman, 1973

52	$CO_3^- + CysSH \xrightarrow{k_{52}} CysS\cdot + HCO_3^-$	$k_{52} = 4.6\times10^7 M^{-1}s^{-1}$ (pH=7.0)	Chen and Hoffman, 1973
53	$CO_3^- + AH_2 \xrightarrow{k_{53}} AH\cdot + HCO_3^-$	$k_{53} = 1.1\times10^9 M^{-1}s^{-1}$ (pH=11.0)	Ross et al., 1998
54	$NO_2 + Trp \xrightarrow{k_{54}} NO_2^- + Trp\cdot$	$k_{54} = 1.0\times10^6 M^{-1}s^{-1}$ (pH=6.5)	Prutz et al., 1985
55	$NO_2 + CysSH \xrightarrow{k_{55}} NO_2^- + CysS\cdot + H^+$	$k_{55} = 5.0\times10^7 M^{-1}s^{-1}$ (pH=7.4)	Ford et al., 2002
56	$NO_2 + AH^- \xrightarrow{k_{56}} NO_2^- + H^+ + A^-\cdot$	$k_{56} = 3.5\times10^7 M^{-1}s^{-1}$ (pH=6.7)	Ross et al., 1998
57	$NO_2 + UH_2^- \xrightarrow{k_{57}} NO_2^- + H^+ + UH\cdot^-$	$k_{57} = 2.0\times10^7 M^{-1}s^{-1}$ (pH=7.4)	Ford et al., 2002
58	$ONOO^- + M^{n+} \xrightarrow{k_{58}} NO_2 + O + M^{(n+1)+}$	$k_{58} = 1.0\times10^5 M^{-1}s^{-1}$	Alvarez and Radi, 2003
59	$ONOOH + proteins \xrightarrow{k_{59}} products$	$k_{59} = 5.0\times10^3 M^{-1}s^{-1}$	Alvarez and Radi, 2003
60	$NO + O_2^- \xrightarrow{k_{60}} ONOO^-$	$k_{60} = 1.0\times10^{10} M^{-1}s^{-1}$	Goldstein and Czapski, 1995
61	$NO_2 + linoleicacid \xrightarrow{k_{61}} products$	$k_{61} = 2.0\times10^5$ (pH=9.5)	Prutz et al., 1985
62	$NO_2 + arachiodicacid \xrightarrow{k_{62}} products$	$k_{62} = 1.0\times10^6$ (pH=9.0)	Prutz et al., 1985

63	$2NO_2 \underset{k_{-63}}{\overset{k_{631}}{\rightleftharpoons}} N_2O_4$	$k_{63} = 4.5\times10^{8}\, M^{-1}s^{-1}$ $k_{-63} = 6.9\times10^{3}\, s^{-1}$	Gratzel et al., 1969 Broszkiewicz, 1976
64	$N_2O_4 + H_2O \xrightarrow{k_{64}} NO_2^- + NO_3^- + 2H^+$	$k_{64} = 1.0\times10^{3}\, s^{-1}$	Schwartz and White, 1983
65	$GS\cdot + AH^- \xrightarrow{k_{65}} GSH + A^-\cdot$	$k_{65} = 6.0\times10^{8}\, M^{-1}s^{-1}$	Wardman and von Sonntag, 1995
66	$Tyr\cdot + AH^- \xrightarrow{k_{66}} Tyr + A^-\cdot$	$k_{66} = 4.4\times10^{8}\, M^{-1}s^{-1}$	Hunter et al., 1989

relative to intracellular reactions, because the concentration driving force for diffusion is so small. Accordingly, for group (iii) species the cell as a whole was regarded as a closed system, with rates of formation exactly balancing rates of consumption. However, internal exchanges between the aqueous and lipid phases were included.

With these assumptions, the steady-state mass balance equation for species i was

$$(1-v)R_i^{(a)} + vR_i^{(m)} = 0 \qquad (2.1)$$

where v is the volume fraction of the lipid phase (estimated as 0.03, or 3% of cell volume(Liu et al., 1998; Moller et al., 2007)) and $R_i^{(a)}$ and $R_i^{(m)}$ are the net rates of formation of species i in the aqueous and lipid (membrane) phases, respectively. These reaction rates are per unit volume of the phase indicated, include all reactions in which species i participates, and are defined as positive for formation and negative for consumption.

The remaining key assumption was that lipid-aqueous mass transfer is rapid enough that concentration ratios between the two phases are very near their equilibrium values. Thus, it was assumed that

$$\frac{[i]_m}{[i]} = Q_i \qquad (2.2)$$

where $[i]$ and $[i]_m$ denote concentrations of i in cytosol and membranes, respectively, and Q_i is the membrane/cytosol partition coefficient. For each species Q_i was viewed as a known constant. Equations 2.1 and 2.2, combined with the rate laws for each reaction, provided the set of algebraic equations that governed the concentrations of all reactive intermediates. Equation 2.2 was used also, where needed, to obtain membrane concentrations from the aqueous values specified for dissolved gases and biomolecular targets.

Estimates of the remaining parameters in the model are given in Table 2.2. These include the cytosolic concentrations that were fixed as inputs, various lipid-aqueous partition coefficients, and certain pK values. The NO concentration of 1 μM is intended to be representative of an inflamed tissue, and the O_2 and CO_2 concentrations each correspond to partial pressures of 40 mmHg. The O_2 value is that in venous blood or typical body tissues, and is about one-fourth of that generally used in cell cultures. The HCO_3^-, CO_3^{2-}, and H^+ concentrations each correspond to an intracellular pH of 7.0. The O_2^- concentration was estimated by us previously (Nalwaya and Deen, 2003), by equating the respiratory production of O_2^- with its consumption by superoxide dismutase (SOD). The rate of O_2^- production was assumed to be 20% of the rate of H_2O_2 production reported in liver cells, and literature values for SOD activity were employed. The antioxidant and amino acid concentrations are all directly from the literature. The amino acid values are for free amino acids only.

The lipid-aqueous partition coefficients tend to be more uncertain. For NO, we chose the higher of two reported values ($Q_{NO} = 9$), to obtain an upper bound on the effects of lipid autoxidation; the effects of using the lower value instead ($Q_{NO} = 3$) will be discussed. Given the absence of direct measurements, Q_{NO_2} and Q_{GSH} were estimated using group-contribution correlations (Meylan and Howard, 1995). However, all of the amino acid values are based on experimental data (Leo et al., 1995). Missing from the table is $Q_{N_2O_3}$, for which there is no literature value. As will be shown, the results are insensitive to the choice of $Q_{N_2O_3}$. The partition coefficients of all ions were assumed to be zero, as already mentioned. Based on pH = 7.0 and the pK values shown, most of the glutathione will be in the neutral form (99.4%), whereas ascorbic acid and uric acid will be mainly anions (99.5% and 97.5%, respectively).

Table 2.2. Concentrations, partition coefficients, and pK values.

Species	Concentration (cytosol) [Ref.]	Partition Coefficient [Ref.]	pK
NO	1 μM (Lewis et al., 1995)	9 (Liu et al., 1998)	
O_2	50 μM (Wardman, 1998)	3 (Liu et al., 1998)	
CO_2	1.2mM (Alvarez and Radi, 2003)	6.8 (Leo et al., 1995)	
HCO_3^-	0.3mM (Roos and Boron, 1981)		
CO_3^{2-}	0.1 μM		
H^+	0.1 μM (Roos and Boron, 1981)		
O_2^-	20pM (Nalwaya and Deen, 2003)		
NO_2		0.3 (Meylan and Howard, 1995)	

GSH	5mM (Ford et al., 2002)	3.9×10^{-6} (Meylan and Howard, 1995)	9.2
AH_2	0.5mM (Alvarez and Radi, 2003; Ford et al., 2002)		4.7
UH_3	0.1mM (Alvarez and Radi, 2003)		5.4
Tyr	100 μM (Bergstrom et al.,1974)	5.5×10^{-3} (Leo et al., 1995)	
Trp	0.3 μM (Fritsche et al., 2007)	8.7×10^{-2} (Leo et al., 1995)	
CysSH	10 μM (Bergstrom et al.,1974)	3.2×10^{-3} (Leo et al., 1995)	
ONOOH			6.8
Proteins	15 mM (Alvarez and Radi, 2003)		
Metals (M^{n+})	0.5 mM		

	(Alvarez and Radi, 2003)		
Linoleic acid	1.0 M*		
Arachidonic acid	0.34 M*		

*Estimated concentration in membrane phase.

With a pK of 6.8 for peroxynitrous acid, 39% of total peroxynitrite will be neutral and 61% anionic. Unless indicated otherwise, all calculations were based on the parameter values in Tables 2.1 and 2.2, and a membrane volume fraction of $\nu = 0.03$.

2.2.4 Peroxynitrite, Hydroxyl Radical and Carbonate Radical

It is simplest algebraically to begin with peroxynitrite. Equation 2.1 was applied first to total peroxynitrite, where [Per] = [$ONOO^-$] + [ONOOH]. The principal reactions that involve either the anion or acid are Reactions 25 and 58-60, which are limited to the aqueous phase. Thus,

$$R_{Per}^{(a)} = 0 = k_{60}[NO][O_2^-] - \left(k_{25} + k_{25'}\right)[CO_2][ONOO^-] - k_{58}[M^{n+}][ONOO^-] - k_{59}[\text{protein}][ONOOH] \tag{2.3}$$

Letting $f = 1/\left(1 + 10^{pK-pH}\right)$ represent the fraction of total peroxynitrite that is present as the anion and 1 - f the fraction present as the acid, Equation 2.3 was rearrranged to

$$[\text{Per}] = \frac{k_{60}[NO][O_2^-]}{f\left\{\left(k_{25} + k_{25'}\right)[CO_2] + k_{58}[M^{n+}]\right\} + (1-f)k_{59}[\text{protein}]} \tag{2.4}$$

Other reactions that involve peroxynitrite are 19, 39, and 42. A comparison with the other sink terms in Equation 2.3 showed the rates of Reactions 19 and 39 to be negligible. Because Reaction 39 is negligible in cytosol, and because Q_{ONOOH} is unlikely to be large, that reaction will be negligible also in the membrane phase. Using Equation 4 and the result for [OH] obtained below, reaction 42 was also confirmed to be unimportant.

A similar approach was used to estimate the concentration of OH radical, which participates in reactions 33 and 39-50. Retaining only the dominant reactions, which are 33, 46

and 47 in the aqueous phase and 40 in the membrane phase, the net rates of formation in the aqueous and membrane phases are

$$R_{OH}^{(a)} = k_{39} f[\text{Per}] - (k_{33}[\text{Tyr}] + k_{46}[\text{GSH}] + k_{47}[\text{AH}^-])[\text{OH}] \qquad (2.5)$$

$$R_{OH}^{(m)} = k_{39}[\text{ONOOH}]_m - k_{40}[\text{NO}]_m \qquad (2.6)$$

Inserting these expressions into Equation 2.1, using $[\text{OH}]_m = Q_{OH}[\text{OH}]$ and $[\text{ONOOH}]_m = Q_{ONOOH}[\text{ONOOH}]$, and rearranging, gives

$$[\text{OH}] = \frac{k_{39}[\text{Per}]\{(1-\nu)f + \nu(1-f)Q_{ONOOH}\}}{(1-\nu)(k_{33}[\text{Tyr}] + k_{46}[\text{GSH}] + k_{47}[\text{AH}^-]) + \nu Q_{OH} k_{40}[\text{NO}]_m} \qquad (2.7)$$

Equation 2.7 can be simplified further by noting that Q_{ONOOH} should not be large, in which case $\nu(1-f)Q_{ONOOH} << (1-\nu)f$. Accordingly, the membrane source term in the numerator is negligible. Likewise, the membrane sink term in the denominator (that involving Q_{OH}) will also be negligible. Thus, the final expression for the OH concentration is

$$[\text{OH}] = \frac{k_{39} f[\text{Per}]}{k_{33}[\text{Tyr}] + k_{46}[\text{GSH}] + k_{47}[\text{AH}^-]} \quad . \qquad (2.8)$$

The major sink for OH was found to be GSH, which accounts for >90% of the denominator in Equation 2.8. It should be noted that this expression will underestimate [OH], because OH is generated by other intracellular reactions. However, as will be discussed, our other results are unaffected even if [OH] is several orders of magnitude larger than implied by Equation 2.8.

For CO_3^- radical, the sources are Reactions 25, 44 and 45 and the sinks are Reactions

20, 26-28, and 51-53. Because CO_3^- is an anion, only aqueous reactions were considered. Retaining only the dominant terms, it was found that

$$[CO_3^-] = \frac{k_{25} f [\text{Per}][CO_2]}{k_{20}[\text{GSH}] + k_{53}[AH^-]} \quad . \tag{2.9}$$

For CO_3^- the major sink is its reaction with ascorbate, which accounts for >90% of the denominator in Equation 2.9.

2.2.5 Nitrogen Dioxide and Nitrous Anhydride

For N_2O_3, Reactions 2, 3, and 18 can occur in the cytosol, and Reactions 2 and 18 can also take place in the lipid membranes. However, by reasoning similar to that used for OH, the membrane sink terms (Reaction 18 and reverse of Reaction 2) were each found to be negligible. The simplified expression for the aqueous N_2O_3 concentration is

$$[N_2O_3] = \frac{k_2[NO][NO_2]\{(1-\nu) + \nu Q_{NO} Q_{NO_2}\}}{(1-\nu)(k_{-2} + k_3 + k_{18}[\text{GSH}])} \tag{2.10}$$

The term in the numerator that contains $Q_{NO}Q_{NO_2}$ represents the augmentation of N_2O_3 production due to intramembrane autoxidation of NO. The concentration of N_2O_3 is depressed by GSH in two ways: via the sink term in the denominator of Equation 2.10 and via the influence of GSH on the NO_2 concentration in the numerator (see below).

The reactions involving NO_2 are much more numerous: 1, 2, 4, 14, 25, 29, 37-39, 43, 54-58, and 61-62. Simplifications were obtained by applying a steady state condition to $GSOONO_2$ in Reaction 14, and assuming that [Tyr·] is small enough to neglect Reactions 37 and 38 for NO_2 (an assumption verified using the tyrosine results discussed later). Retaining only the dominant

sources and sinks in the remaining reactions in each phase, and neglecting Reaction 2 in the membrane, the aqueous NO_2 concentration was found to be

$$[NO_2] = \frac{(1-v)A + 2vk_1Q_{NO}^2Q_{O_2}[NO]^2[O_2]}{(1-v)B + vQ_{NO_2}(k_2Q_{NO}[NO] + k_{61}[LA] + k_{62}[AA])} \quad (2.11a)$$

$$A = 2k_1[NO]^2[O_2] + f[Per](k_{25}[CO_2] + k_{58}[M^{n+}]) \quad (2.11b)$$

$$B = k_2[NO] + k_4[GSH] + k_{56}[AH^-] + k_{57}[UH_2^-] \quad (2.11c)$$

The term in the numerator of Equation 2.11a that involves $Q_{NO}^2Q_{O_2}$ represents the increased rate of NO_2 formation due to membrane autoxidation. The NO_2 concentration is reduced by the presence of antioxidants and unsaturated fatty acids, as shown by the various terms in the denominator.

2.2.6 Glutathionyl Radical, S-nitroso Glutathione, and Tyrosyl Radical

The reactions that involve GS· are 4-8, 10, 20, 21, 23, 24, 46, and 65. Of these, Reactions 8, 20, 21 and 65 will occur only in the cytosol. Simplifications were obtained by applying steady state assumptions to GSOO·, $GSSG^-$, and GSO·. For GSOO·, it was found that only Reaction 7 was important; for GSO·, Reaction 6 could be ignored because it is a second-order reaction between radicals, each of which will have a very small concentration. Reactions 20, 21 and 46 were found to be negligible sources of GS· and reverse Reaction 23 was a negligible sink. Also, all membrane reactions were found to be negligible compared to those in the aqueous phase. After considerable manipulation, it was found that

$$[GS\cdot] = \frac{k_4[NO_2][GSH] + k_{20}[CO_3^-][GSH] + k_{23}[Tyr\cdot][GSH]}{k_{65}[AH^-] + k_5[NO] + k_8[GS^-] - C + k_{10}[GSNO] - D[GSH]} \quad (2.12a)$$

$$C = \frac{k_8 k_{-8}[GS^-]}{k_{-8} + k_9[O_2]} \quad (2.12b)$$

$$D = \frac{k_7 k_{17}[O_2]}{k_{-7}} . \quad (2.12c)$$

Note that $[GS^-] = 10^{pH-pK}[GSH] = 0.0063\,[GSH]$ for pH = 7.0 and pK = 9.2. Before [GS·] can be evaluated, it is necessary to calculate [GSNO] and [Tyr·], as described next.

For GSNO, the relevant reactions were 5, 10-13, and 18. Reaction 12 could be ignored because it is a third-order reaction among trace species. All membrane reactions were negligible here because of the small Q_i values. Applying Equation 2.1 once again, it was found that

$$[GSNO] = \frac{k_5[GS\cdot][NO] + k_{18}[N_2O_3][GSH]}{k_{10}[GS\cdot] + k_{11}[GSH] + k_{13}[GSOO\cdot]} \quad (2.13a)$$

$$[GSOO\cdot] = \frac{k_7[GS\cdot][O_2]}{k_{-7} + k_{17}[GSH]} . \quad (2.13b)$$

The reactions that involve Tyr· are 23, 28-30, 32-34, 36-38, and 66. Simplifications were obtained by neglecting Reaction 36 (a second-order reaction among trace species), applying steady state conditions to Tyr-NO and Tyr(OH)·, and identifying the dominant sources and sinks among the terms that remained. All reactions in the membrane were found to be negligible in this case. The result was

$$[Tyr\cdot] = \frac{k_{-23}[GS\cdot][Tyr\cdot] + k_{28}[CO_3^-][Tyr\cdot] + k_{29}[NO_2][Tyr\cdot]}{k_{23}[GSH] + k_{30}[NO] + k_{66}[AH^-]} . \quad (2.14)$$

As seen in Equations 2.12a and 2.14, the expressions for [GS·] and [Tyr·] are coupled. However, it was found that, for physiological concentrations of GSH and Tyr, the terms that cause the coupling are negligible. Also, for physiological concentrations of AH^-, the ascorbate terms in the denominators of Equations 2.12a and 2.14 were easily the dominant sinks for GS· and Tyr·. In addition, because $[CO_3^-]$ is greatly depressed at physiological levels of AH^- (Equation 2.9), CO_3^- radical is ordinarily not an important source for GS·. Accordingly, for normal values of $[AH^-]$, Equations 2.12a and 2.14 could be simplified to

$$[GS\cdot] = \frac{k_4[NO_2][GSH]}{k_{65}[AH^-]} \qquad (2.15)$$

$$[Tyr\cdot] = \frac{k_{28}[CO_3^-][Tyr] + k_{29}[NO_2][Tyr]}{k_{66}[AH^-]} \quad . \qquad (2.16)$$

2.2.7 Reaction Rates

In addition to providing estimates of the concentrations of key intermediates, the analysis permitted us to calculate the rate of each reaction in Table 1. The rates of formation of nitrotyrosine and dityrosine are of particular interest, as these end products have been proposed as biomarkers for NO_2 and peroxynitrite activity. The rates of formation of these tyrosine derivatives are given by

$$R_{NO_2-Tyr} = k_{38}[NO_2][Tyr] = \frac{k_{38}[Tyr]}{k_{66}[AH^-]}(k_{29}[NO_2]^2 + k_{28}[NO_2][CO_3^-]) \qquad (2.17)$$

$$R_{diTyr} = 2k_{36}[Tyr]^2 \quad . \qquad (2.18)$$

2.3 Results

2.3.1 Effects of NO on RNS concentrations

In this kinetic model all reactive nitrogen species (RNS) are derived ultimately from NO. Figure 2.5 shows the predicted concentrations of total peroxynitrite (Per), NO_2, and N_2O_3 as functions of the NO concentration. Those concentrations are linear, weakly quadratic (almost linear) and cubic, respectively, in [NO], and differ by several orders of magnitude. Whereas [NO] in macrophage cultures (and presumably sites of inflammation) is on the order of 1 μM, the concentrations of Per, NO_2, and N_2O_3 were found to be in the nM, pM and fM ranges, respectively. The prediction that [Per] is in the nM range is consistent with our previous peroxynitrite model (Nalwaya and Deen, 2003). To our knowledge, these are the first estimates of $[NO_2]$ and $[N_2O_3]$ that take into account the effects of antioxidants, proteins, lipids and other cellular components.

2.3.2 Effects of GSH on RNS concentrations

Among the various antioxidants, GSH is predicted to have a particularly strong effect on RNS concentrations, because of its relatively high intracellular concentrations (mM range). The expected effect of [GSH] on $[NO_2]$ is shown in Figure 2.6, for three scenarios. For the baseline conditions (Q_{NO_2} = 0.3 and lipids included), $[NO_2]$ declined sharply with increasing [GSH], the relationship being nearly hyperbolic ($[NO_2] \propto [GSH]^{-1}$). When the membrane phase was omitted ($v = 0$), the results were nearly the same, indicating that lipid reactions do not strongly influence the NO_2 concentration. Only when the relative solubility of NO_2 in the membrane phase was assumed to be much larger than the baseline value (Q_{NO_2} = 3 instead of 0.3) was there

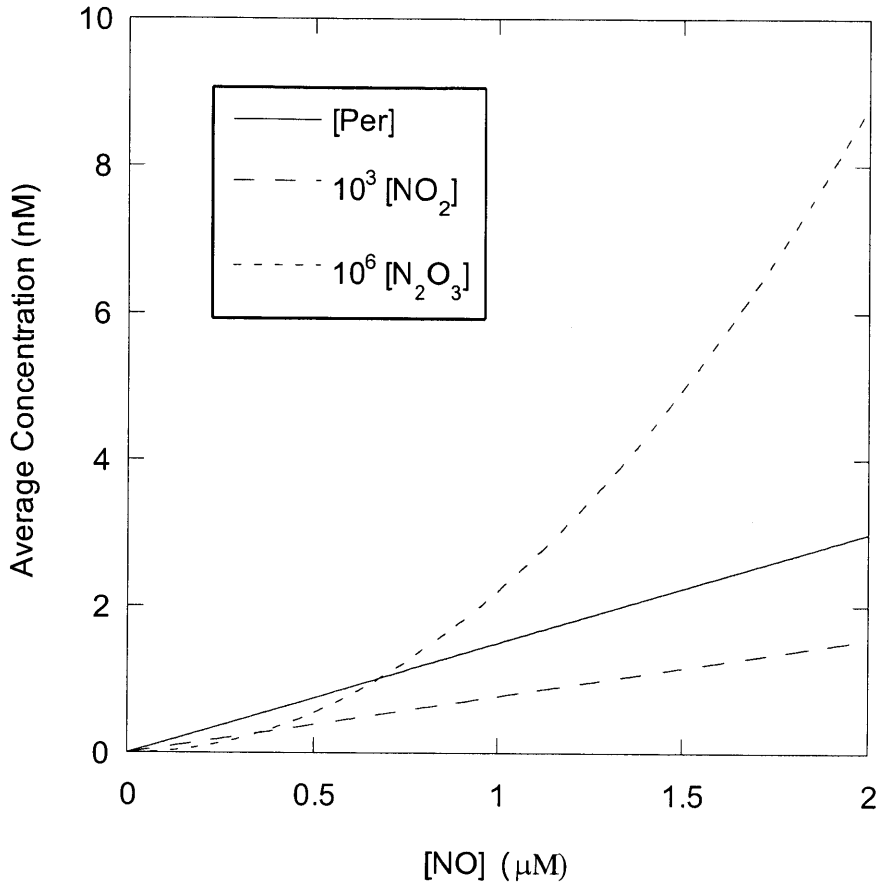

Figure 2.5. Effects of NO concentration on RNS concentrations. Values are shown for total peroxynitrite (Per), NO_2, and N_2O_3. The concentrations in this and subsequent plots are volume-weighted averages of cytosolic and membrane values. The values for Per, NO_2, and N_2O_3 are in the nM, pM and fM ranges, respectively.

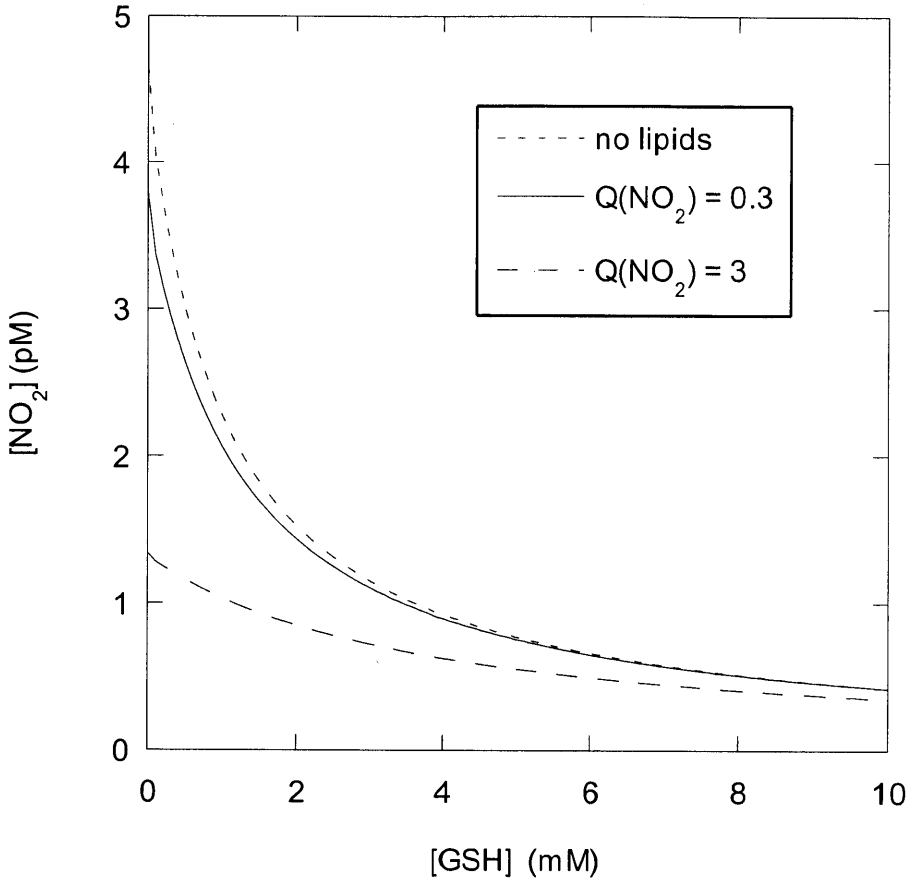

Figure 2.6. Effects of glutathione concentration on the concentration of NO_2. Results are shown for three situations: the baseline case ($Q_{NO_2} = 0.3$); a high relative solubility of NO_2 in the lipid phase ($Q_{NO_2} = 3$); and a simplified model in which the lipid phase was omitted.

a significant reduction in [NO_2], relative to the baseline curve. Varying $Q_{N_2O_3}$ from 0 to 10 (not shown) did not have a noticeable effect on either [NO_2] or [N_2O_3], indicating that this partition coefficient is not an important parameter.

Figure 2.7 shows the effects of [GSH] on [N_2O_3], for the same three scenarios just discussed. As with [NO_2], there was a marked decrease in [N_2O_3] with increasing [GSH]. Close examination reveals that at high GSH concentrations, [N_2O_3] was even more sensitive to [GSH] than was [NO_2] (i.e., $[N_2O_3] \propto [GSH]^{-2}$). This increased sensitivity stems from the fact that GSH influences [N_2O_3] both by scavenging NO_2 (needed to produce N_2O_3) and by scavenging N_2O_3 itself. Except at low values of [GSH], neither increases in Q_{NO_2} nor the removal of lipids had a significant effect on [N_2O_3].

As indicated by Equation 4, peroxynitrite concentrations are predicted to be unaffected by GSH levels.

2.3.3 RNS Sources and Sinks

Figure 2.8 depicts the primary sources and sinks for NO_2. Conversion of peroxynitrite, mediated either by metals or CO_2, was calculated to account for 98% of intracellular NO_2 production. Autoxidation in cytosol (not shown in the graph) produced only 0.2% of the NO_2 and autoxidation in membranes only 1.8%. Autoxidation in membranes was calculated to be more important than that in cytosol, despite the relatively small membrane volume (3% of cell volume), because of the favorable partitioning of NO and O_2 into lipids. Scavenging of NO_2 by GSH was found to be the dominant sink (79%), followed by reaction with ascorbate (14%).

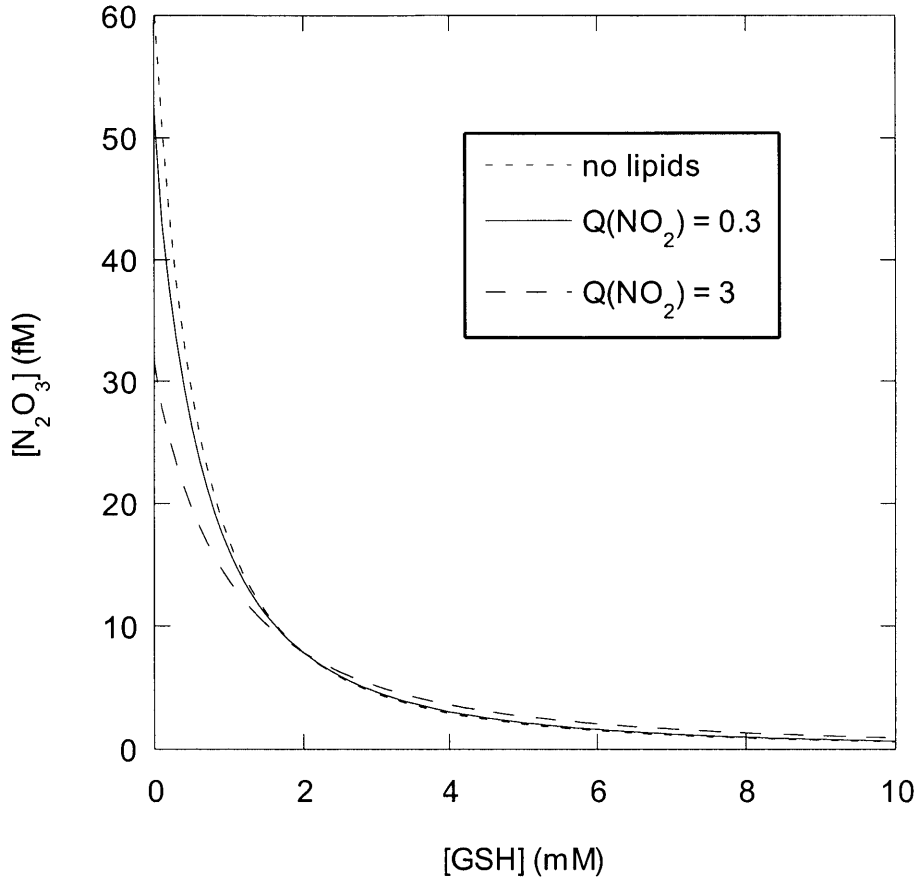

Figure 2.7. Effects of glutathione concentration on the concentration of N_2O_3, for the same conditions as in Figure 2.6.

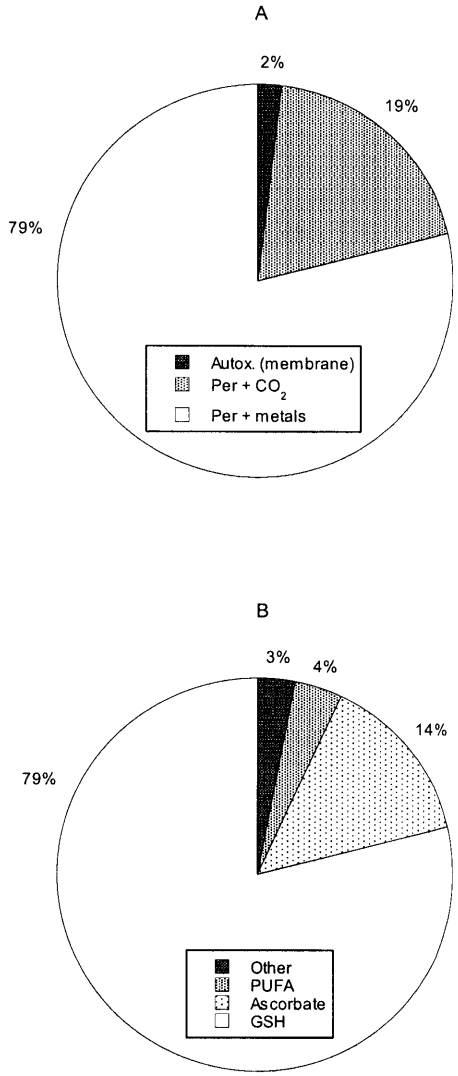

Figure 2.8. Sources (panel A) and sinks (panel B) for NO_2. In decreasing order of importance, the sources are the reaction of peroxynitrite with metals or selenium, the reaction of peroxynitrite with CO_2, and autoxidation of NO in membranes. Autoxidation in the cytosol (not shown) is negligible. The sinks (also in decreasing order) are the reaction with glutathione, the reaction with ascorbate, the reaction with unsaturated fatty acids, and all other reactions.

Reactions of NO_2 with polyunsaturated fatty acids (PUFA, 4%) and other targets (3%) were found to be minor sinks. These results reemphasize the importance of GSH as a scavenger of NO_2, as indicated already by Figure 2.6.

The origin and fate of N_2O_3 are depicted in Figure 2.9. In this case the only source was autoxidation. Again, the lipid contribution was disproportionate to membrane volume (8% of N_2O_3 produced in 3% of cell volume). However, unlike NO_2 formation, the total rate of production of N_2O_3 via autoxidation in cytosol was much larger than that via membrane autoxidation. The reason for this is that partitioning of NO_2 into the membrane is unfavorable ($Q_{NO_2} = 0.3$), and NO_2 is required to produce N_2O_3. All N_2O_3 consumption in the model was cytosolic, with scavenging by GSH being most important (79%), followed by decomposition into NO and NO_2 (20%). Only 1% of the N_2O_3 formed was calculated to be hydrolyzed to NO_2^-.

2.3.4 Glutathione Products

Of the various reaction products of GSH with RNS, GSNO was found to be present at the highest concentration. For [GSH] = 1 mM, 5 mM, and 10 mM, [GSNO] = 5.4 μM, 2.2 μM, and 1.4 μM, respectively. The reason that [GSNO] varies inversely with [GSH] is that N_2O_3 produces GSNO, and $[N_2O_3]$ decreases rapidly with increasing [GSH] (Figure 2.7). The concentrations of GSOH, GSO, and GSOO were all found to be negligible relative to that of GSNO. Depending on the GSH/GSSG redox potential, each cellular compartment cytosol, mitochondria, nucleus) has its own GSH/GSSG concentration ratio (Hansen et al., 2006). Because GSSG levels are maintained by enzymatic processes, and because the concentration of GSSG is at most 3% of that of GSH, concentrations of GSSG were not calculated in our analysis.

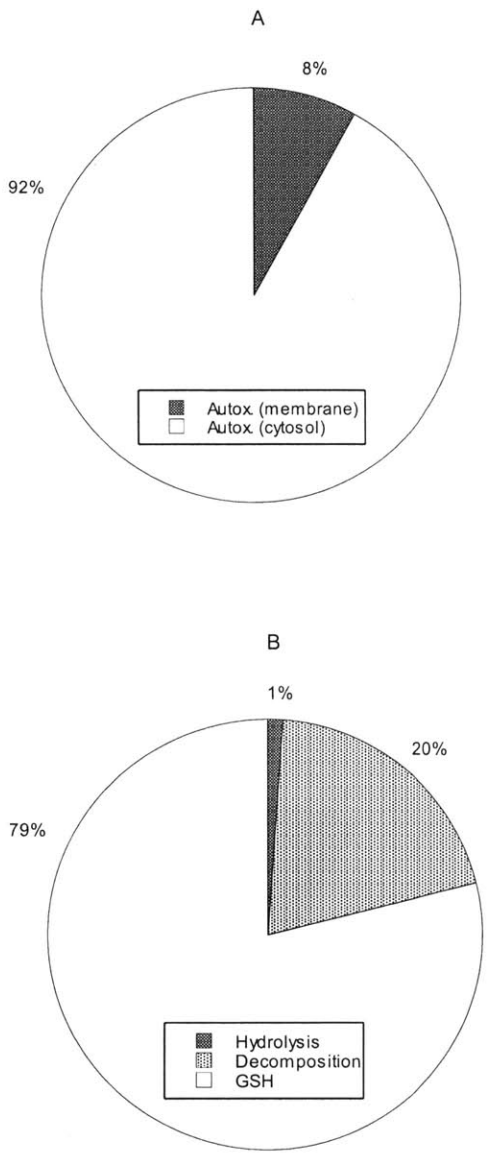

Figure 2.9. Sources (panel A) and sinks (panel B) for N_2O_3. The dominant source is autoxidation of NO in cytosol, the contribution from autoxidation in membranes being minor. The sinks (in decreasing order of importance) are the reaction with glutathione, decomposition to NO and NO_2, and hydrolysis to NO_2^-.

Concerning the lumping together of aqueous compartments in the model, it is worth noting that mitochondrial GSH concentrations are generally similar to cytosolic values (Garcia-Ruiz et al., 1994).

2.3.5 Tyrosine Products

In the presence of ascorbate (our baseline conditions) it was found that 3-nitrotyrosine (NO_2-Tyr) was the only significant tyrosine product; dityrosine (diTyr) was nearly absent, accounting for only 0.01% of the moles of Tyr going to either product. The reason for this is that the rate of diTyr formation is proportional to the square of the Tyr· concentration (Equation 2.18), and ascorbate is an extremely effective Tyr· scavenger (Equation 2.16). When ascorbate was assumed to be absent, NO_2-Tyr remained the major product; however, diTyr was no longer entirely negligible, accounting then for 6% of the molar consumption of Tyr. For all combinations of antioxidant levels considered (1 mM ≤ [GSH] ≤ 10 mM and 0 ≤ [AH^-] ≤ 0.5 mM), NO_2-Tyr formation accounted for at least 91% of the consumption of Tyr.

2.4 Discussion

The present kinetic analysis provides what seem to be the first estimates of the intracellular concentrations of NO_2 and N_2O_3, two key reactive species derived from NO. Incorporating the effects of the antioxidants, proteins, and lipids present in cells yielded concentrations which were much smaller than those in simple aqueous solutions containing the same levels of NO. For example, with [NO] = 1.0 μM and [O_2] = 50 μM, which should be representative of inflamed tissues, we found that [NO_2] = 0.8 pM and [N_2O_3] = 2.2 fM when the kinetic effects of cellular constituents were included (Figure 2.5). The corresponding steady-state concentrations in simple aqueous solutions, where only autoxidation (Reactions 1-3) occurs,

are calculated to be 30 pM and 400 fM at ambient O_2 levels ($[O_2]$ = 200 μM) and 8 pM and 100 fM at tissue O_2 levels ($[O_2]$ = 50 μM). The latter are still some 10 and 45 times the respective intracellular values. In a 0.01 M phosphate buffer at pH = 7.0 and ambient O_2, the accelerated hydrolysis of N_2O_3 (Reaction 3) is calculated to yield $[NO_2]$ = 8 pM and $[N_2O_3]$ = 100 fM, concentrations which are coincidentally the same as those at tissue O_2 levels in simple solutions without phosphate. Differences in $[O_2]$ aside, the main reason for the lower intracellular concentrations is the reaction of both NO_2 and N_2O_3 with glutathione (Reactions 4 and 18). As shown in Figures 2.6 and 2.7, GSH has a particularly strong effect on $[N_2O_3]$, because it scavenges NO_2 (needed to form N_2O_3) as well as N_2O_3 itself. The marked ability of GSH to scavenge NO_2, and thereby prevent the formation of N_2O_3, has been recognized previously (Goldstein and Czapski, 1996; Jourd'heuil et al., 2003; Schrammel et al., 2003; Sovitj and Rose, 1998).

In addition to containing antioxidants such as glutathione and ascorbate, a distinctive feature of cells is the possibility of lipid-phase reactions as well as aqueous ones. It has been shown by Lancaster and co-workers that, in various hydrophobic media, the rate of autoxidation per unit volume is greatly amplified by the high solubilities of NO and O_2 in such media relative to water (Liu et al., 1998; Moller et al., 2007). Thus, the favorable partitioning of NO and O_2 into lipids may lead to large volumetric rates of autoxidation in cell membranes, even though the rate constants in the two phases are equal or nearly so (Liu et al., 1998; Moller et al., 2007). The present analysis included the effects of membrane autoxidation, and allowed also for the possibility of intramembrane reactions involving other uncharged species. Because reported rate constants for lipid phases were usually lacking, we assumed each to be equal to the

corresponding aqueous value. Thus, the predicted magnitude of the lipid effects depended entirely on the membrane/cytosol partition coefficients (Q_i for species i) and the fraction of cell volume occupied by lipids (v, fixed at 0.03 or 3%).

Autoxidation in the membrane (lipid) phase was found not to have a significant effect on the predicted RNS concentrations. For NO_2 and N_2O_3, the results are affected somewhat by uncertainties in Q_{NO}, with Liu et al. (1998) giving a value of 9 and Miller et al. (2007) a value of 3. This corresponds to an order-of-magnitude difference in the rate of NO consumption by O_2 in membranes, which is proportional to $Q_{NO}^2 Q_{O_2}$. However, even adopting the higher value of Q_{NO} as a baseline parameter (Table 2.2), we found the effects of membrane autoxidation on NO_2 and N_2O_3 levels to be small. As shown in Figures 8 and 9, only about 2% and 8%, respectively, of the synthesis of NO_2 and N_2O_3 was associated with membrane autoxidation. If it was assumed that $Q_{NO} = 3$, the membrane contributions to synthesis were reduced to 0.2% for NO_2 and 3% for N_2O_3. Another partition coefficient that affected the levels of NO_2 and N_2O_3 was Q_{NO_2}. However, as shown in Figures 2.6 and 2.7, it became significant only when it was assumed to greatly exceed the baseline estimate of 0.3. Uncertainties in the other relevant partition coefficient, $Q_{N_2O_3}$, were found to have negligible effect.

In addition to accelerating autoxidation, membranes might alter the concentrations of RNS by reacting with them directly. The possibility considered in the analysis was the reaction of NO_2 with polyunsaturated fatty acids (PUFA, Reactions 61 and 62). As shown in Figure 2.8, the reaction with PUFA was found to be only a minor sink for NO_2. In summary, although they influence the rate of NO consumption by autoxidation, intramembrane reactions appear to have little effect on the concentrations of RNS. Although having a negligible effect on RNS

concentrations, membrane reactions with RNS might still be an important pathway for cellular damage.

A similarly detailed treatment of intracellular nitrogen oxide chemistry was provided by Lancaster (2006). Most of the reactions found in Table 1 were included also in that analysis and the two sets of calculations employ similar or identical values of the rate constants. However, the present model includes a number of additional reactions, namely, Reactions 11, 12, 21, 22, 24, 33-35, 42, 44-59, 61-66. Of these, it seems especially important to include the reaction of peroxynitrite with transition metal centers or selenium-containing compounds (Reaction 58) as a source for NO_2, as pointed out by Radi et al. (Alvarez and Radi, 2003; Radi, 2004). As shown in Figure 8, this accounted for nearly 79% of our calculated NO_2 production. The reaction of peroxynitrite with proteins (Reaction 59) is also noteworthy, as a sink for peroxynitrite. Ascorbate should not be ignored, mainly because of its ability to scavenge tyrosyl radicals (see below), but also because it is a moderately important sink for NO_2 (Figure 2.8). Lancaster (2006) also chose to consider only aqueous chemistry, but this decision is supported by our finding that membrane reactions do not strongly influence RNS levels.

According to the present analysis, the only significant products of glutathione and tyrosine are GSNO and NO_2-Tyr, respectively. This differs from the findings of Lancaster (2006), where the main glutathione products predicted were GSOH, GSOO and GSO, and dityrosine (dityr) was important, in addition to NO_2-tyr. These differences stem not only from the inclusion of somewhat different sets of reactions in the two models, but also from a large discrepancy in the assumed levels of $O_2^{\cdot-}$. The $O_2^{\cdot-}$ synthesis rates used by Lancaster (2006) were two orders of magnitude larger than what led to the $O_2^{\cdot-}$ concentration in Table 2.2 (as much as

200 μM/s, as compared with 1 μM/s). A high O_2^- concentration, for example, will favor the reaction of Tyr· with O_2^- over the reaction of Tyr· with NO.

With regard to glutathione products, the model predicts [GSNO] ranging from 1 to 5 μM for [GSH] of 1 to 10 mM, under conditions of steady-state exposure to 1 μM NO and 50 μM O_2. These predictions for [GSNO] are reasonable, given the micromolar levels determined in various tissues from humans and animal models of human disease. For example, Kluge et al. measured [GSNO] of 6-8 μM in normal rat cerebellum (Kluge et al.1997), while Stamler and coworkers have found nitrosothiol levels in general ranging from 7 μM in blood to 15-20 μM in pulmonary fluids (Gaston et al., 1993;Stamler et al, 1992) Further studies are needed to assess [GSNO] under conditions of inflammation in vivo.

The ratio of the rate of NO_2-Tyr formation to that of diTyr is predicted to vary as $[NO_2]/[Tyr\cdot]$, as indicated by Equations 2.17 and 2.18. Carbonate radical tends to be the dominant source of Tyr· (more important than NO_2 or GS·), and ascorbate its main scavenger. Accordingly, [Tyr·] is very nearly proportional to $[CO_3^-][Tyr]/[AH^-]$ (Equation 2.16). The concentration of CO_3^-, in turn, varies as $1/[AH^-]$ (Equation 2.9). Accordingly, when ascorbate is present, the rate of NO_2-Tyr formation relative to that of diTyr will vary nearly as $[NO_2][AH^-]^2/[Tyr]$. This illustrates why NO_2-Tyr is predicted to be favored so strongly over diTyr at typical intracellular levels of ascorbate, which range from 0.5-2 mM (Washko et al., 1989). It should be noted, however, that $[CO_3^-]$ may be underestimated in the present model to some extent, because CO_3^- is formed also from the reaction of H_2O_2 with HCO_3^- and Cu-Zn SOD

(Karunakaran et al., 2005;Ramirez et al., 2005;Zhang et al., 2000); a higher [CO_3^-] would favor more diTyr formation.

The concentration of OH radical may be underestimated considerably by Equation 2.8, because there are sources of OH in addition to those included in the model. For example, the reaction of reduced transition metal ions such as copper (I) and iron (II) with H_2O_2 can give rise to OH (Halliwell and Gutteridge, 1998). However, none of the other results are affected noticeably even if [OH] is increased by a factor of 10^3, and the effect on RNS concentrations is negligible even if [OH] is increased by a factor of 10^9.

Another pathway for generating NO_2 in an inflamed tissue is the conversion of NO_2^- to NO_2 by the extracellular myeloperoxidase (MPO) activity associated with neutrophils (Burner et el., 2000) We are unaware of any data that would allow quantification of this source of NO_2, so it was not included in the present model. It is conceivable that, in some circumstances, MPO activity might lead to NO_2 concentrations that exceed those predicted here. If extracellular concentrations of NO_2 could be estimated, along with a cell membrane permeability to NO_2, then the steady-state mass balance in Eq. 1 could be altered to include a source term that corresponds to NO_2 diffusion into the cell.

The list of RNS sinks that were considered is also incomplete. For example, N_2O_3 is known to react with DNA, nucleotides, and amino acids (Nguyen et al., 1992). Of the potential N_2O_3 targets that were not included in the model, perhaps the most abundant is ATP, which may be present at concentrations as high as 10 mM (Traut, 1994). Based on preliminary data obtained using dATP (V. Dendroulakis and P.C. Dedon, unpublished) the rate constant for N_2O_3 with ATP is estimated as 5.0×10^6 $M^{-1}s^{-1}$. However, even at the high ATP concentration just

mentioned, including ATP decreased the predicted value of $[N_2O_3]$ only from 2.2 fM to 1.9 fM. In summary, the effect of GSH scavenging on $[N_2O_3]$ is already so strong that reactions with other biomolecular targets are unlikely to depress $[N_2O_3]$ below the predicted fM range.

The model predicts a roughly order-of-magnitude increase in $[N_2O_3]$ as [GSH] decreases from 10 to 1 mM (Figure 2.7), and a corresponding 3- to 4-fold increase in [GSNO]. Such a large increase in $[N_2O_3]$ would be expected to lead to increased reactions with DNA and other cellular molecules. However, we previously observed that the level of nitrosatively-induced deamination products in DNA increased by at most 40 percent in cells exposed to a steady-state level of 0.6 μM NO for 8 hr when GSH levels were decreased by more than 10-fold with buthionine sulfoximine treatment (Li et al., 2005). This relatively small increase in N_2O_3-induced DNA damage is consistent with a role for GSH in scavenging N_2O_3, but suggests that other factors intervene to possibly mask the effects of increased N_2O_3, such as a balance between DNA repair and N_2O_3-induced damage. Indeed, the level of nitrosative DNA damage may not serve as a useful index of $[N_2O_3]$, given our observation of a 3- to 4-fold protective effect when comparing levels of nitrosative DNA damage in cells and purified DNA, both exposed to identical [NO] and $[O_2]$ (Dong et al., 2003; Dong and Dedon, 2006), and evidence for significantly higher levels of nitrosative damage in RNA compared to DNA (Pang et al., manuscript in preparation).

The present model can be modified to develop more accurate predictions of intracellular RNS concentrations as the chemistry becomes more completely understood. The algebraic expressions that are presented for the concentrations of RNS and other reactive intermediates permit one to easily update the calculations as new data concerning any of the rate constants or

partition coefficients become available. Those expressions also provide a way to assess the importance of including additional intracellular reactions. In general, for an additional source to be important, it must be at least comparable to terms already present in the numerator of a given concentration expression; new sinks may be compared with the terms in the denominator. Because of the analytical form of the results, no special software is needed to assess the effects either of new parameter values or additional reactions.

Chapter 3

Prediction of NO Concentrations in Cell Coculture System

3.1 Introduction

Nitric oxide (NO) endogenously generated by activated macrophages can produce other reactive nitrogen species (RNS) through successive reactions. In particular, adding NO to a solution that contains O_2 and O_2^- (such as cytosol) will produce nitrogen dioxide (NO_2), nitrous anhydride (N_2O_3), and peroxynitrite ($ONOO^-$), which show diverse reactivities with critical cellular components, including proteins, nucleic acids, and lipids (Tamir et al., 1996). Although NO and its oxidation products (RNS) can assist in killing invading microorganisms, the concurrent chemical damage to host cells may initiate or contribute to diseases such as certain forms of cancer through chronic inflammation (deRojas et al., 1995; Lewis et al., 1995; Tamir and Tannenbaum, 1996). In other words, sustained high local rates of NO generation may result in a significant health risk.

Several methods for NO delivery to biological solutions have been developed so far. Both addition of NO-saturated aqueous solutions (Liu et al., 1998; Thomas et al., 2001) and release from NO donor compounds (Estevez et al., 1999; Gasco et al., 1996) are not suited for long-term, constant levels of NO exposure to cell cultures. However, NO delivery by gas permeation through membranes (Chen et al., 2003; Lewis et al., 1994; Tamir et al., 1993) can achieve steady state NO concentrations indefinitely (up to at least 72h).

Another approach for achieving constant levels of NO for long periods is to co-culture target cells with activated macrophages. A novel co-culture method was developed recently in the laboratory of Gerald N. Wogan at MIT. Transwell™ permeable supports (Corning, NY),

consist of 100 mm culture dishes each containing a 75 mm diameter insert having a polycarbonate membrane with 0.4 μm pores that separates two chambers (Figure 3.1).Target cells are placed on the top of a porous membrane and macrophages adhered to the bottom side. This system allows diffusional exchange but no direct contact between generator (macrophage) and the target cells, and also enables the separation between these two types of cells, even when both are adherent. In addition, target cells can be recovered separately for viability and mutation assays. Due to these features, this co-culture system might better mimic the inflammation in vivo.

The objective of the present work was to develop a model for predicting NO concentration as a function of height (z) by using the measured nitrite (NO_2^-) data in co-culture systems. As will be shown, the NO and O_2 concentration are functions of z only. Concerning how these NO and O_2 concentrations depend on z, it is apparent that the net NO production rate and O_2 consumption rate by generator cells and the target cells have important effects on these concentration profiles. The fraction of NO loss by diffusion to the head space depends strongly on the cellular rate of NO synthesis. A graphical method was developed to allow the cellular NO concentrations under various conditions to be determined from the rate of NO_2^- accumulation.

3.2 Model Development

3.2.1 Model Geometry and Simplification

The co-culture system is shown schematically in Figure 3.1. The cells are placed on both sides of an insert of radius a, which fits within a dish of radius b. The vertical coordinate is z, with $z = -H$ at the bottom of the outer dish, $z = 0$ at the membrane, and $z = L$ at the gas-liquid interface. The fixed dimensions are $a = 37.5$ mm, $b = 50$ mm, and $H = 1$ mm; the liquid depth

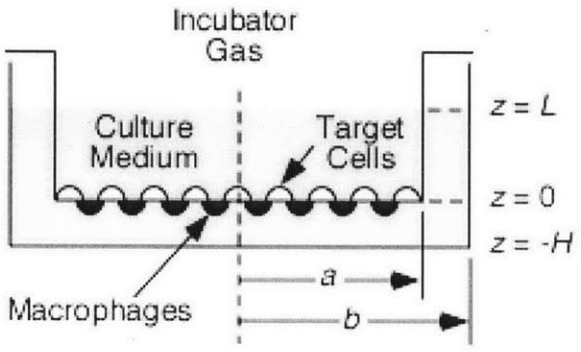

Figure 3.1. Schematic of the co-culture system. Target cells were placed on the top side of a porous membrane positioned at $z = 0$ and macrophages adhered to the bottom side. The thickness of the insert was negligible relative to the other dimensions shown.

can be varied, but in all experiments to be discussed $L = 2$ mm. The thickness of the porous membrane separating the macrophages (bottom of the insert) from the target cells (top of the insert) is 10 μm. This is small enough that, in modeling NO and O_2 diffusion, both cell layers may be viewed as residing at $z = 0$. The porosity of the membrane (fraction of its area occupied by pores) is 0.13.

There are two pathways for entry of O_2 and loss of NO from the stagnant liquid. The more direct one is diffusion in the z direction, including through the cell layers and the insert membrane. Less direct is radial diffusion within the bottom chamber combined with vertical diffusion in the annular space between the insert and dish. The resistance of the second pathway relative to the first is approximately $a^2/(4HL) = 180$ (see Appendix, Section 3.5). Accordingly, the second pathway was neglected and the concentrations of O_2 and NO were viewed as functions of height only. The concentration of species i is denoted as $C_i(z)$. A steady state model is appropriate because the time required for diffusion of either species across a 2 mm film ($L^2/D = 22$ min) is much shorter than the duration of the experiments (48 h).

3.2.2 Autoxidation Reaction

Competing with the diffusional loss of NO to the incubator gas is its reaction with O_2. The aqueous oxidation of NO by O_2 is described by 3 successive elementary reactions as follows.

$$2NO + O_2 \xrightarrow{k_1} 2NO_2 \tag{3.1}$$

$$NO + NO_2 \underset{k_{-2}}{\overset{k_2}{\rightleftarrows}} N_2O_3 \tag{3.2}$$

$$N_2O_3 + H_2O \xrightarrow{k_3} 2NO_2^- + 2H^+ \tag{3.3}$$

The intermediates (NO_2 and N_2O_3) are present only in tiny amounts (Lewis et al., 1994), and the rate-limiting step is reaction (3.1). Under these conditions, the overall reaction, which is called autoxidation reaction, can be simplified to

$$4NO + O_2 + 2H_2O \xrightarrow{k_1} 4NO_2^- + 4H^+ \tag{3.4}$$

The autoxidation reaction is second order in NO and first order in O_2 because reaction (3.1) is the rate-controlling. Hence, the formation rate of nitrite (R) is

$$R = \frac{dC_{NO_2^-}}{dt} = 4k_1 C_{NO}{}^2 C_{O_2} \tag{3.5}$$

whereas the volumetric rate of O_2 consumption in the medium is $R/4$.

Oxygen is plentiful enough and autoxidation slow enough that the effect of Reaction (3.1) on C_{O_2} is negligible. However, cellular consumption by respiration can be an important sink for O_2. Because NO inhibits respiration, and because the availability of O_2 influences the trapping of NO as NO_2^-, the concentrations of NO and O_2 are linked. In the remainder of this section the governing equations will be stated, the parameters that affect $C_{O_2}(z)$ and $C_{NO}(z)$ will be defined, and the solution procedure will be described. How the model can be used to infer the cellular NO concentration from measurements of R will be explained.

3.2.3 Reaction-Diffusion Equation

Assuming no bulk motion in the liquid solution (no free convection), the one-dimensional conservation equation for species i is

$$\frac{\partial C_i}{\partial t} = D_i \frac{\partial^2 C_i}{\partial z^2} + R_i \tag{3.6}$$

where t is time, C_i is the molar concentration, D_i is the liquid diffusivity, and R_i is the net rate of formation of species i by chemical reactions, per unit volume (Deen, 1998). Under cellular conditions, the species are at steady-state. Then,

$$D_i \frac{d^2 C_i}{dz^2} + R_i = 0 \tag{3.7}$$

3.2.4 Model Formulation

The autoxidation Damköhler number for O_2 which is the ratio of a reaction velocity ($k_1 C_{NO}^{*2} L$) to a diffusion velocity (D_{O_2} / L) ($\mathrm{Da}_{O_2} = k_1 C_{NO}^{*2} L^2 / D_{O_2}$) is very small. (For $C_{NO}^{*} = 1\mu\mathrm{M}$, $\mathrm{Da}_{O_2} = 3.4 \times 10^{-3}$). This dimensionless number is a measure of the intrinsic rate of reaction relative that of diffusion (Deen, 1998). This tiny Damköhler number for O_2 means that the reaction of O_2 with NO will have a negligible effect on the O_2 concentration. Hence, the reaction term is ignored for O_2. Therefore, the application of the conservation Eq. (3.7) to O_2 is

$$D_{O_2} \frac{d^2 C_{O_2}}{dz^2} = 0 \tag{3.8}$$

$$C_{O_2}(L) = C_{O_2}^{*} \tag{3.9}$$

$$\frac{dC_{O_2}}{dz}(-H) = 0 \tag{3.10}$$

$$-D_{O_2} \left.\frac{dC_{O_2}}{dz}\right|_{z=0^+} + D_{O_2} \left.\frac{dC_{O_2}}{dz}\right|_{z=0^-} = -M \tag{3.11}$$

where D_{O_2} is the aqueous oxygen diffusivity, $C_{O_2}^{*}$ is the aqueous concentration of O_2 in equilibrium with the chamber gas and Eq. (3.10) expresses the assumption that the bottom of the dish is impermeable to O_2. The total cellular O_2 consumption rate by the target cells and

generator cells based on total area of the insert is denoted as M (e.g., mol m^{-2} s^{-1}). As will be described, M depends on both the O_2 and the NO concentrations. The solution for oxygen is

$$C_{O_2}(z) = C^*_{O_2} + \frac{M}{D_{O_2}}(z - L) \quad (0 \le z \le L) \tag{3.12}$$

$$C_{O_2}(z) = C^*_{O_2} - \frac{ML}{D_{O_2}} \quad (-H \le z \le 0) \tag{3.13}$$

As shown, the O_2 concentration in the upper chamber increases with z, whereas that in the lower chamber is constant.

The autoxidation Damköhler number for NO (Da_{NO}, Eq. 3.18) is order one. (For $N = 1$ nmol m^{-2} s^{-1}, Da_{NO}=1.7) This implies that the reaction and diffusion have comparable rates. Hence, the NO conservation equation should keep both terms and

$$D_{NO}\frac{d^2C_{NO}}{dz^2} = 4k_1 {C_{NO}}^2 C_{O_2} \tag{3.14}$$

$$C_{NO}(L) = 0 \tag{3.15}$$

$$\frac{dC_{NO}}{dz}(-H) = 0 \tag{3.16}$$

$$-D_{NO}\left.\frac{dC_{NO}}{dz}\right|_{z=0^+} + D_{NO}\left.\frac{dC_{NO}}{dz}\right|_{z=0^-} = N \tag{3.17}$$

$$\mathrm{Da_{NO}} = \frac{4k_1 C^*_{O_2} N L^3}{D^2_{NO}} \tag{3.18}$$

where k_1 is the rate constant for the reaction of NO with O_2 and N is the net NO production rate by the target cells and generator cells based on the total area of the insert. (e.g., mol m^{-2} s^{-1}) Plugging Eq. (3.12) and (3.13) into the NO governing equation,

$$D_{NO}\frac{d^2C_{NO}}{dz^2} = 4k_1C_{NO}{}^2(C_{O_2}^* + \frac{M}{D_{O_2}}(z-L)) \quad (0 \le z \le L) \tag{3.19}$$

$$D_{NO}\frac{d^2C_{NO}}{dz^2} = 4k_1C_{NO}{}^2(C_{O_2}^* - \frac{ML}{D_{O_2}}) \quad (-H \le z \le 0) \tag{3.20}$$

To minimize the number of parameters and simplify the numerical solution, it is advantageous to employ scaled dimensionless variables. The dimensionless position and NO concentrations are defined as

$$\xi = z/L, \quad \theta = C_{NO}D_{NO}/NL \tag{3.21}$$

Using the dimensionless NO concentration and dimensionless length, the governing equations for NO are

$$\frac{d^2\theta}{d\xi^2} = \mathrm{Da}_{NO}\theta^2(1-A) + \mathrm{Da}_{NO}A\theta^2\xi \quad (0 \le \xi \le 1) \tag{3.22}$$

$$\frac{d^2\theta}{d\xi^2} = \mathrm{Da}_{NO}\theta^2(1-A) \quad (-H/L \le \xi \le 0) \tag{3.23}$$

$$A = \frac{ML}{D_{O_2}C_{O_2}^*} \tag{3.24}$$

where A is the ratio of the total O_2 consumption flux (M) to the maximum O_2 diffusional flux ($D_{O_2}C_{O_2}{}^*/L$). The dimensionless number A is a measure of the total O_2 consumption rate relative to that of diffusion, such that $0 \le A \le 1$. Hence, A=0 and A=1 corresponds to zero and maximum O_2 consumption respectively. There is one additional parameter, H/L, which in the experiments was fixed at 0.5.

Now the dimensionless boundary conditions are as follows.

$$\theta(1) = 0 \tag{3.25}$$

$$\frac{d\theta}{d\xi}(-0.5) = 0 \tag{3.26}$$

$$-\left.\frac{d\theta}{d\xi}\right|_{\xi=0^+} + \left.\frac{d\theta}{d\xi}\right|_{\xi=0^-} = 1 \tag{3.27}$$

What remains to be described are the effects of O_2 and NO on respiration, which influences the evaluation of the O_2 consumption parameter, A.

3.2.5 Oxygen Consumption Parameter

Taking into account the effects of both O_2 limitations and NO inhibition on respiration, the oxygen consumption rate can be expressed as

$$M = \frac{R_{\max} C_{O_2}(0)}{C_{O_2}(0) + K_M(1 + C_{NO}(0)/K_I)} \tag{3.28}$$

where R_{max} is the maximum rate of O_2 consumption per unit area contributed by both generator cells and the target cells and K_M and K_I are constants previously determined (Nalwaya and Deen, 2005). Using "G" and "T" to denote NO generator cells (macrophages) and target cells, respectively,

$$R_{\max} = \frac{m_G R_{\max,G} + m_T R_{\max,T}}{\pi R^2} \tag{3.29}$$

where m_i is the number of viable cells present of type i and $R_{max,i}$ is the maximum rate of O_2 consumption for that cell type. The values of K_M and K_I are expected to be similar for all cells, as they are properties of the respiratory enzymes (Nalwaya and Deen, 2005). Likewise, R_{max} can be estimated reasonably well for combinations of macrophages and various kinds of target cells. Thus, the main reason that M (and thus A) is not known in advance is that it depends on the O_2 and NO concentrations at $z = 0$, which depend on the experimental conditions.

Using Eq. (3.13) to eliminate $C_{O_2}(0)$ from Eq. (3.29) leads to a quadratic equation for M. Keeping only the root that yields positive values of $C_{O_2}(0)$, the O_2 consumption parameter is

$$A = \frac{M}{D_{O_2} C_{O_2}^{*} / L} = \frac{1+\alpha+\beta+\gamma}{2}\left[1-\sqrt{1-\frac{4\alpha}{(1+\alpha+\beta+\gamma)^2}}\right] \tag{3.30}$$

$$\alpha = \frac{R_{\max} L}{D_{O_2} C_{O_2}^{*}}, \beta = \frac{K_M}{C_{O_2}^{*}}, \quad \gamma = \frac{K_M C_{NO}(0)}{K_I C_{O_2}^{*}} = \frac{Da_{NO} K_M D_{NO}}{4k_1 C_{O_2}^{*} K_I L^2}\theta(0) \tag{3.31}$$

Whereas α and β are constants, γ makes A dependent on the calculated NO concentration at $z = 0$. This implies that A cannot be determined beforehand and is one of the final results. In the absence of NO ($\gamma = 0$), A has its maximum value denoted as A_0.

$$A_0 = \frac{1+\alpha+\beta}{2}\left[1-\sqrt{1-\frac{4\alpha}{(1+\alpha+\beta)^2}}\right] \tag{3.32}$$

As shown in Eq. (3.32), A_0 is zero when α is zero and approaches 1 as α approaches infinity. The ratio of A to A_0 is a function of $C_{NO}(0)$, provided that α is fixed at specific experimental conditions. The ratio is,

$$\frac{A}{A_0} = \frac{1+\alpha+\beta+\gamma}{1+\alpha+\beta}\left[\frac{1-\sqrt{1-4\alpha/(1+\alpha+\beta+\gamma)^2}}{1-\sqrt{1-4\alpha/(1+\alpha+\beta)^2}}\right] \tag{3.33}$$

As α approaches to zero, A_0 and A has the following asymptote.

$$A(\alpha \to 0) = \frac{\alpha}{1+\alpha+\beta+\gamma} \tag{3.34}$$

$$A_0(\alpha \to 0) = \frac{\alpha}{1+\alpha+\beta} \tag{3.35}$$

Hence, as α approaches to zero, the ratio of A to A_0 is

$$\frac{A}{A_0} = \frac{1+\beta}{1+\beta+\gamma} \tag{3.36}$$

As obvious in Eqs. (3.34) and (3.35), A and A_0 eventually approaches 1 as α approaches infinity. Hence, the ratio of A to A_0 is 1 as α approaches infinity.

3.2.6 Solution Procedure

Equations (3.22) and (3.23) were solved numerically for both regions using Maple 12 (Maplesoft, Waterloo, Ontario, Canada). All calculations assumed initially that $A = A_0$, and the value of A was then refined using an iterative procedure. The algorithm used depended on whether or not the rate of NO production, and therefore the value of Da_{NO}, was assumed to be known. If Da_{NO} was given, Eqs. (3.22) and (3.23) were solved repeatedly, adjusting the value of $\theta(0)$ until Eq. (3.27) was satisfied to within 0.01 %. If the left-hand side of Eq. (3.27) was larger than 1, it was necessary to decrease $\theta(0)$, and vice versa. Equation (3.30) was then used to find a new value of A. Usually, only 1-3 adjustments of A were needed for its value to converge to within 1%.

When inferring the cellular NO concentration from the measured rate of NO_2^- formation, a value of R was given but Da_{NO} was unknown. For these cases an initial guess for Da_{NO} was made and then the above procedure was followed until the convergence of A was satisfactory. A new value of Da_{NO} was calculated from the solution using

$$\mathrm{Da_{NO}} = \frac{L^2}{D_{NO}}\sqrt{\frac{4k_1 C_{O_2}^* R}{J}} \tag{3.37}$$

$$J = \left(\frac{L}{H+L}\right)(1-A)\int_{-H/L}^{0}\theta^2\,d\zeta + \left(\frac{L}{H+L}\right)\left[(1-A)\int_{0}^{1}\theta^2\,d\zeta + A\int_{0}^{1}\theta^2\zeta\,d\zeta\right] \tag{3.38}$$

where J is the dimensionless rate of autoxidation obtained from the NO and O_2 concentration profiles in the two chambers. If the value of Da_{NO} from Eq. (3.37) differed from the trial value by more than 1%, it was used as the new trial value and the procedure was repeated. Typically, the convergence was satisfactory after 2-3 iterations. An adequate initial guess for Da_{NO} can be obtained from Eqs. (3.37) and (3.38) by assuming that $\theta(\zeta) = 1$ in the lower chamber and $\theta(\zeta) = 1 - \zeta$ in the upper chamber. This algorithm is summarized in Figure 3.2.

The values of the physicochemical parameter used in all the calculations, and their sources, are given in Table 3.1.

Table 3.1. Physicochemical parameters

Quantity	Value	References
k_1	$2.4\times10^{6}\ M^{-2}s^{-1}$	Lewis and Deen, 1994
$C_{O_2}^{*}$	$200\ \mu M$	Chen and Deen, 2003
D_{NO}	$3.0\times10^{-9}\ m^2s^{-1}$	Zacharia and Deen, 2005
D_{O_2}	$2.8\times10^{-9}\ m^2s^{-1}$	Goldstick and Fatt, 1970
K_M	$7\ \mu M$	Nalwaya and Deen, 2005
K_I	$18\ nM$	Nalwaya and Deen, 2005

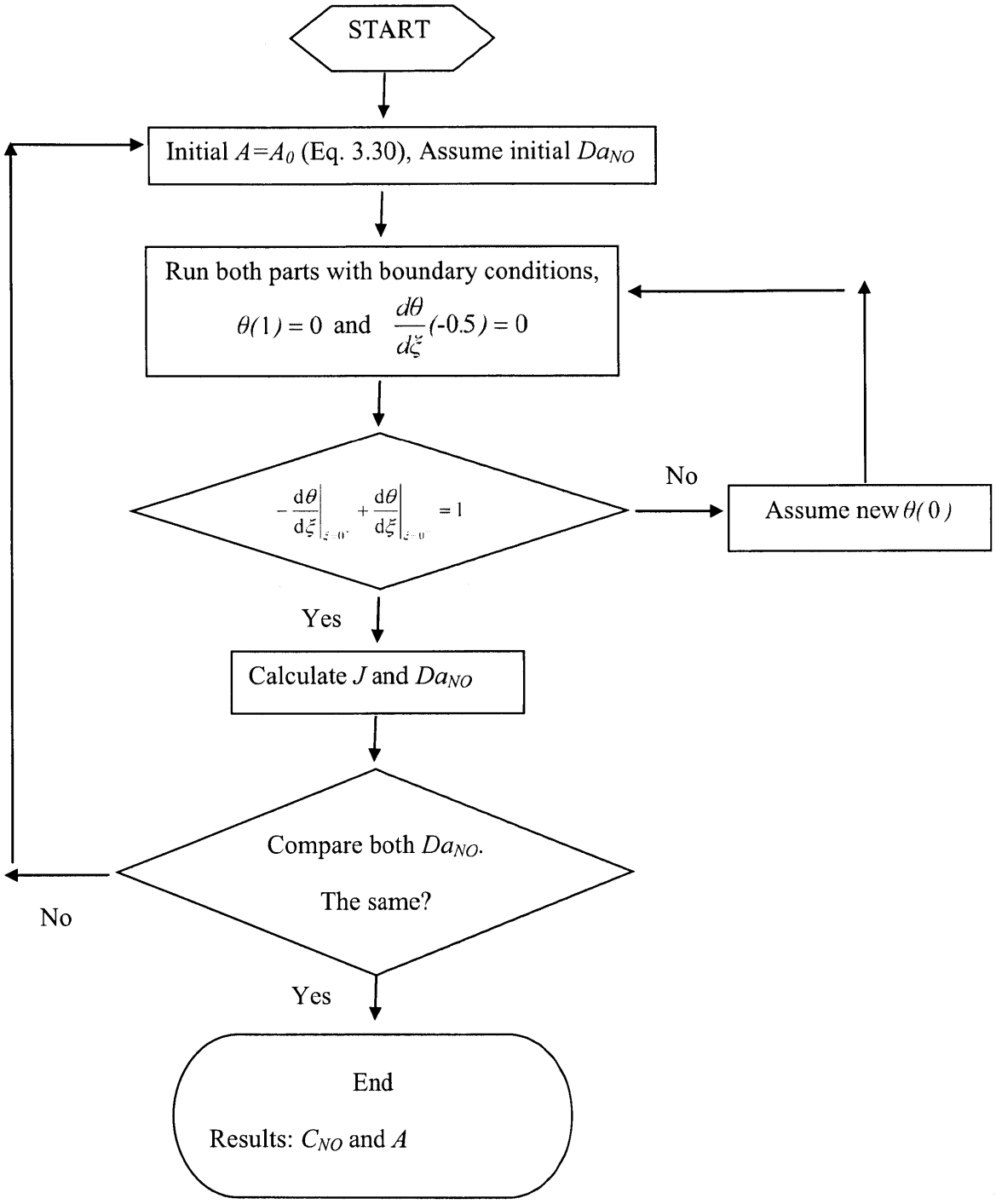

Figure 3.2. Algorithm Flow Chart

3.3 Results

3.3.1 Concentration Profiles of O_2 and NO

According to equations (3.12), (3.13), and (3.24), the dimensionless O_2 concentration can be expressed in terms of A as follows.

$$C_{O_2}(z)/C^*_{O_2} = 1 + A(z/L - 1) \quad (0 \le z \le L) \tag{3.39}$$

$$C_{O_2}(z)/C^*_{O_2} = 1 - A \quad (-H \le z \le 0) \tag{3.40}$$

All the following results are based on L = 2mm. As previously mentioned, H is fixed as 1 mm. Figure 3.3 shows three different dimensionless O_2 concentration profiles, corresponding to A = 0, 0.5 and 1. As mentioned above, A = 0 means zero O_2 consumption and this results in the same O_2 concentration everywhere, which is $C^*_{O_2}$. The other extreme case is A = 1, which corresponds to the maximum O_2 diffusional flux. This results in zero O_2 concentration throughout the lower chamber. Finally, A = 0.5 gives an intermediate O_2 concentration profile between above two extreme cases. These O_2 concentration profiles are linear because the reaction of O_2 with NO has a negligible effect on the O_2 concentration, as previously explained. The effect of Da_{NO} on A is described by Eqs. (3.30) and (3.31).

For NO, the concentration profile is not linear because the autoxidation reaction with O_2 is not negligible compared with the diffusion. For this reason, both Da_{NO} and A explicitly affect the concentration profile. Figure 3.4 shows NO concentration profiles for three different N values at constant A. C_{NO} has a maximum value at z = 0 because the NO generating cells are located at the membranes (z = 0). As N increases, the NO concentration profile goes upward as a result of more generation. Also, the NO concentration profile is more sharply peaked at higher N because high N means high Da_{NO}.

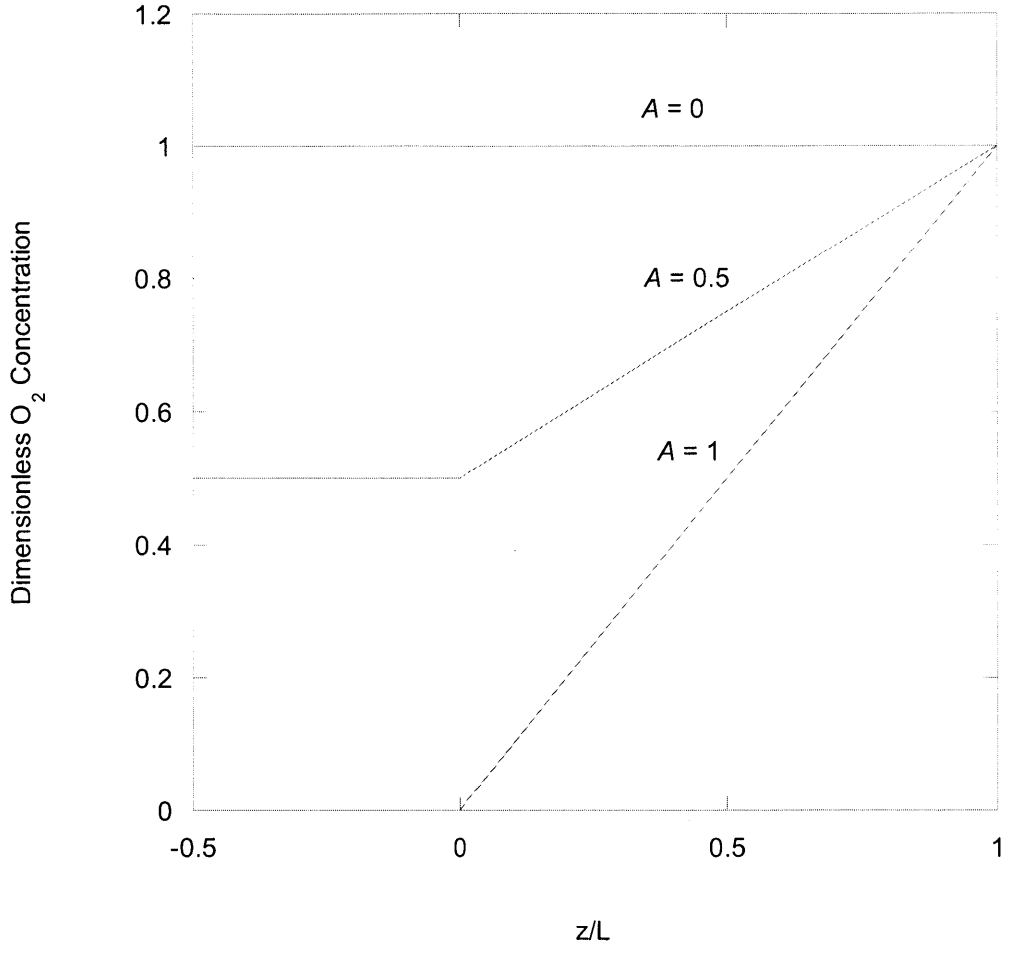

Figure 3.3. O_2 Concentration Profile for $A = 0$, 0.5 and 1

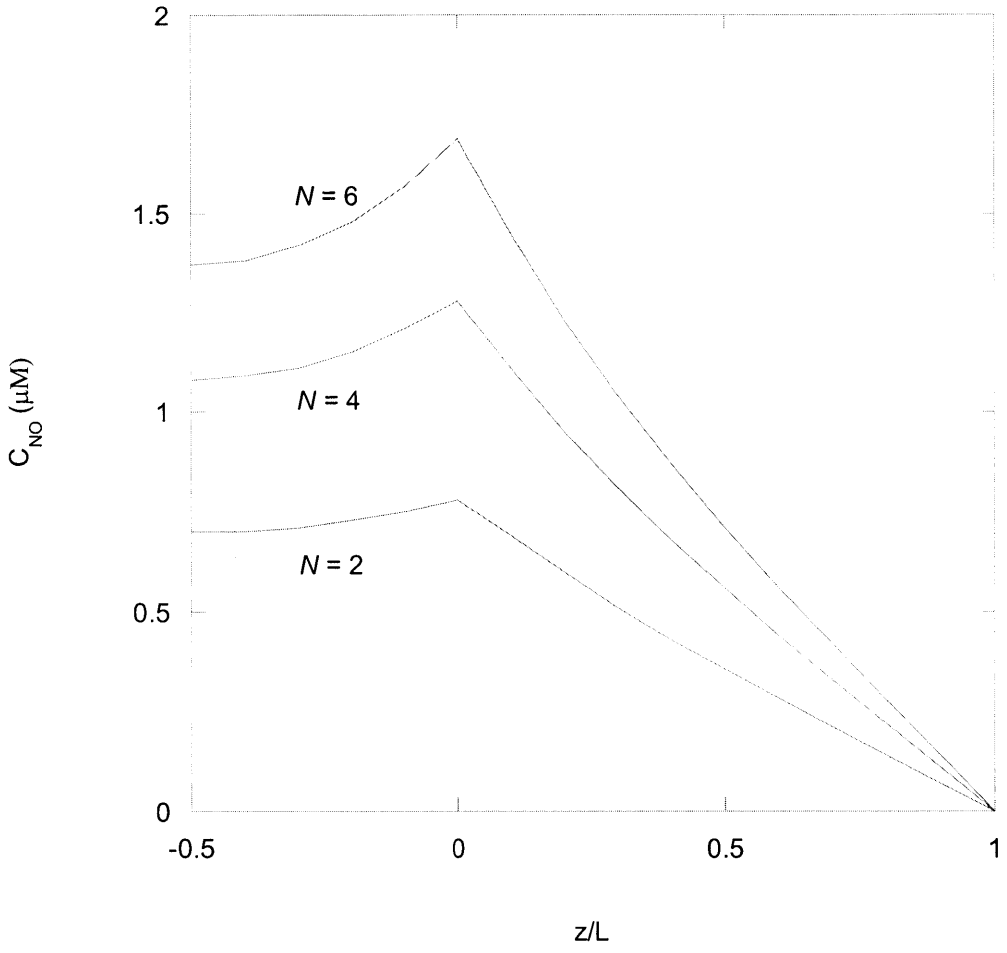

Figure 3.4. NO Concentration Profile for $N = 2$, 4 and 6 nmol m^{-2} s^{-1} ($A = 0.5$)

Figure 3.5 shows NO concentration profiles for three different A values at constant N. Again, C_{NO} has its maximum value at $z = 0$. As A increases, the NO concentration profile goes upward because the loss of NO through autoxidation reaction is reduced with the reduced O_2 concentration at higher A. When $A = 1$, the NO concentration in the lower chamber is constant because the zero O_2 concentration in the lower chamber (Figure 3.3, A=1) means no reaction loss of NO in this special case.

3.3.2 Total NO flux and Diffusion Loss

After NO is produced at $z = 0$, it can diffuse upward or downward. As proven in the Appendix, the diffusion pathway via the lower chamber is negligible. In addition, the bottom is an impenetrable surface. Hence, the only possible way for NO to escape is by diffusion through the gas-liquid interface. Figure 3.6 shows the correlation between nitrite formation rate R and the total NO generation rate. The total rate of NO generated per unit volume is the product of N with the insert area, divided by total volume. Overall, R increases as N increases because more NO produces more nitrite. However, the entire NO is not consumed to make the stable end product, nitrite. The gap between the identity line (zero diffusion loss) and the specific A value line reflects the loss of NO by diffusion. As A increases, the percentage of NO lost increases because less O_2 is available for the autoxidation reaction.

Figure 3.7 shows the predicted loss of NO as a function of the net rate of NO synthesis (N), for three values of the O_2 consumption parameter (A). For the range of conditions shown, 30-100% of the NO is lost. The reason that the loss becomes complete as $N \rightarrow 0$ is that the rate of autoxidation varies as C_{NO}^2, whereas diffusion varies as C_{NO}. Consequently, the lower the NO concentration, the less effective autoxidation is at trapping NO as NO_2^-. Also, for this reason,

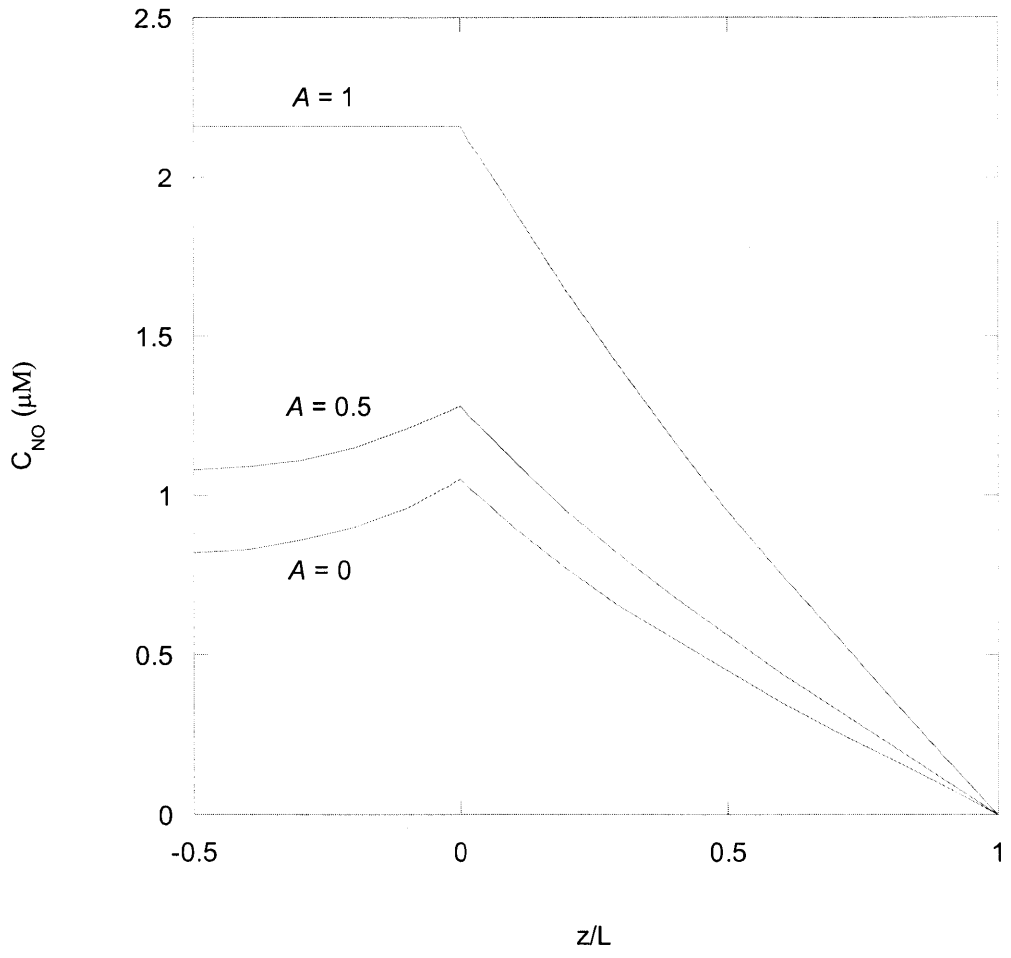

Figure 3.5. NO Concentration Profile for $A = 0$, 0.5 and 1 ($N = 4$ nmol m^{-2} s^{-1})

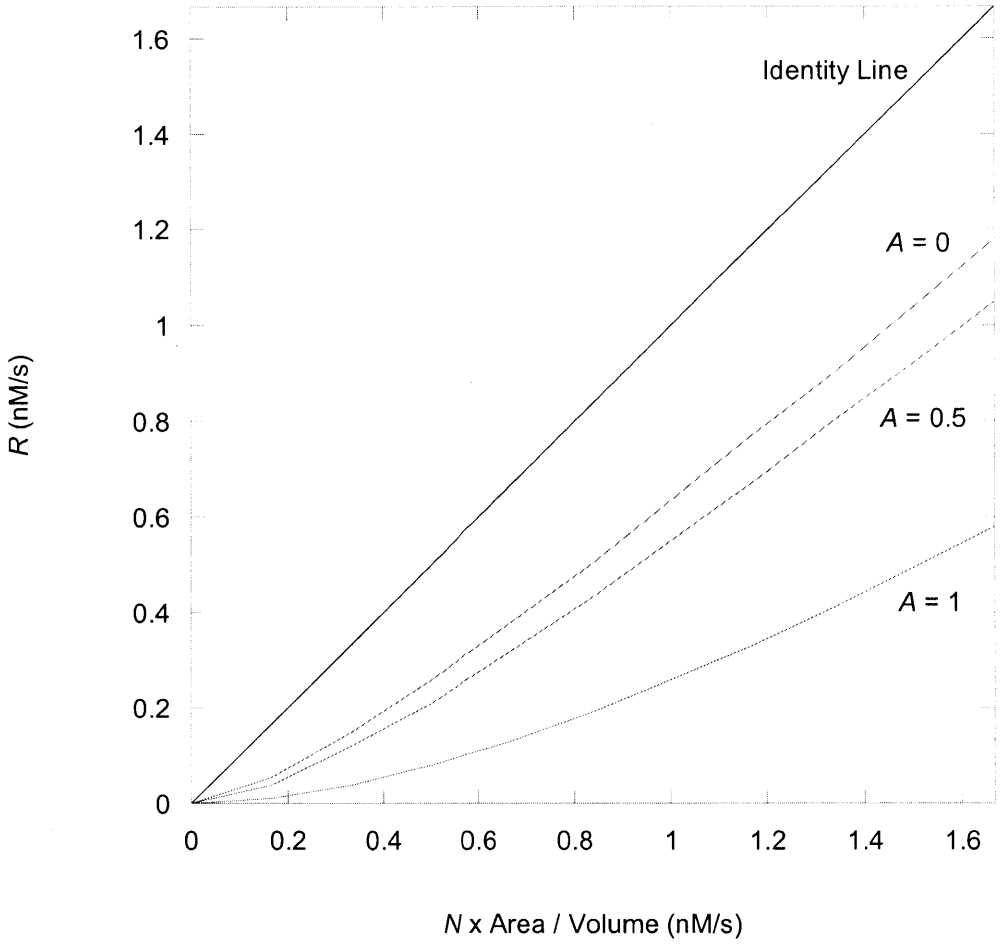

Figure 3.6. Nitrite Formation Rate (R) .vs. Total NO Flux

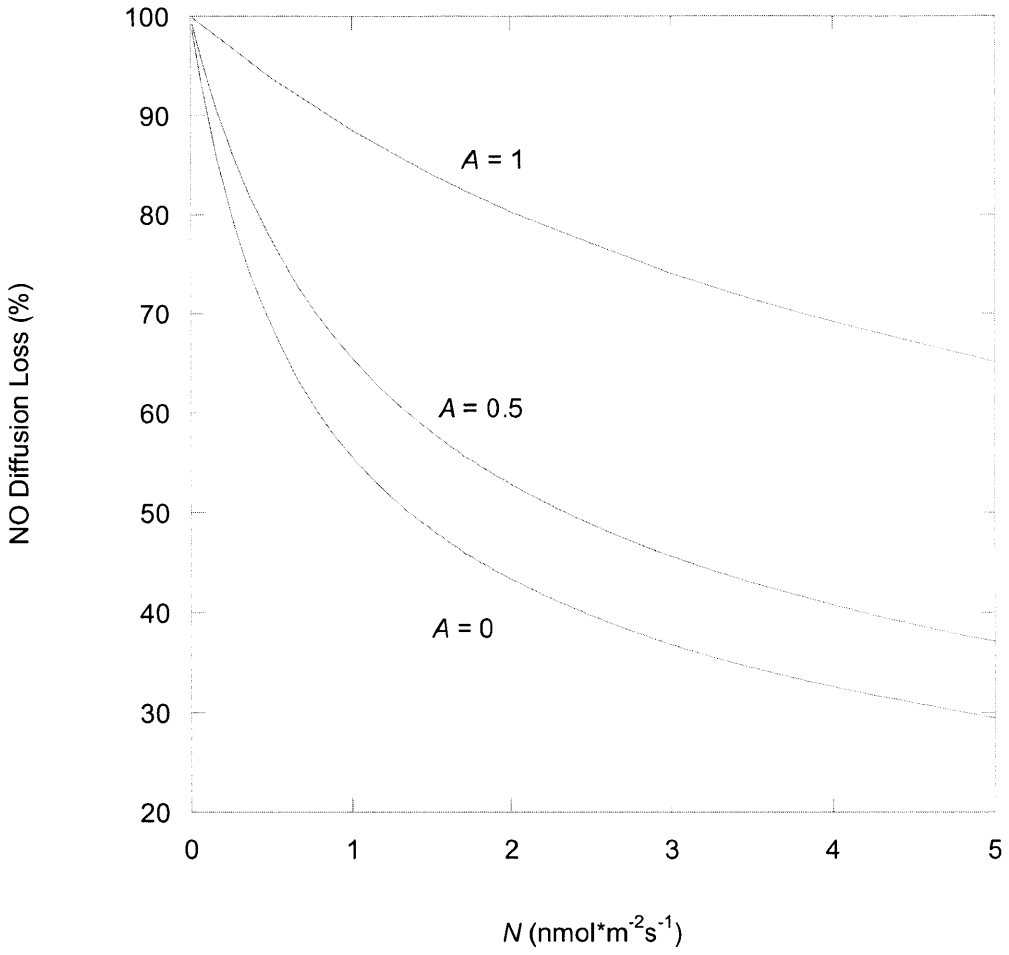

Figure 3.7. Percentage loss of NO to the incubator gas as a function of the net rate of NO synthesis. Results are shown for three values of the O_2 consumption parameter, A. It was assumed in each case that $H = 1$ mm and $L = 2$ mm.

more diffusion loss occurs at higher values of A. An important feature of the mathematical model is that it accounts for these losses in calculating cellular NO concentrations from observed rates of NO_2^- accumulation.

3.4 Discussion

As stated, the purpose of this work was to develop a model for predicting the NO concentration as a function of height (z) by using measured nitrite data. Specially, it is important to know the NO concentration at the target cells, $C_{NO}(0)$. However, the main problem is that the dimensionless O_2 consumption parameter A is a variable rather than a pre-determined constant, as already indicated in model development. This required development of an iterative numerical algorithm, as explained in the model development. However, to make the results more broadly accessible, a graphical method to calculate the cellular NO concentration was also developed. That method is described now and is illustrated using experimental results from the Wogan laboratory.

Before digging into the specific examples, how the ratio of A to A_0 (Eq. 3.33) changes as a function of $C_{NO}(0)$ is shown in Figure 3.8 for 2 cases of α. This ratio equals 1 at zero NO concentration and decreases with increasing $C_{NO}(0)$. Figure 3.8 shows that the difference between the small α asymptote (Eq. 3.34) and the result for $\alpha = 1$ is very small. This means that it is possible to use Eq. (3.34) to correct A for a wide range of α.

Co-culture of AS52 cells with macrophages (RAW264.7) was performed using Transwell^{TM} permeable supports (Corning, NY) by our collaborators. (Minyoung Kim, Laura J. Trudel, and Gerald N. Wogan at MIT) AS 52 cells were co-cultured with macrophages at a ratio of 1:10 ($1x10^6$: $1x10^7$, respectively) for 48 hr before the main experiment. IFN-γ and LPS were

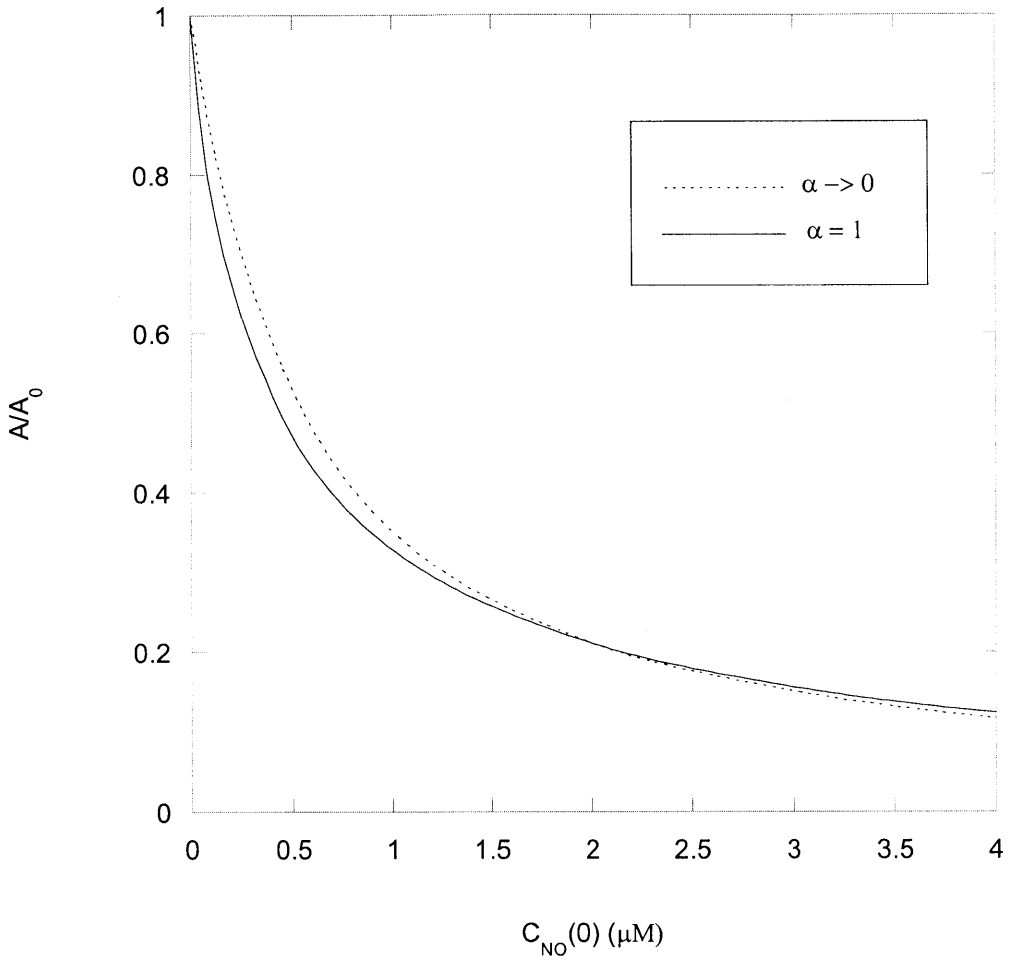

Figure 3.8. *A* correction (the ratio of *A* to A_0) as a function of $C_{NO}(0)$

placed into the lower chamber and suspended AS 52 cells was placed into the upper compartment. After 48 hr, total NO_2^- was measured. It was found that 26% of the AS52 cells were viable in the absence of NOS inhibitors and 83% were viable with NMA present. Based on previous results for RAW264.7 cells at similarly high coverages (Zhuang and Wogan, 1997), the corresponding values are 12% without NMA and 24% with NMA. Using the respective doubling times of 19 h (Hollenbach et al., 1999) and 22 h (Zhuang and Wogan, 1997), we estimate the numbers of viable cells at the start of the experimental period as $m_T = 1.5 \times 10^6$ and $m_G = 5.4 \times 10^6$. Combining these cell numbers with maximum respiration rates of 60 pmol s^{-1} $(10^6 \text{ cells})^{-1}$ for AS52 (Lai et al., 1982) and 100 pmol s^{-1} $(10^6 \text{ cells})^{-1}$ for RAW264.7 (Nalwaya and Deen, 2005), $R_{max} = 1.4 \times 10^{-7}$ mol m^{-2} s^{-1} from Eq. (3.28). The important parameters are summarized in Table 3.2. From Eqs. (3.30) and (3.31), the initial guess for A was then $A_0 = 0.48$. For the experiments without inhibition of NOS, the increase in NO_2^- concentration of 123 μM over the 42 h experimental period corresponds to $R = 0.81$ nM/s. The final value of the O_2 consumption parameter obtained via the iterative procedure was $A = 0.15$, and the cellular NO concentration was 1.1 μM . The net rate of NO synthesis was calculated as $N = 3.7 \times 10^{-9}$ mol m^{-2} s^{-1}, corresponding to $Da_{NO} = 4.3$. For the experiments with NMA, $R = 0.076$ nM/s, $A = 0.47$, $C_{NO}(0) = 0.36$ μM , $N = 0.74 \times 10^{-9}$ mol m^{-2} s^{-1}, and $Da_{NO} = 0.85$. Thus, although the rate of NO_2^- accumulation with NMA was only 9% of that without NOS inhibition, the NO concentration was 33% of that without inhibition. This disproportionality is a consequence of the nonlinear rate law for autoxidation. For each of the other experiments with NOS inhibitors, the estimated NO concentration again was about 0.3-0.5 μM , as shown in Table 3.3.

Table 3.2. Cell parameters

Quantity	Value	References
RAW 264.7 doubling time	22hr	Zhuang and Wogan, 1997
RAW 264.7 R_{max}	100 pmol s^{-1} $(10^6$ cells$)^{-1}$	Nalwaya and Deen, 2005
AS52 doubling time	19hr	Hollenbach et al., 1999
AS52 R_{max}	60 pmol s^{-1} $(10^6$ cells$)^{-1}$	Lai et al., 1982

3.4.1 Simplified Estimation of NO Concentrations

The NO concentrations experienced by cells in experiments such as those reported here can be estimated graphically from measured rates of NO_2^- accumulation, using Fig. 3.9. The NO concentration at the cells is plotted here as a function of the NO_2^- formation rate (R) for several values of the O_2 consumption parameter and a liquid depth of 2 mm in the upper chamber. Overall, C_{NO} (0) varies nearly as $R^{1/2}$. To find C_{NO} (0) from a measured value of R, the first step is to obtain an initial value for A. This requires knowledge of the numbers of viable cells and measured or estimated values of their maximum rates of O_2 consumption. By choosing the curve in Fig. 3.9 that corresponds to this initial value of A, a first estimate of $C_{NO}(0)$ is found from R. To refine the estimated concentration, the parameters β and γ are calculated from Eq. (3.31). Whereas β is the same for all such experiments, γ depends on $C_{NO}(0)$. The value of A is refined then using Eq. (3.36)

$$\frac{A}{A_0} = \frac{1+\beta}{1+\beta+\gamma} \tag{3.36}$$

As shown in Fig. 3.8, this relationship remains quite accurate even for α as large as unity. Using the improved value of A, $C_{NO}(0)$ is updated by returning to Fig. 3.9. This procedure converges rapidly enough that only 1-2 updates of $C_{NO}(0)$ are likely to be needed. When the graphical method was applied to the present data without NOS inhibition, two-digit accuracy [$C_{NO}(0)$ = 1.1 μM] was obtained with just one update.

Table 3.3. NO concentration for various treatments

Treatment	NO_2^- concentration (μM)	R (nM/s)	NO concentration (μM)
IFN-γ + LPS	122.6	0.81	1.1
IFN-γ + LPS+ NMA	11.3	0.076	0.36
IFN-γ + LPS+ Tiron	25.7	0.17	0.51
IFN-γ + LPS+ Uric acid	22.8	0.15	0.47
IFN-γ + LPS+ NMA+ Tiron	8.6	0.057	0.31
IFN-γ + LPS+ NMA+ Tiron+ Uric acid	9.0	0.060	0.32

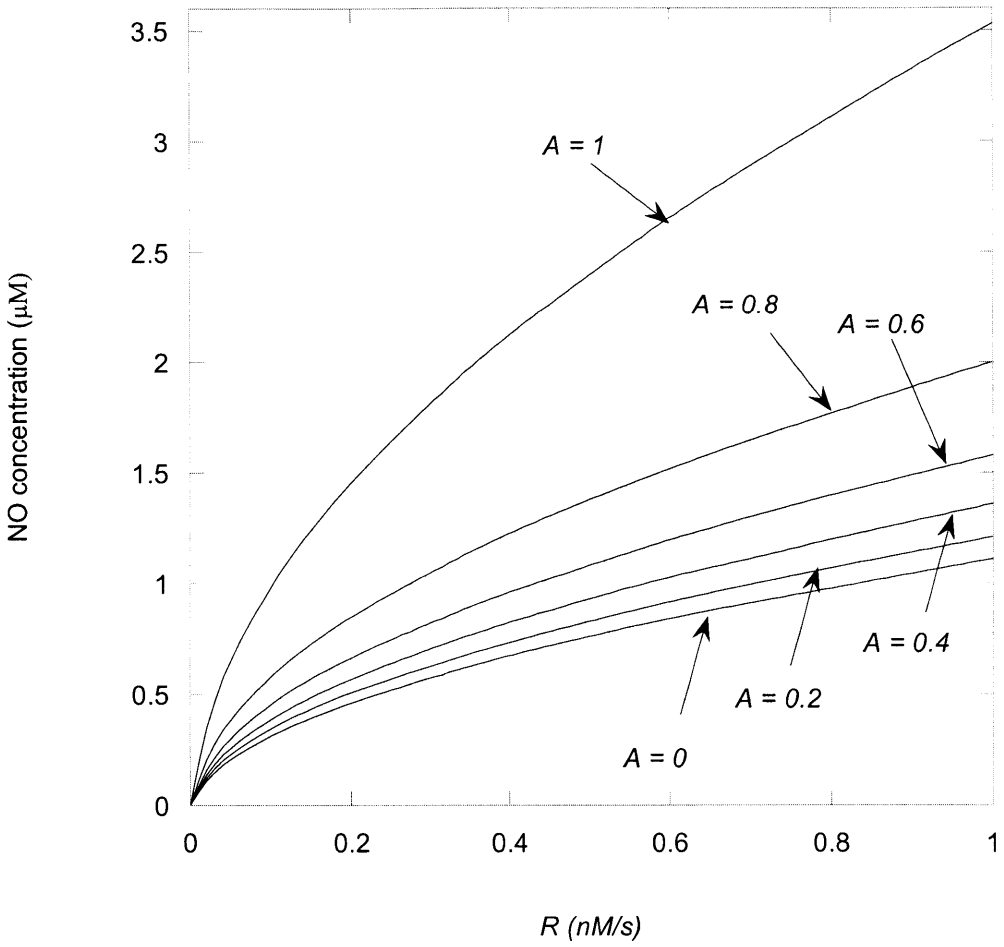

Figure 3.9. Relationship between cellular NO concentration and rate of NO_2^- formation (R) calculated assuming an upper-chamber depth of $L = 2$ mm. How to estimate the O_2 consumption parameter (A) is described in the text in connection with Eq. (25).

3.4.2 Effect of the Liquid Depth of Upper Chamber on NO Concentrations

Although Fig. 3.9 assumes an upper chamber depth of L = 2 mm, satisfactory estimates can be obtained also for other depths. Figure 3.10 shows the ratio of $C_{NO}(0)$ for L = 1mm and L = 3mm to $C_{NO}(0)$ for L = 2mm under R= 1nM/s. The important fact is that these NO concentration corrections are nearly independent of A up to 0.6. For practical purpose, this fact is very important because A is usually less than 0.5 for most cases. If $A \leq 0.6$, as is likely, it is recommended that the value of $C_{NO}(0)$ found from Fig. 3.9 be increased by 15% if L = 3 mm and decreased by 24% if L = 1 mm. (The precise correction factors range from a 14-18% increase for L = 3 mm to a 21-27% decrease for L = 1 mm, depending on the value of R.) Although it is recommended to set the upper chamber liquid depth as L = 2mm for convenience, it is possible to obtain $C_{NO}(0)$ for different liquid depths using Fig.3.9.

Once the NO concentration at the target cells is determined in this way, it is possible to predict concentrations of other reactive nitrogen species such as NO_2, N_2O_3, and peroxynitrite plus all relevant reactive radicals such as tyrosyl and glutationyl radicals in this cell coculture system (Chapter 2 and Lim et al., 2008). In addition, concentrations of all stable end products such as 3-nitrotyrosine and S-nitrosoglutathione (GSNO) can be predicted in this system.

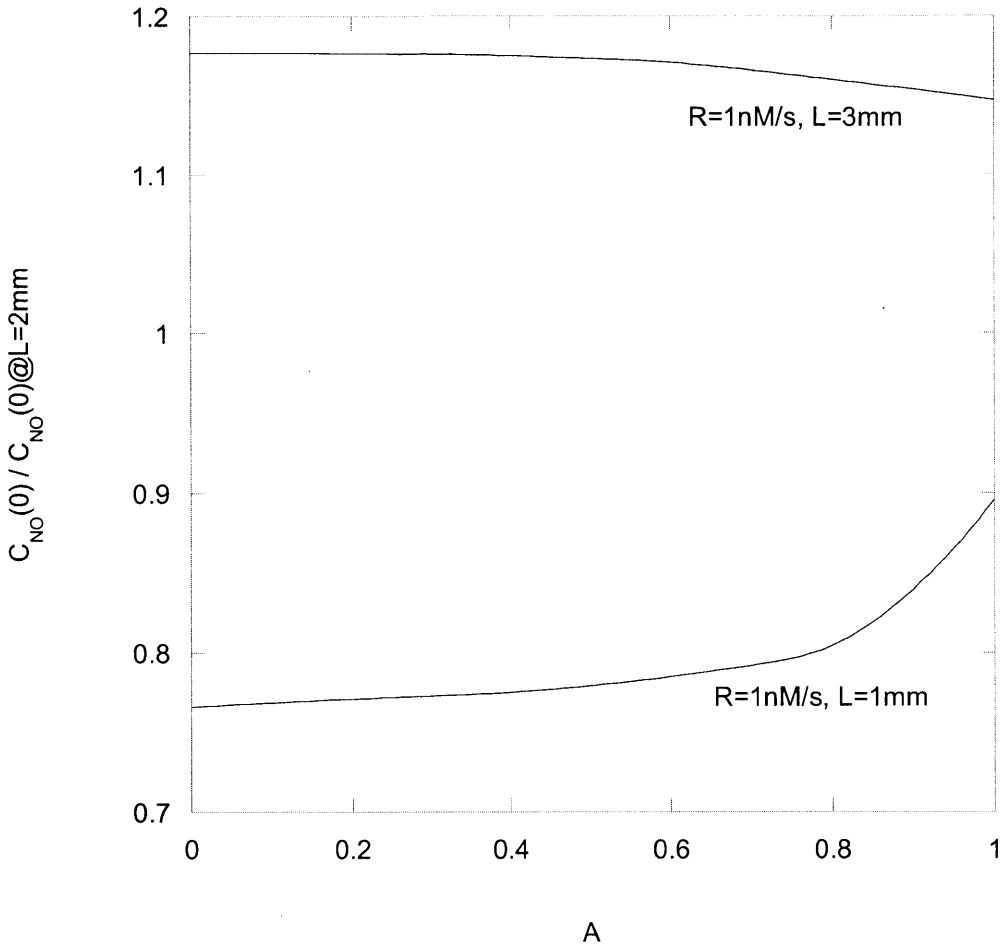

Figure 3.10. Effect of liquid depth on the NO concentration at the target cells

3.5 Appendix

Comparative Resistance Calculations. The diffusional resistance of each is defined as the ratio of concentration difference to flux based on the total area of the insert. As shown in Figure 3.1, there are two pathways for NO diffusion from the generator cells (macrophages) to the gas-liquid interface. The first is made up of the lower chamber and outer annulus, and the second consists of the membrane and upper chamber. The resistances of the lower chamber, outer annulus, membrane, and upper chamber are denoted as R_L, R_A, R_M, and R_U respectively. It will be shown that $(R_L+R_A)/(R_M+R_U)$ is large, making the first pathway negligible.

The upward flux throug the membrane is

$$N\big|_{z>0} = \frac{D_{NO}\Delta C_M}{h}\varepsilon \tag{A1}$$

where D_{NO} is the diffusivity of NO in the solution, ΔC_M is the concentration difference across the membrane, h is the membrane thickness ($10\,\mu m$), and ε is the porosity of the membrane. Hence, the resistance inside the membrane is

$$R_M = \frac{\Delta C_M}{N\big|_{z)0}} = \frac{h}{\varepsilon D_{NO}} \tag{A2}$$

Likewise, the flux through the upper chamber is

$$N\big|_U = \frac{D_{NO}\Delta C_U}{L\text{-}h} \tag{A3}$$

where ΔC_U is the concentration difference in the upper chamber, and L is the liquid depth in the upper chamber. Hence, the resistance of the upper chamber is

$$R_U = \frac{L-h}{D_{NO}} \cong \frac{L}{D_{NO}} \tag{A4}$$

Unlike the upper chamber, the lower chamber is open in the radial direction. Its large ratio of radius to height, this suggests that $C_{NO} = C_{NO}(r)$ only, as a good approximation. Given that $C_{NO} = C_{NO}(r)$, the local value can be replaced by the cross-sectional average (at constant r). This average is

$$\bar{C}_{NO}(r) \equiv \frac{1}{H}\int_{-H}^{0} C_{NO}(r,z)dz \tag{A5}$$

The boundary conditions are

$$\frac{\partial C_{NO}}{\partial z}(r,0) = -\frac{N|_{z<0}}{D_{NO}} \tag{A6}$$

$$\frac{\partial C_{NO}}{\partial z}(r,-H) = 0 \tag{A7}$$

where $N|_{z<0}$ is the downward NO flux based on the total area of the insert. The diffusion equation for the lower chamber is

$$\frac{1}{r}\frac{\partial}{\partial r}(r\frac{\partial C_{NO}}{\partial r}) + \frac{\partial^2 C_{NO}}{\partial z^2} = 0 \tag{A8}$$

Averaging each term over height gives

$$\frac{1}{H}\int_{-H}^{0}\frac{1}{r}\frac{\partial}{\partial r}(r\frac{\partial C_{NO}}{\partial r})\,dz = \frac{1}{r}\frac{d}{dr}(r\frac{d}{dr}(\frac{1}{H}\int_{-H}^{0} C_{NO}dz)) = \frac{1}{r}\frac{d}{dr}(r\frac{d\bar{C}_{NO}}{dr})$$

$$\frac{1}{H}\int_{-H}^{o}\frac{\partial^2 C_{NO}}{\partial z^2}dz = \frac{1}{H}\frac{\partial C_{NO}}{\partial z}\Big|_{z=-H}^{z=0} = -\frac{1}{H}\frac{N|_{z<0}}{D_{NO}}$$

The diffusion equation is now

$$\frac{1}{r}\frac{d}{dr}(r\frac{d\overline{C}_{NO}}{dr})-\frac{1}{H}\frac{N|_{z<0}}{D_{NO}}=0 \tag{A9}$$

Integrating equation (9) once and using the symmetry condition $d\overline{C}_{NO}(0)/dr=0$,

$$\frac{d\overline{C}_{NO}}{dr}=\frac{r}{2H}\frac{N|_{z<0}}{D_{NO}} \tag{A10}$$

For calculating the resistance, only the concentration difference is important. Hence, it is justified to set $\overline{C}_{NO}(a)=0$. Integrating equation (10),

$$\overline{C}_{NO}(r)=\frac{N|_{z<0}}{4HD_{NO}}a^2\left[(\frac{r}{a})^2-1\right] \tag{A11}$$

The concentration difference in the lower chamber is

$$\Delta C_L=\overline{C}_{NO}(a)-\overline{C}_{NO}(0)=\frac{N|_{z<0}a^2}{4HD_{NO}} \tag{A12}$$

Hence, the resistance in lower chamber is

$$R_L=\frac{a^2}{4HD_{NO}}. \tag{A13}$$

R_A is the same as R_U, except for the different flux area because all resistances are defined based on total area of the insert (πa^2). The area of the outer annulus is $\pi(b^2-a^2)$ where b is the outer radius. Hence, the resistance of annulus is,

$$R_A=\frac{L}{D_{NO}}\frac{1}{\left(\frac{b}{a}\right)^2-1} \tag{A14}$$

Accordingly, the ratio of the first pathway resistance to the second pathway resistance is

$$\frac{R_L + R_A}{R_M + R_U} = \frac{\varepsilon a^2(b^2 - a^2 + 4HL)}{4H(h + \varepsilon L)(b^2 - a^2)} \cong \frac{a^2}{4HL}. \tag{A15}$$

For L = 2 mm, H = 1 mm, and a = 37.5 mm, this ratio is 703. This means that the first pathway, which involves radial diffusion in the lower chamber and vertical diffusion in the annulus, is negligible. This justifies the one-dimensional model formulation that was used.

Chapter 4

Theoretical Analysis of Controlled NO_2 Delivery to Biological Solutions

4.1 Introduction

As mentioned in Chapter 1, methods for the controlled delivery of NO_2 over relatively long periods of time (i.e., from several hours to days) are needed to better characterize its biological effects and isolate them from the effects of other RNS. Two possible NO_2 delivery methods were investigated theoretically. One was the direct contact of NO_2 gas mixtures with stirred aqueous solutions, and the other was diffusion of NO_2 through gas-permeable tubing such as polydimethylsiloxane (PDMS) into such solutions. Schematics for both methods are shown in Fig 4-1.

The objective of this work was to analyze the two controlled NO_2 delivery methods mentioned above and compare their performance. This was done by developing both macroscopic and microscopic models. The macroscopic model consists of a set of time-dependent differential equations which show the balance of species based on the aqueous volume-averaged (bulk) concentrations. Although the macroscopic model is complete in that it represents the measurable data such as the NO_2^- formation rate, its ability is reduced by the fact that the liquid-phase mass transfer coefficients depend on composition. Furthermore, there is no direct measuring tool for the aqueous volume-averaged bulk NO_2 concentration ($\overline{C}_{NO_2}$).To investigate the factors that determine the composition dependence of the parameters and to predict the aqueous NO_2 concentration, various microscopic diffusion-reaction models were developed. The microscopic models describe spatial variations in concentrations near the gas-liquid interface, or within the tubing wall and immediately adjacent liquid. Coordinates for the

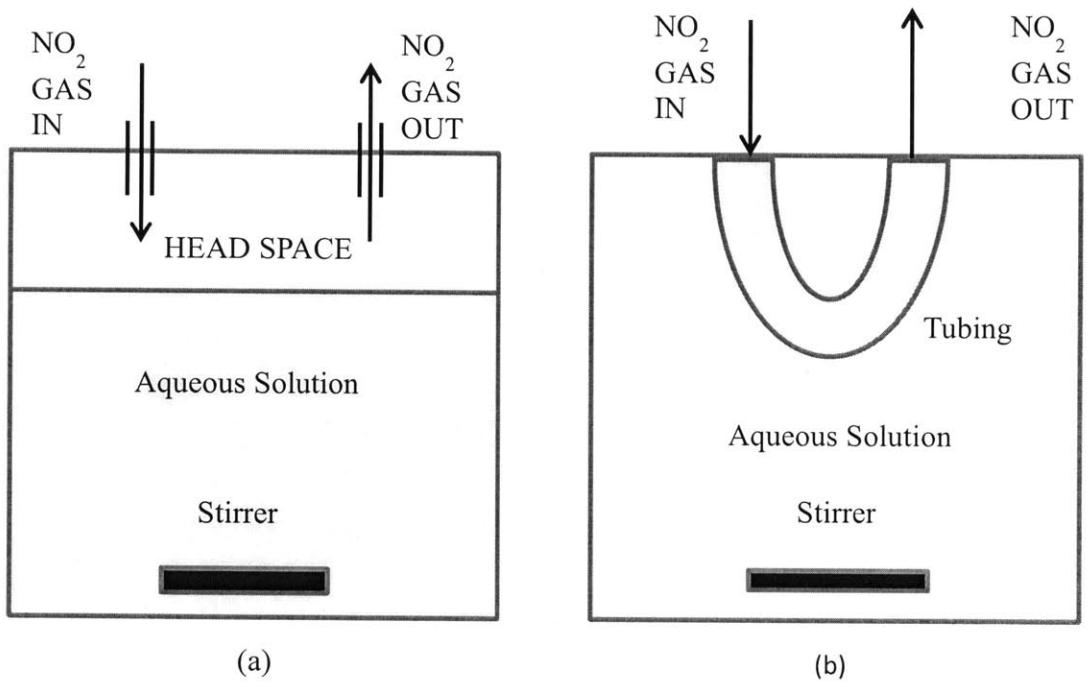

Figure 4.1. Two possible approaches for controlled delivery of NO_2 into aqueous solutions: (a) direct gas-liquid contacting; and (b) diffusion through gas-permeable tubing (e.g., PDMS)

microscopic models are shown in Fig. 4-2. Each used a stagnant film approximation for the liquid. The aqueous model (Section 4.5), PDMS membrane model (Section 4.7), and combined model (Section 4.8) are presented successively. For both delivery methods, the bulk NO_2 and N_2O_4 levels were predicted. A few comparisons were made with quantities such as NO_2^- formation rates.

After this introduction, the basic NO_2 reactions are presented (Section 4.2). Following that are the equilibrium relationships between NO_2 and N_2O_4 (Section 4.3). Then, diffusivities and length scales for the microscopic models are given (Section 4.4). With this background, the aqueous microscopic model is analyzed (Section 4.5) and followed by the macroscopic model (Section 4.6). Afterwards, the microscopic model for PDMS membrane (Section 4.7) and combined membrane-aqueous model (Section 4.8) are investigated. After these all models, experimental methods (Section 4.9) are shown. Finally, results (Section 4.10) and discussion (Section 4.11) are shown.

4.2 Basic NO_2 Reactions

In aqueous solutions, nitrogen dioxide (NO_2) coexists with its dimer, dinitrogen tetroxide (N_2O_4). Once formed, N_2O_4 reacts rapidly with water to produce nitrite and nitrate. The reactions and rate expressions are as follows:

$$2NO_2 \underset{k_{-1}}{\overset{k_1}{\rightleftharpoons}} N_2O_4 \tag{4.1}$$

$$N_2O_4 + H_2O \xrightarrow{k_2} NO_2^- + NO_3^- + 2H^+ \tag{4.2}$$

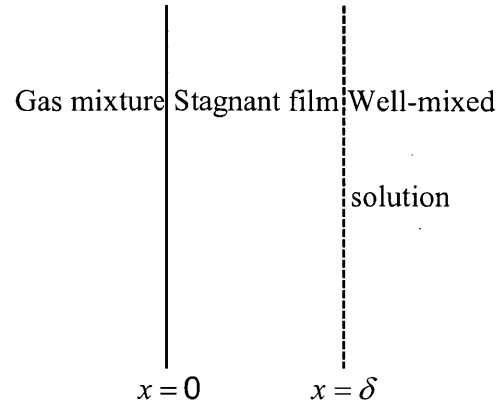

(a)

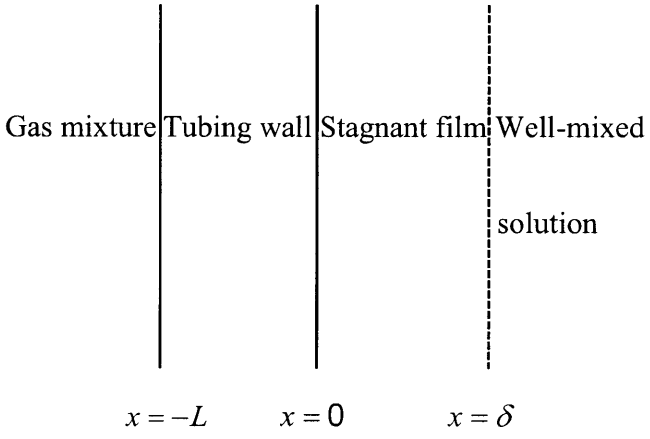

(b)

Figure 4.2. Coordinates for microscopic models: (a) direct gas-liquid contacting; and (b) diffusion through gas-permeable tubing (e.g., PDMS)

$$R_{NO_2} = -2k_1 C_{NO_2}{}^2 + 2k_{-1} C_{N_2O_4} \tag{4.3}$$

$$R_{N_2O_4} = k_1 C_{NO_2}{}^2 - (k_{-1} + k_2) C_{N_2O_4} \tag{4.4}$$

$$R_{NO_2^-} = k_2 C_{N_2O_4} \tag{4.5}$$

where k_1 and k_{-1} are the rate constants for the forward and reverse directions of reaction (4.1) in the aqueous phase, respectively. The net rates of NO_2 and N_2O_4 formation per unit volume are R_{NO_2} and $R_{N_2O_4}$, respectively. The aqueous equilibrium constant (K) is defined as the ratio of k_1 to k_{-1}:

$$K = \frac{k_1}{k_{-1}} = \left. \frac{C_{N_2O_4}}{C_{NO_2}{}^2} \right|_{eq} \tag{4.6}$$

The rate constant for the N_2O_4 hydrolysis reaction in the aqueous phase is denoted as k_2. Likewise, the rate of NO_2^- formation per unit volume is $R_{NO_2^-}$.

In PDMS, only reaction (4.1) occurs because the reaction (4.2) products are ions. The corresponding rate constants for reaction (4.1) in PDMS are denoted as $\tilde{k}_1$ and $\tilde{k}_{-1}$. The rate constants for the reverse direction of reaction (4.1) are assumed to be the same in the aqueous phase and PDMS phase. The equilibrium constant in the PDMS tubing is denoted as $\tilde{K}$. $\tilde{K}$ is defined as the ration of $\tilde{k}_1$ to $\tilde{k}_{-1}$:

$$\tilde{K} = \frac{\tilde{k}_1}{\tilde{k}_{-1}} = \left. \frac{\tilde{C}_{N_2O_4}}{\tilde{C}_{NO_2}{}^2} \right|_{eq} \tag{4.7}$$

The $\widetilde{K}$ value is not known in advance because there is no information about the rate constants for reaction (4.1) in the PDMS tubing.

In the gas-phase, NO_2 also exists in equilibrium with its dimer, N_2O_4. The rate constants for reaction (4.1) in the gas phase are denoted as k_{1g} and k_{-1g}. The gas-phase equilibrium constant (K_p) is defined in terms of the NO_2 and N_2O_4 partial pressures:

$$K_p = \frac{P_{N_2O_4}}{P_{NO_2}^2} \tag{4.8}$$

In the gas-phase, N_2O_4 reacts with water vapor to produce nitric acid and nitrous acid, instead of reaction (4.2). The rate constant for this reaction is represented as k_{2g} .All of the known rate constants and equilibrium constants are given in Table 4.1.

4.3 Equilibrium Properties and Relationships

4.3.1 Solubilities and Partition Coefficients

In order to estimate the dissolved NO_2 and N_2O_4 concentrations, information about the gas solubilities is needed. The aqueous solubilities of NO_2 and N_2O_4 are denoted as α_{NO_2} and $\alpha_{N_2O_4}$, respectively. The solubility of N_2O_4 is about 100 times larger than that of NO_2 (Gratzel et al., 1969; Broszkiewicz, 1976; Schwartz et al., 1981). The reported solubility of N_2O_4, $1.4\times10^{-5}\,\mathrm{MPa}^{-1}$ in Schwartz et al., (1981), was slightly adjusted based on the aqueous phase equilibrium constant, for internal consistency. The relationship between partial pressure and the aqueous concentration at gas-liquid interface (assumed to be equilibrium, justified later) is,

$$C^0_{NO_2} = \alpha_{NO_2} P_{NO_2},\ C^0_{N_2O_4} = \alpha_{N_2O_4} P_{N_2O_4} = K C^{0\,2}_{NO_2} \tag{4.9}$$

Table 4.1. Rate and equilibrium constants.

Quantity	Units	Values	References
k_1	$M^{-1}s^{-1}$	4.5×10^{8}	Gratzel et al., 1969; Broszkiewicz, 1976
k_{-1}	s^{-1}	6.9×10^{3}	Gratzel et al., 1969; Broszkiewicz, 1976
k_{1g}	$M^{-1}s^{-1}$	6.0×10^{8}	Atkinson et al.,2004
k_{-1g}	s^{-1}	$3.8\times10^{6}(296K)$	Atkinson et al.,2004
k_2	s^{-1}	1.0×10^{3}	Schwartz et al., 1981
k_{2g}	s^{-1}	8.0×10^{2}	England and Corcoran, 1974
K	M^{-1}	6.5×10^{4}	Calculated from k_1 and k_{-1}
K_p	Pa^{-1}	$7.577\times10^{-5}(296K)$	Schwartz et al., 1981

From Eq. (4.6) to (4.9), the relation between K and K_p can be expressed as follows,

$$\frac{K}{K_p} = \frac{\alpha_{N_2O_4}}{\alpha_{NO_2}^{\ 2}} \tag{4.10}$$

Thus, $\alpha_{N_2O_4}$ cannot be specified independently of K, K_p, and α_{NO_2}. The value used (Table 4.2) is about 10% smaller than that in Schwartz et al., (1981).

The solubility of species i in the PDMS tubing is denoted as $\tilde{\alpha}_i$. The equilibrium partition coefficient between PDMS and water is defined as

$$Q_i = \frac{\tilde{\alpha}_i}{\alpha_i} \tag{4.11}$$

The value of Q_{NO_2} is given in Table 4.2. Because no data are available for the N_2O_4 solubility in the PDMS tubing ($\tilde{\alpha}_{N_2O_4}$), it is not possible to obtain $Q_{N_2O_4}$ directly. Similar to Eq. (4.10), the relation between $\tilde{K}$ and K_p is,

$$\frac{\tilde{K}}{K_p} = \frac{\tilde{\alpha}_{N_2O_4}}{\tilde{\alpha}_{NO_2}^{\ 2}} \tag{4.12}$$

The value of $Q_{N_2O_4}$ can be inferred indirectly using Eqs. (4.10) to (4.12), which indicate that

$$\varepsilon = \frac{\tilde{K}}{K} = \frac{Q_{N_2O_4}}{Q_{NO_2}^{\ 2}} = \frac{\tilde{k}_1}{k_1} \tag{4.13}$$

The last equality comes from the assumption that the rate constants for the reverse reaction (4.1) are the same in both phases. Solubilities and partition coefficients of NO_2 and N_2O_4 are given in Table 4.2. This equilibrium constant ratio will be an important parameter in the combined membrane and aqueous models.

Table 4.2. Solubilities and partition coefficients.

Quantity	Units	Values	References
α_{NO_2}	MPa^{-1}	1.2×10^{-7}	Mertes et al., 1995
$\alpha_{N_2O_4}$	MPa^{-1}	1.24×10^{-5}	Calculated
$\tilde{\alpha}_{NO_2}$	MPa^{-1}	2.0×10^{-6}	Robb, 1968
Q_{NO_2}		16.7	Calculated

4.3.2 Gas Composition and Liquid Interface Concentrations

As pointed out in Section 4.2, NO_2 and N_2O_4 are always present together. Commercial gas mixtures are denoted as % NO_2 and are available down to 0.001%. The stated percentage (X) is related to the partial pressures of NO_2, N_2O_4 and an inert gas such as N_2 as follows:

$$P_{NO_2} + P_{N_2O_4} + P_{Inert} = P_{atm} \tag{4.14}$$

$$\frac{P_{NO_2} + 2P_{N_2O_4}}{P_{NO_2} + 2P_{N_2O_4} + P_{Inert}} = \frac{X}{100} \tag{4.15}$$

where P_{NO_2}, $P_{N_2O_4}$ and P_{Inert} are the partial pressure of NO_2, N_2O_4, and the inert gas, respectively. Eq. (4.14) assumes that the total pressure is atmospheric as would be the case when the gas mixture reaches the reactor. Solving Eqs. (4.14), (4.15) with (4.8), relates the partial pressure of N_2O_4 to X and the partial pressure of NO_2.

$$K_p(200 - X)P_{NO_2}{}^2 + 100P_{NO_2} - P_{atm}X = 0 \tag{4.16}$$

$$P_{N_2O_4} = \frac{P_{atm}X - 100P_{NO_2}}{200 - X} \tag{4.17}$$

From Eq. (4.16) and (4.17), the gas phase concentrations (in terms of partial pressures) of NO_2 and N_2O_4 at the gas-liquid interface are obtained.

The fractions of total nitrogen as NO_2 in the gas and liquid at the gas-liquid interface are defined as,

$$F_G = \frac{P_{NO_2}}{P_{NO_2} + 2P_{N_2O_4}} = \frac{1}{1 + 2K_pP_{NO_2}} \tag{4.18}$$

$$F_L = \frac{C^0_{NO_2}}{C^0_{NO_2} + 2C^0_{N_2O_4}} = \frac{1}{1 + 2KC^0_{NO_2}} = \frac{1}{1 + \left(\frac{\alpha_{N_2O_4}}{\alpha_{NO_2}}\right)2K_pP_{NO_2}} \tag{4.19}$$

where C_i° is the concentration in the liquid. The gas (F_G) and liquid (F_L) fractions differ greatly because of the differing solubilities of NO_2 and N_2O_4, as will be shown.

In the gas entrance line, there will be a significant pressure drop at the regulator. Accordingly, whether the equilibrium between NO_2 and N_2O_4 still holds after the sudden pressure drop was examined by comparing an estimate of the transit time to the reactor with a characteristic reaction time. Characteristic reaction time from the gas-phase analog of Eq. (4.3) is

$$t_R = \frac{1}{2k_{1g}C^*_{NO_2}} \tag{4.20}$$

where $C^*_{NO_2}$ is the NO_2 concentration at the regulator. For $C^*_{NO_2} \sim$ mM, t_R is about 1 μs. The t time for the gas to travel through a typical line (t_t = length / mean velocity) is about one second. This indicates that the dimerization reaction is fast enough to reestablish the equilibrium between NO_2 and N_2O_4.

In the case where the gas directly contacts the PDMS membrane, the concentrations of NO_2 and N_2O_4 at the gas-PDMS membrane interface are

$$\tilde{C}^0_{NO_2} = \tilde{\alpha}_{NO2} P_{NO2}, \quad \tilde{C}^0_{N_2O_4} = \tilde{\alpha}_{N_2O_4} P_{N_2O_4} = \tilde{K}\tilde{C}^{0\ 2}_{NO_2} \tag{4.21}$$

4.4 Diffusivities and Length Scales for Microscopic Models

In order to set up the microscopic diffusion-reaction equations, information about the diffusivities is also needed. D_{NO_2} and $D_{N_2O_4}$ are the aqueous diffusivities of NO_2 and N_2O_4, respectively. The aqueous diffusivity of N_2O_4 was obtained by using Wilke-Chang method, which is an empirical modification of the Stokes-Einstein relation. $\tilde{D}_{NO_2}$ and $\tilde{D}_{N_2O_4}$ are the

diffusivities of NO_2 and N_2O_4 in the PDMS tubing. Because it is impossible to estimate $\widetilde{D}_{N_2O_4}$ with the Wilke-Chang method, the diffusivity ratio was assumed to be the same in both phases. That is,

$$a = \frac{\widetilde{D}_{NO_2}}{\widetilde{D}_{N_2O_4}} = \frac{D_{NO_2}}{D_{N_2O_4}} \tag{4.22}$$

From this diffusivity ratio, $\widetilde{D}_{N_2O_4}$ can be estimated. The PDMS membrane thickness (L) is the same as in the reactor of Wang and Deen (2003). The boundary layer next to the membrane or the gas was modeled as a stagnant film from $x = 0$ (Interface) to $x = \delta$ (bulk liquid). Its film thickness (δ) is expected to be about $100\mu m$. For example, Wang and Deen (2003) found $\delta = 70\mu m$ for liquid in contact with loops of PDMS tubing in their stirred reactor, and Brian Skinn in our laboratory found $\delta = 78\mu m$ for direct gas-liquid contact in a similar device (personal communication). The diffusivities and thicknesses are summarized in Table 4.3.

4.5 Aqueous Microscopic Model

Although the concentrations are time dependent, they are pseudosteady. The longest time scale in the liquid film is $\delta^2/D \cong 3-5s$, which is much shorter than the experimental time scales (at least 30-60 min). Hence, time derivatives were deleted and the species conservation equations for NO_2 and N_2O_4 in the aqueous film were written as follows:

$$D_{NO_2}\frac{d^2C_{NO_2}}{dx^2} - 2k_1C_{NO_2}{}^2 + 2k_{-1}C_{N_2O_4} = 0 \tag{4.23}$$

$$D_{N_2O_4}\frac{d^2C_{N_2O_4}}{dx^2} + k_1C_{NO_2}{}^2 - (k_{-1}+k_2)C_{N_2O_4} = 0 \tag{4.24}$$

Table 4.3. Diffusivities and film thickness

Quantity	Units	Values	References
D_{NO_2}	m^2s^{-1}	1.85×10^{-9}	Mertes et al., 1995
$D_{N_2O_4}$	m^2s^{-1}	1.3×10^{-9}	Estimated
$\widetilde{D}_{NO_2}$	m^2s^{-1}	1.1×10^{-9}	Mertes et al., 1995
$\widetilde{D}_{N_2O_4}$	m^2s^{-1}	7.7×10^{-10}	Estimated
L	m	2.45×10^{-4}	Wang and Deen, 2003
δ	m	$\sim10^{-4}$	See the text

where $C_{NO_2}(x)$ and $C_{N_2O_4}(x)$ are the concentration of NO_2 and N_2O_4 in the aqueous film. The starting point (x = 0) in the film represents the gas-liquid interface. The boundary conditions at x = 0 representing gas-liquid equilibrium at the interface, are

$$C_{NO_2}(0) = C^0_{NO_2} \tag{4.25}$$

$$C_{N_2O_4}(0) = C^0_{N_2O_4} = K{C^0_{NO_2}}^2 \tag{4.26}$$

It is assumed in Eq. (4.26) that NO2 and N_2O_4 are in equilibrium at the gas-liquid interface. The boundary conditions at $x = \delta$ are,

$$-D_{NO_2}\frac{dC_{NO_2}(\delta)}{dx} = \frac{V}{A_C}[2k_1 C_{NO_2}(\delta)^2 - 2k_{-1}C_{N_2O_4}(\delta)] \tag{4.27}$$

$$-D_{N_2O_4}\frac{dC_{N_2O_4}(\delta)}{dx} = \frac{V}{A_C}[-k_1 C_{NO_2}(\delta)^2 + (k_{-1}+k_2)C_{N_2O_4}(\delta)] \tag{4.28}$$

where A_C is the contact area between gas and the liquid and V is the volume of the well-stirred part of the solution (which will be almost the same as the total liquid volume). At the edge of the aqueous film ($x = \delta$), the flux of each species must be the same as its net consumption in the well-stirred solution, per unit area of film.

To minimize the number of parameters and simplify the numerical solution, it is advantageous to employ scaled dimensionless variables. The dimensionless position and concentrations are defined as

$$\zeta = \frac{y}{\delta}, \quad \Theta = \frac{C_{NO_2}}{C^0_{NO_2}}, \quad \Phi = \frac{C_{N_2O_4}}{C^0_{N_2O_4}} \tag{4.29}$$

Based on these dimensionless variables and using the diffusivity ratio a (Eq. (4.22)), conversion to dimensionless variables gives

$$\frac{d^2\Theta}{d\zeta^2} - \mathrm{Da}_1(\Theta^2 - \Phi) = 0 \tag{4.30}$$

$$\frac{d^2\Phi}{d\zeta^2} + \mathrm{Da}_1 b\Theta^2 - \left(1 + \frac{k_{-1}}{k_2}\right)\mathrm{Da}_2\Phi = 0 \tag{4.31}$$

$$\mathrm{Da}_1 = \frac{2k_1\delta^2 C^0_{NO_2}}{D_{NO_2}}, \quad \mathrm{Da}_2 = \frac{k_2\delta^2}{D_{N_2O_4}}, \quad b = \frac{a}{2KC^0_{NO_2}} = \frac{a}{2}\frac{C^0_{NO_2}}{C^0_{N_2O_4}}, \quad \mathrm{Da}_1 b = \frac{k_{-1}\delta^2}{D_{N_2O_4}} \tag{4.32}$$

where Da_1 and Da_2 are the Damkohler numbers for reactions (4.1) and (4.2), respectively. Note that b is proportional to the ratio of NO_2 to N_2O_4 concentration with a proportionality factor $a/2$. Also note that both $\mathrm{Da}_1 b$ and Da_2 are concentration-independent. The dimensionless boundary conditions are

$$\Theta(0) = 1 \tag{4.33}$$

$$\Phi(0) = 1 \tag{4.34}$$

$$\frac{d\Theta(1)}{d\zeta} = \frac{V}{A_c\delta}\left[-\mathrm{Da}_1\Theta(1)^2 + \mathrm{Da}_2\Phi(1)\right] \tag{4.35}$$

$$\frac{d\Phi(1)}{d\zeta} = \frac{V}{A_c\delta}\left[\mathrm{Da}_1 b\Theta(1)^2 - \left(1 + \frac{k_{-1}}{k_2}\right)\mathrm{Da}_2\Phi(1)\right] \tag{4.36}$$

As pointed out in the introduction, the macroscopic model contains the aqueous volume-averaged (bulk) concentrations. These concentrations are denoted as $\overline{C}_i$ and they are related to those in the microscopic model as

$$\overline{C}_i = \left[1 + \frac{A_C}{VC_i(\delta)} \int_0^\delta C_i(y)dy\right] C_i(\delta) \tag{4.37}$$

$$\kappa_i = 1 + \frac{A_C}{VC_i(\delta)} \int_0^\delta C_i(y)dy \tag{4.38}$$

where $C_i(\delta)$ is the well-mixed concentration of species i, and κ_i is the volume averaged (bulk) concentration divided by the concentration in the well-mixed region. The liquid boundary layer also contributes to the dimerization reaction rate, so a correction factor (γ) that accounts for this is defined as

$$\gamma = 1 + \frac{A_C}{Vk_1 \overline{C}_{NO_2}^{\,2}} \int_0^\delta k_1 C_{NO_2}(y)^2 dy \tag{4.39}$$

This correction factor, which indicates the degree of the concentration non-uniformity, will appear in the macroscopic equations presented later.

4.5.1 Quasi-Equilibrium Approximation (QEA) for Aqueous Microscopic Model

If the NO_2 and N_2O_4 concentrations are assumed to be near their equilibrium ratio throughout the liquid film, which is termed the quasi-equilibrium approximation (QEA), the microscopic model can be simplified significantly. The QEA formulation is described next. As will be shown later, this is an excellent approximation for the expected operating conditions in NO_2 delivery. From Eqs. (4.23) and (4.24), the following is always true.

$$\frac{d^2(D_{NO_2}C_{NO_2} + 2D_{N_2O_4}C_{N_2O_4})}{dx^2} - 2k_2 C_{N_2O_4} = 0 \tag{4.40}$$

It is convenient then to define the total nitrogen concentration as

$$C_N = aC_{NO_2} + 2C_{N_2O_4} \tag{4.41}$$

where a is the diffusivity ratio in Eq. (4.22). In terms of C_N, Eq. (4.40) becomes which is always true.

$$\frac{d^2C_N}{dx^2} - \frac{2k_2C_{N_2O_4}}{D_{N_2O_4}} = 0 \tag{4.42}$$

If the QEA is accurate, then

$$C_{N_2O_4} = KC_{NO_2}^{\ 2} \tag{4.43}$$

Combining Eq. (4.41) and (4.43) and solving the quadratic equation for the NO_2 concentration gives the NO_2 and N_2O_4 concentrations as functions of C_N,

$$C_{NO_2} = \frac{-a + a\sqrt{1 + \dfrac{8KC_N}{a^2}}}{4K} \tag{4.44}$$

$$C_{N_2O_4} = \frac{C_N}{2} - \frac{aC_{NO_2}}{2} = \frac{C_N}{2} + \frac{a^2}{8K}\left(1 - \sqrt{1 + \frac{8KC_N}{a^2}}\right) \tag{4.45}$$

Putting Eq. (4.45) into Eq. (4.42), the governing differential equation for C_N with the QEA is obtained. This reduces the two differential equations for NO_2 and N_2O_4 to a single differential equation, namely

$$\frac{d^2C_N}{dx^2} = \frac{k_2}{D_{N_2O_4}}\left[C_N + \frac{a^2}{4K}\left(1 - \sqrt{1 + \frac{8KC_N}{a^2}}\right)\right] \tag{4.46}$$

The boundary conditions are now

$$C_N(0) = C_N^0 = aC_{NO_2}^0 + 2C_{N_2O_4}^0 \tag{4.47}$$

$$-D_{N_2O_4}\frac{dC_N(\delta)}{dx} = \frac{Vk_2}{A_C}\left[C_N(\delta) + \frac{a^2}{4K}\left(1-\sqrt{1+\frac{8KC_N(\delta)}{a^2}}\right)\right] \tag{4.48}$$

Using a dimensionless total nitrogen concentration (Θ_N),

$$\Theta_N = \frac{C_N}{C_N^0} \tag{4.49}$$

$$\frac{d^2\Theta_N}{d\zeta^2} = \mathrm{Da}_2\left[\Theta_N + ab_N\left(1-\sqrt{1+\frac{2\Theta_N}{ab_N}}\right)\right] \tag{4.50}$$

$$b_N = \frac{a}{4KC_N^0} \tag{4.51}$$

where b_N is analogous to b in Eq. (4.32). The dimensionless boundary conditions are

$$\Theta_N(0) = 1 \tag{4.52}$$

$$\frac{d\Theta_N(1)}{d\zeta} = -\frac{V}{A_c\delta}\mathrm{Da}_2\left[\Theta_N(1) + ab_N\left(1-\sqrt{1+\frac{2\Theta_N(1)}{ab_N}}\right)\right] \tag{4.53}$$

The concentration gradients of NO_2 and N_2O_4 at $x = 0$ (gas-liquid interface) will be important for the macroscopic model. For this reason, analytical expressions for those slopes are presented here for the QEA. Using the following mathematical relationship (Eq. (4.54)), Eq. (4.50) is changed into Eq. (4.55).

$$\frac{d^2\Theta_N}{d\zeta^2} = \frac{d\Theta_N}{d\zeta}\frac{d}{d\Theta_N}\left(\frac{d\Theta_N}{d\zeta}\right) = \frac{1}{2}\frac{d}{d\Theta_N}\left(\frac{d\Theta_N}{d\zeta}\right)^2 \tag{4.54}$$

$$\frac{d}{d\Theta_N}\left(\frac{d\Theta_N}{d\zeta}\right)^2 = 2\mathrm{Da}_2\left[\Theta_N + ab_N\left(1-\sqrt{1+\frac{2\Theta_N}{ab_N}}\right)\right] \tag{4.55}$$

Integrating both sides and using the approximation $d\Theta_N(1)/d\psi \cong 0$, $\Theta_N(1) \cong 0$

$$\left(\frac{d\Theta_N(0)}{d\zeta}\right)^2 = \mathrm{Da}_2(1+2ab_N) - \frac{2}{3}\mathrm{Da}_2(ab_N)^2\left(\left(1+\frac{2}{ab_N}\right)^{\frac{3}{2}}-1\right) \tag{4.56}$$

Using Eqs. (4.41), (4.43), and (4.49), the gradients are

$$\frac{dC_{NO_2}(0)}{dx} = \frac{C_N^0}{(a+4KC_{NO_2}^0)\delta}\frac{d\Theta_N(0)}{d\zeta} \tag{4.57}$$

$$\frac{dC_{N_2O_4}(0)}{dx} = 2KC_{NO_2}^0\frac{dC_{NO_2}(0)}{dy} = \frac{2KC_{NO_2}^0 C_N^0}{(a+4KC_{NO_2}^0)\delta}\frac{d\Theta_N(0)}{d\zeta} \tag{4.58}$$

4.5.2 Limiting Form of QEA for Low Total Nitrogen Concentration

For low C_N, it is possible to simplify the QEA solution more. This can be done under following conditions:

$$2\Theta_N << ab_N = \frac{a^2}{4KC_N^0}, \quad C_N << \frac{A^2}{8K} = 3.9\mu\mathrm{M} \tag{4.59}$$

Using a binomial expansion up to three terms,

$$\sqrt{1+\frac{2\Theta_N}{ab_N}} \cong 1+\frac{\Theta_N}{ab_N}-\frac{1}{8}\left(\frac{2\Theta_N}{ab_N}\right)^2 \tag{4.60}$$

Then, Eq. (4.50) is changed into

$$\frac{d^2\Theta_N}{d\zeta^2} \cong \mathrm{Da}_2\left[\Theta_N + ab_N\left(1-\left(1+\frac{\Theta_N}{ab_N}-\frac{{\Theta_N}^2}{2(ab_N)^2}\right)\right)\right] = \frac{\mathrm{Da}_2}{2ab_N}{\Theta_N}^2 \tag{4.61}$$

The modified boundary conditions are,

$$\Theta_N(0) = 1 \tag{4.62}$$

$$\frac{d\Theta_N(1)}{d\zeta} \cong -\frac{V\mathrm{Da}_2}{A_c\delta}\frac{\Theta_N(1)^2}{2ab_N} \tag{4.63}$$

Expanding $\left[1+(2/ab_N)\right]^{3/2}$ up to the fourth terms by using the binomial theorem and Eq. (4.56) gives

$$\left(\frac{d\Theta_N(0)}{d\zeta}\right)^2 = \frac{\mathrm{Da}_2}{3ab_N} \tag{4.64}$$

Because total nitrogen is consumed in the film only, the negative root is meaningful. Combined with Eq. (4.57) and (4.58), the NO_2 and N_2O_4 initial slopes are

$$\frac{dC_{NO_2}(0)}{dx} = -\frac{C_N^0}{(a+4KC_{NO_2}^0)\delta}\sqrt{\frac{\mathrm{Da}_2}{3ab_N}} \tag{4.65}$$

$$\frac{dC_{N_2O_4}(0)}{dx} = 2KC_{NO_2}^0\frac{dC_{NO_2}(0)}{dx} = -\frac{2KC_{NO_2}^0C_N^0}{(a+4KC_{NO_2}^0)\delta}\sqrt{\frac{\mathrm{Da}_2}{3ab_N}} \tag{4.66}$$

4.5.3 Limiting Form of QEA for High Total Nitrogen Concentration

For high C_N, it is not possible to simplify the QEA formulation more, even though that looks possible at first sight. The reason is that every term in Eq. (4.50) is important in much of the film, the dominant terms changing in different regions of the film. However, it is possible to simplify the expressions for the initial slopes in this high nitrogen limit. The diffusivity ratio a is

order of magnitude one. As evident in Eq. (4.51), b_N approaches zero as the total nitrogen increases. Thus, ab_N approaches zero at high total nitrogen. So, in this limit, Eq. (4.56) is reduced to

$$\left(\frac{d\Theta_N(0)}{d\zeta}\right)^2 = \mathrm{Da}_2 \tag{4.67}$$

Combined with Eq. (4.57) and (4.58), the NO_2 and N_2O_4 initial slopes in the high nitrogen limit are

$$\frac{dC_{NO_2}(0)}{dx} = -\frac{C_N^0}{(a+4KC_{NO_2}^0)\delta}\sqrt{\mathrm{Da}_2} \tag{4.68}$$

$$\frac{dC_{N_2O_4}(0)}{dx} = 2KC_{NO_2}^0\frac{dC_{NO_2}(0)}{dx} = -\frac{2KC_{NO_2}^0 C_N^0}{(a+4KC_{NO_2}^0)\delta}\sqrt{\mathrm{Da}_2} \tag{4.69}$$

4.5.4 Limiting Form of Aqueous Model for Very Low Total Nitrogen Concentration

For very low total nitrogen concentration, it is possible to obtain an analytical solution for the aqueous microscopic model without introducing the QEA. According to Eqs. (4.13) ,(4.14) and the K_p values in Table 4.1, the NO_2 partial pressure is much greater than the N_2O_4 partial pressure even if its value is extremely small compared to that of the atmospheric pressure. This means that almost all of the gas consists of NO_2 in this limit. So, in this limit, it is expected that the diffusion rate of NO_2 is much faster than the reaction rate of NO_2. Actually, this can be easily verified by calculating Da_1 (Eq. (4.32)). The species conservation equation for NO_2 in this very low nitrogen limit is then,

$$D_{NO_2}\frac{d^2C_{NO_2}}{dx^2}=0 \tag{4.70}$$

However, the reaction terms for N_2O_4 cannot be eliminated like those for NO_2. If the N_2O_4 reaction terms are ignored, then Eq. (4.40) cannot be satisfied. Furthermore, the Da_1b and Da_2 values in the dimensionless N_2O_4 equation (Eq. (4.31)) are enormous as well as concentration-independent [Eq. (4.32), Tables 4.1 and 4.3]. For these reasons, the N_2O_4 conservation equation in this very low nitrogen limit is the same as Eq. (4.24). All boundary conditions except Eq. (4.27) are the same. The new boundary condition for NO_2 at the edge of the liquid film is the well-mixed NO_2 concentration. The solution for NO_2 that satisfies Eq. (4.70) with Eq. (4.25) and new boundary condition is

$$C_{NO_2}(x)=\left(\frac{C_{NO_2}(\delta)-C^0_{NO_2}}{\delta}\right)x+C^0_{NO_2} \tag{4.71}$$

$$M=\left(\frac{C_{NO_2}(\delta)-C^0_{NO_2}}{\delta}\right) \tag{4.72}$$

At this stage, M is still undetermined because the well-mixed concentration of NO_2 [$C_{NO_2}(\delta)$] is not yet known. Substitution of Eq. (4.71) into Eq. (4.24) and solving with the boundary conditions (Eq. (4.26) and (4.28)) gives

$$C_{N_2O_4}(x)=P\cosh(\lambda x)+Q\sinh(\lambda x)+\frac{k_1}{k_{-1}+k_2}C_{NO_2}(x)^2+\frac{2D_{N_2O_4}k_1}{(k_{-1}+k_2)^2}M^2 \tag{4.73}$$

$$\lambda=\sqrt{\frac{k_{-1}+k_2}{D_{N_2O_4}}}=\frac{\sqrt{\mathrm{Da}_1b+\mathrm{Da}_2}}{\delta} \tag{4.74}$$

$$P = \frac{k_2}{k_{-1}+k_2} C^0_{N_2O_4} - \frac{2D_{N_2O_4}k_1}{(k_{-1}+k_2)^2} M^2 \tag{4.75}$$

$$Q = -\left(\frac{\tanh(\lambda\delta) + \frac{V\lambda}{A_C}}{1 + \frac{V\lambda}{A_C}\tanh(\lambda\delta)} \right) P - \left(\lambda\cosh(\lambda\delta) + \frac{V\lambda^2}{A_C}\sinh(\lambda\delta) \right)^{-1} \frac{2k_1 M}{k_{-1}+k_2} \left(\frac{VM}{A_C} + C^0_{NO_2} \right) \tag{4.76}$$

The value of $\lambda\delta$ is about 200, for which the hyperbolic cosine and sine are nearly equal. So, the value of $\tanh(\lambda\delta)$ is one, and Eq. (4.76) is reduced to

$$Q = -P = -\frac{k_2}{k_{-1}+k_2} C^0_{N_2O_4} + \frac{2D_{N_2O_4}k_1}{(k_{-1}+k_2)^2} M^2 \tag{4.77}$$

Thus, the N_2O_4 concentration expression is reduced to,

$$C_{N_2O_4}(x) = P\exp(-\lambda x) + \frac{k_1}{k_{-1}+k_2} C_{NO_2}(x)^2 + \frac{2D_{N_2O_4}k_1}{(k_{-1}+k_2)^2} M^2 \tag{4.78}$$

The exponential terms in both the N_2O_4 concentration and its gradient vanish at $x = \delta$. Simplifying the expressions and substituting them into Eq. (4.28) gives, after some rearrangement,

$$\frac{C^0_{NO_2}}{C_{NO_2}(\delta)} = 1 + \frac{A_c\delta}{V} \tag{4.79}$$

$$M = -\frac{\frac{A_c}{V} C^0_{NO_2}}{1 + \frac{A_c\delta}{V}} \tag{4.80}$$

$$\frac{C^0_{N_2O_4}}{C_{N_2O_4}(\delta)} = \frac{\left(1 + \frac{A_c\delta}{V}\right)^2}{\frac{k_{-1}}{k_{-1}+k_2} + \frac{2D_{N_2O_4}k_{-1}}{(k_{-1}+k_2)^2}\left(\frac{A_c\delta}{V}\right)^2} \cong \frac{k_{-1}+k_2}{k_{-1}}\left(1 + \frac{A_c\delta}{V}\right)^2 \tag{4.81}$$

Now, M is completely determined and expressed in terms of known parameters. The NO_2 concentration is

$$C_{NO_2}(x) = \left(\frac{-\frac{A_c}{V} C^0_{NO_2}}{1 + \frac{A_c \delta}{V}} \right) x + C^0_{NO_2} \tag{4.82}$$

Substitution of Eq. (4.71) into Eq. (4.38) and integrating

$$\kappa_{NO_2} = 1 + \frac{A_C \delta}{2V} \left(1 + \frac{C^0_{NO_2}}{C_{NO_2}(\delta)} \right) = 1 + \frac{A_c \delta}{2V} \left(2 + \frac{A_c \delta}{V} \right) \cong 1 + \frac{A_c \delta}{V} \tag{4.83}$$

The second equality comes from Eq. (4.79). In a similar manner, substituting Eq. (4.78) into Eq. (4.38) and integrating, the integral is

$$\int_0^\delta C_{N_2O_4}(x) dx = \frac{I}{\lambda}(1 - e^{-\lambda \delta}) + \frac{k_1}{k_{-1} + k_2} \int_0^\delta C_{NO_2}(x)^2 dx + \frac{2 D_{N_2O_4} k_1 M^2}{(k_{-1} + k_2)^2} \delta \tag{4.84}$$

In the first term, $e^{-\lambda \delta}$ vanishes and substitution of Eq. (4.75) into Eq. (4.84) gives

$$\int_0^\delta C_{N_2O_4}(x) dx = \frac{k_2 C^0_{N_2O_4}}{k_{-1} + k_2} \frac{\delta}{\lambda} + \frac{k_1}{k_{-1} + k_2} \int_0^\delta C_{NO_2}(x)^2 dx + \frac{2 D_{N_2O_4} k_1 M^2}{(k_{-1} + k_2)^2} \delta \left(1 - \frac{1}{\lambda}\right) \tag{4.85}$$

From an order of magnitude analysis, the first and third terms are both much smaller than the second term. Dropping both terms and substituting Eq. (4.82) into Eq. (4.85),

$$\int_0^{\delta} C_{N_2O_4}(x)dx = \frac{k_{-1}}{k_{-1}+k_2}\frac{C^0_{N_2O_4}}{\left(1+\frac{A_c\delta}{V}\right)^2}\frac{V}{3A_c}\left[\left(1+\frac{A_c\delta}{V}\right)^3-1\right] \tag{4.86}$$

Then, $\kappa_{N_2O_4}$ is,

$$\kappa_{N_2O_4} = 1+\frac{A_c\delta}{V}\left\{\frac{k_{-1}}{k_{-1}+k_2}\frac{1}{\left(1+\frac{A_c\delta}{V}\right)^2}\frac{V}{3A_c\delta}\left[\left(1+\frac{A_c\delta}{V}\right)^3-1\right]\right\}\frac{C^0_{N_2O_4}}{C_{N_2O_4}(\delta)} \tag{4.87}$$

Substitution of Eq. (4.81) into Eq. (4.87) gives

$$\kappa_{N_2O_4} = 1+\frac{A_c\delta}{V}\left\{\frac{V}{3A_c\delta}\left[\left(1+\frac{A_c\delta}{V}\right)^3-1\right]\right\} \cong 1+\frac{A_c\delta}{V} \tag{4.88}$$

Also, it is possible to obtain the analytical expression for the dimerization reaction correction factor. Substituting Eq. (4.82) into Eq. (4.39) and integrating,

$$\gamma = 1+\frac{A_c {C^0_{NO_2}}^2}{V\overline{C}_{NO_2}{}^2}\frac{1}{\left(1+\frac{A_c\delta}{V}\right)^2}\frac{V}{3A_c}\left[\left(1+\frac{A_c\delta}{V}\right)^3-1\right] \tag{4.89}$$

By using the definition of $\kappa_{N_2O_4}$, Eq. (4.79), and Eq. (4.83),

$$\gamma = 1+\frac{1}{3\kappa_{NO_2}{}^2}\left[\left(1+\frac{A_c\delta}{V}\right)^3-1\right] \cong 1+\frac{A_c\delta}{V} \tag{4.90}$$

As shown in Eqs. (4.83), (4.88), and (4.90), all values of κ and γ approaches the same value.

4.6 Macroscopic Model

To characterize the performance of this delivery system in terms of mass transfer coefficients for NO_2 and N_2O_4, a macroscopic model was set up in which the control volume was the entire solution. The concentration of species i averaged over the liquid volume is denoted as $\overline{C}_i$, which has already been defined in Eq. (4.37). In general, the balances for NO_2 and N_2O_4 and the rates of NO_2^- and NO_3^- formation were written as

$$V\frac{d\overline{C}_{NO_2}}{dt} = k_{NO_2}A_C(\alpha_{NO_2}P_{NO_2} - \overline{C}_{NO_2}) - 2\gamma k_1\overline{C}_{NO_2}{}^2V + 2k_{-1}\overline{C}_{N_2O_4}V \tag{4.91}$$

$$V\frac{d\overline{C}_{N_2O_4}}{dt} = k_{N_2O_4}A_C(\alpha_{N_2O_4}P_{N_2O_4} - \overline{C}_{N_2O_4}) + \gamma k_1\overline{C}_{NO_2}{}^2V - (k_{-1}+k_2)\overline{C}_{N_2O_4}V \tag{4.92}$$

$$\frac{d\overline{C}^-_{NO_2}}{dt} = \frac{d\overline{C}^-_{NO_3}}{dt} = k_2\overline{C}_{N_2O_4} \tag{4.93}$$

The liquid-phase mass transfer coefficient for species i is denoted as k_i and γ is the correction factor for the dimerization reaction [Eq. (4.39)]. The time constant (τ) for species i to reach the steady-state can be determined by fitting the time-dependent concentration as

$$C_i(t) = \overline{C}_i^s(1-e^{-t/\tau}) \tag{4.94}$$

where the steady-state concentration of species i is denoted as $\overline{C}_i^s$. As will be shown, the values of τ for NO_2 and N_2O_4 are quite small (< 1 s for the direct gas contact), so that steady conditions are reached very quickly and the time derivatives in Eqs. (4.91) and (4.92) can be ignored for most purposes.

With $\alpha_{NO_2} P_{NO_2} >> \overline{C}_{NO_2}$ and $\alpha_{N2O4} P_{N2O4} >> \overline{C}_{N_2O_4}$, the steady-state N_2O_4 concentration is,

$$\overline{C}^{s}_{N_2O_4} = \frac{\left(k_{NO_2}\alpha_{NO_2}P_{NO_2} + 2k_{N_2O_4}\alpha_{N_2O_4}P_{N_2O_4}\right)A_c}{2k_2V} \tag{4.95}$$

Substitution of the steady state N_2O_4 concentration into the NO_2 mass balance at steady-state,

$$\overline{C}^{s}_{NO_2}{}^{2} = \frac{A_c}{2\gamma k_1 V}\left(k_{NO_2}\alpha_{NO_2}P_{NO_2} + \frac{k_{-1}}{k_2}(k_{NO_2}\alpha_{NO_2}P_{NO_2} + 2k_{N_2O_4}\alpha_{N_2O_4}P_{N_2O_4})\right) \tag{4.96}$$

The mass transfer coefficients are related to the microscopic model as follows:

$$-D_{NO_2}\frac{dC_{NO_2}(0)}{dx} = k_{NO_2}(\alpha_{NO_2}P_{NO_2} - \overline{C}_{NO_2}) \tag{4.97}$$

$$-D_{N_2O_4}\frac{dC_{N_2O_4}(0)}{dx} = k_{N_2O_4}(\alpha_{N_2O_4}P_{N_2O_4} - \overline{C}_{N_2O_4}) \tag{4.98}$$

4.7 PDMS Membrane Microscopic Model

Because the PDMS membrane thickness is of the same order as that of the liquid film (Table 4.3), the longest time scale in the PDMS membrane is the same order of magnitude as that of the liquid film. For the same reason as in the liquid film, the species conservation equations for NO_2 and N_2O_4 are pseudosteady in the membrane. Only reaction (4.1) occurs in the PDMS membrane, so the conservation equations are written as

$$\widetilde{D}_{NO_2}\frac{d^2\widetilde{C}_{NO_2}}{dx^2} - 2\widetilde{k}_1\widetilde{C}_{NO_2}{}^{2} + 2\widetilde{k}_{-1}\widetilde{C}_{N_2O_4} = 0 \tag{4.99}$$

$$\widetilde{D}_{N_2O_4}\frac{d^2\widetilde{C}_{N_2O_4}}{dx^2}+\widetilde{k}_1\widetilde{C}_{NO_2}{}^2-\widetilde{k}_{-1}\widetilde{C}_{N_2O_4}=0 \tag{4.100}$$

where $\widetilde{C}_{NO_2}(x)$ and $\widetilde{C}_{N_2O_4}(x)$ are the concentration of NO_2 and N_2O_4 in the PDMS membrane. The starting point (x = -L) in the PDMS membrane represents the gas-PDMS membrane interface (Fig 4.2 (b)), and the interface between the PDMS membrane and the liquid film is denoted as x = 0. The boundary conditions are

$$\widetilde{C}_{NO_2}(-L)=\widetilde{C}^0_{NO_2} \tag{4.101}$$

$$\widetilde{C}_{N_2O_4}(-L)=\widetilde{C}^0_{N_2O_4}=\widetilde{K}\widetilde{C}^0_{NO_2}{}^2 \tag{4.102}$$

As already shown in Eq. (4.21), the equilibrium between NO_2 and N_2O_4 holds at x = -L.

$$\widetilde{C}_{NO_2}(0)=\widetilde{C}^*_{NO_2} \tag{4.103}$$

$$\widetilde{C}_{N_2O_4}(0)=\widetilde{C}^*_{N_2O_4} \tag{4.104}$$

However, at the aqueous edge of the PDMS membrane (x = 0), there is no equilibrium relationship between NO_2 and N_2O_4.

The dimensionless position, NO_2, and N_2O_4 concentrations in the PDMS membrane are defined as,

$$\eta=\frac{x+L}{L},\quad \theta=\frac{\widetilde{C}_{NO_2}}{\widetilde{C}^0_{NO_2}},\quad \phi=\frac{\widetilde{C}_{N_2O_4}}{\widetilde{C}^0_{N_2O_4}} \tag{4.105}$$

Conversion to dimensionless variables gives

$$\frac{d^2\theta}{d\eta^2} - \mathrm{Da_m}(\theta^2 - \phi) = 0 \tag{4.106}$$

$$\frac{d^2\phi}{d\eta^2} + \mathrm{Da_m}\tilde{b}(\theta^2 - \phi) = 0 \tag{4.107}$$

$$\mathrm{Da_m} = \frac{2\tilde{k}_1 L^2 \tilde{C}^0_{NO_2}}{\tilde{D}_{NO_2}}, \quad \tilde{b} = \frac{a}{2\tilde{K}\tilde{C}^0_{NO_2}} = \frac{a}{2}\frac{\tilde{C}^0_{NO_2}}{\tilde{C}^0_{N_2O_4}}, \quad \mathrm{Da_m}\tilde{b} = \frac{\tilde{k}_{-1}L^2}{\tilde{D}_{N_2O_4}} \tag{4.108}$$

where $\mathrm{Da_m}$ is the Damkohler number for the forward reaction (4.1) in the PDMS membrane, and $\tilde{b}$ is the diffusivity-weighted concentration ratio of NO_2 to N_2O_4 in the PDMS membrane. Note that $\mathrm{Da_m}\tilde{b}$ is concentration-independent. The dimensionless boundary conditions are,

$$\theta(0) = 1 \tag{4.109}$$

$$\phi(0) = 1 \tag{4.110}$$

$$\theta(1) = \alpha \tag{4.111}$$

$$\phi(1) = \beta \tag{4.112}$$

$$\alpha = \frac{\tilde{C}^*_{NO_2}}{\tilde{C}^0_{NO_2}}, \quad \beta = \frac{\tilde{C}^*_{N_2O_4}}{\tilde{C}^0_{N_2O_4}} \tag{4.113}$$

4.7.1 Core solution in the PDMS membrane

In the membrane is one region where the dimerization reaction is nearly at equilibrium and a second one where it is not. The equilibrium region, termed the "core", encompasses most of the membrane, extending from the gas-membrane interface almost to the membrane-aqueous

interface. The nonequilibrium region is a boundary layer next to the aqueous side. The existence of the boundary layer was a significant complication in formulating and solving the microscopic model for the membrane phase. The governing equations for the core are presented first, followed by those for the boundary layer.

From Eq. (4.99) and (4.100), the following is always true:

$$\frac{d^2(\tilde{D}_{NO_2}\tilde{C}_{NO_2} + 2\tilde{D}_{N_2O_4}\tilde{C}_{N_2O_4})}{dx^2} = 0 \tag{4.114}$$

Integrating twice and using all boundary conditions from Eq. (4.101) to (4.104),

$$\tilde{D}_{NO_2}\tilde{C}_{NO_2} + 2\tilde{D}_{N_2O_4}\tilde{C}_{N_2O_4} = (\tilde{D}_{NO_2}\tilde{C}^0_{NO_2} + 2\tilde{D}_{N_2O_4}\tilde{C}^0_{N_2O_4})\left(-\frac{x}{L}\right) + (\tilde{D}_{NO_2}\tilde{C}^*_{NO_2} + 2\tilde{D}_{N_2O_4}\tilde{C}^*_{N_2O_4})\left(1+\frac{x}{L}\right)$$

(4.115)

Using the dimensionless variables (Eq. (4.105), (4.108), and (4.113)), Eq. (4.115) is expressed as

$$\tilde{b}\,\theta + \phi = (\tilde{b}+1)(1-\eta) + (\tilde{b}\,\alpha + \beta)\eta \tag{4.116}$$

Once again, it is emphasized that Eq. (4.116) is true throughout the PDMS membrane, without any assumptions. From Eqs. (4.106) and (4.107), if the second derivative is ignored, the core solution is

$$\theta^2 = \phi \tag{4.117}$$

Combining Eq. (4.116) with Eq. (4.117), and solving the quadratic equation for θ and ϕ,

$$\theta_{Core}(\eta) = \frac{-\tilde{b} + \sqrt{\tilde{b}^2 + 4[(\tilde{b}+1)(1-\eta) + (\tilde{b}\alpha + \beta)\eta]}}{2} \tag{4.118}$$

$$\phi_{core}(\eta) = (\tilde{b}+1)(1-\eta) + (\tilde{b}\alpha + \beta)\eta + \frac{\tilde{b}^2}{2} - \tilde{b}\sqrt{(\tilde{b}+1)(1-\eta) + (\tilde{b}\alpha + \beta)\eta + \frac{\tilde{b}^2}{4}} \tag{4.119}$$

These core solutions satisfy the boundary conditions at the gas-PDMS membrane interface [Eq. (4.109) and (4.110)], because the equilibrium relation at x = -L satisfies Eq. (4.117). However, the core solutions cannot satisfy the boundary conditions at the liquid-PDMS membrane interface [Eq. (4.111) and (4.112)], because NO_2 and N_2O_4 might not be in equilibrium at x = 0. This is because of the diffusion and hydrolysis of N_2O_4 in the liquid. In other words, the second derivative cannot be ignored near at x = 0. Also, this means that there is a membrane boundary layer near x = 0. So, a different scaled variable is needed for this membrane boundary layer.

4.7.2 PDMS Membrane Boundary Layer

To rescale the coordinate for the boundary layer, let

$$Z = (1-\eta)\mathrm{Da_m}^{C} \tag{4.120}$$

The quantity $(1-\eta)$, which is small in the membrane boundary layer, is stretched by $\mathrm{Da_m}^{C}$ to obtain a new coordinate Z which is of order one. Transforming the coordinate in Eq. (4.106),

$$\mathrm{Da_m}^{2C}\frac{d^2\theta}{dZ^2} - \mathrm{Da_m}(\theta^2 - \phi) = 0 \tag{4.121}$$

Both terms are balanced when C = 1/2. Thus, the boundary coordinate is

$$Z = (1-\eta)\mathrm{Da_m}^{1/2} \tag{4.122}$$

Based on the new boundary coordinate, the dimensionless conservation equations are

$$\frac{d^2\hat{\theta}}{dZ^2} - \hat{\theta}^2 + \hat{\phi} = 0 \tag{4.123}$$

$$\frac{d^2\hat{\phi}}{dZ^2} + \tilde{b}(\hat{\theta}^2 - \hat{\phi}) = 0 \tag{4.124}$$

To distinguish between the core and boundary layer regions, the concentrations in the boundary layer are denoted as $\hat{\theta} = \hat{\theta}(Z)$ and $\hat{\phi} = \hat{\phi}(Z)$. The boundary conditions at $x = 0$ which correspond to $Z = 0$ are

$$\hat{\theta}(0) = \alpha \tag{4.125}$$

$$\hat{\phi}(0) = \beta \tag{4.126}$$

The other conditions are obtained by asymptotic matching with the core solution. The main problem with Eq. (4.123) and (4.124) is that both are nonlinear, second-order differential equations. Thus, it is not possible to obtain analytical solutions for the boundary layer. For this reason, the matching cannot be done in a typical asymptotic manner. However, there is an analytical solution in the core region as already mentioned. For large values of the boundary coordinate Z, the concentrations in both regions must be the same. This means that

$$\lim_{Z\to\infty} \hat{\theta}(Z) = \lim_{Z\to\infty} \theta_{Core}(Z) = \lim_{Z\to\infty} \left\{ \frac{-\tilde{b} + \sqrt{\tilde{b}^2 + 4[(\tilde{b}+1)ZDa_m^{-1/2} + (\tilde{b}\alpha + \beta)(1 - ZDa_m^{-1/2})]}}{2} \right\} \tag{4.127}$$

$$\lim_{Z\to\infty}\hat{\phi}(Z)=\lim_{Z\to\infty}\phi_{core}(Z)$$

$$=\lim_{Z\to\infty}\left\{(\tilde{b}+1)ZDa_m^{-1/2}+(\tilde{b}\alpha+\beta)(1-ZDa_m^{-1/2})+\frac{\tilde{b}^2}{2}-\tilde{b}\sqrt{(\tilde{b}+1)ZDa_m^{-1/2}+(\tilde{b}\alpha+\beta)(1-ZDa_m^{-1/2})+\frac{\tilde{b}^2}{4}}\right\} \tag{4.128}$$

Practically, for large values of Z,

$$\hat{\theta}(Z)=\frac{-\tilde{b}+\sqrt{\tilde{b}^2+4[(\tilde{b}+1)ZDa_m^{-1/2}+(\tilde{b}\alpha+\beta)(1-ZDa_m^{-1/2})]}}{2} \tag{4.129}$$

$$\hat{\phi}(Z)=(\tilde{b}+1)ZDa_m^{-1/2}+(\tilde{b}\alpha+\beta)(1-ZDa_m^{-1/2})+\frac{\tilde{b}^2}{2}-\tilde{b}\sqrt{(\tilde{b}+1)ZDa_m^{-1/2}+(\tilde{b}\alpha+\beta)(1-ZDa_m^{-1/2})+\frac{\tilde{b}^2}{4}} \tag{4.130}$$

Eqs. (4.123) and (4.124) with the boundary conditions in Eqs. (4.125), (4.126), (4.129) and (4.130), were solved numerically to compute the solution for the PDMS membrane. For the matching conditions, values of Z were found that were large enough that further increases did not affect the results significantly. Values about 20 were found to be satisfactory for 10^{-6}% accuracy in the concentration gradient (flux).

4.8 Combined Membrane-Aqueous Microscopic Model

The microscopic models for the PDMS membrane and the aqueous solution (liquid film) will be combined now. Both NO_2 and N_2O_4 gases are delivered through the PDMS tubing which is in contact with the liquid. In this combined case, from Eqs. (4.105) to (4.110) still apply. However, the boundary conditions at the aqueous edge of PDMS membrane [Eq. (4.111) and (4.112)] are now changed. At the interface between the PDMS membrane and the liquid film,

which corresponds to $x = 0$ ($Z = 0$), the fluxes of NO_2 and N_2O_4 should be continuous. Accordingly,

$$\widetilde{D}_{NO_2}\frac{d\widetilde{C}_{NO_2}(0)}{dx} = D_{NO_2}\frac{dC_{NO_2}(0)}{dx} \tag{4.131}$$

$$\widetilde{D}_{N_2O_4}\frac{d\widetilde{C}_{N_2O_4}(0)}{dx} = D_{N_2O_4}\frac{dC_{N_2O_4}(0)}{dx} \tag{4.132}$$

In terms of the dimensionless variables previously defined,

$$-\frac{\widetilde{D}_{NO_2}\sqrt{Da_m}\widetilde{C}^0_{NO_2}}{L}\frac{d\hat{\theta}(0)}{dZ} = \frac{D_{NO_2}C^0_{NO_2}}{\delta}\frac{d\Theta(0)}{d\zeta} \tag{4.133}$$

$$-\frac{\widetilde{D}_{N_2O_4}\sqrt{Da_m}\widetilde{C}^0_{N_2O_4}}{L}\frac{d\hat{\phi}(0)}{dZ} = \frac{D_{N_2O_4}C^0_{N_2O_4}}{\delta}\frac{d\Phi(0)}{d\zeta} \tag{4.134}$$

The other boundary conditions at the interface between the membrane and liquid film are

$$\widetilde{C}^*_{NO_2} = Q_{NO_2}C^0_{NO_2} \tag{4.135}$$

$$\widetilde{C}^*_{N_2O_4} = Q_{N_2O_4}C^0_{N_2O_4} \tag{4.136}$$

Note that NO_2 and N_2O_4 do not have to be in equilibrium at the membrane-liquid interface. In terms of the dimensionless variables,

$$\widetilde{C}^0_{NO_2}\hat{\theta}(0) = Q_{NO_2}C^0_{NO_2}\Theta(0) \tag{4.137}$$

$$\widetilde{C}^0_{N_2O_4}\hat{\phi}(0) = Q_{N_2O_4}C^0_{N_2O_4}\Phi(0) \tag{4.138}$$

For the liquid film part, the governing equations are slightly changed compared to the previous ones [Eqs. (4.30) to (4.32)] because the equilibrium relationship between NO_2 and N_2O_4 is not valid any more at the membrane-liquid interface. The modified equations are

$$\frac{d^2\Theta}{d\zeta^2} - \mathrm{Da}_1(\Theta^2 - c\Phi) = 0 \tag{4.139}$$

$$\frac{d^2\Phi}{d\zeta^2} + \mathrm{Da}_1 b'\Theta^2 - \left(1 + \frac{k_{-1}}{k_2}\right)\mathrm{Da}_2\Phi = 0 \tag{4.140}$$

$$\mathrm{Da}_1 = \frac{2k_1\delta^2 C^0_{NO_2}}{D_{NO_2}}, \quad \mathrm{Da}_2 = \frac{k_2\delta^2}{D_{N_2O_4}}, \quad b' = \frac{a}{2cKC^0_{NO_2}} = \frac{a}{2c}\frac{C^0_{NO_2}}{C^0_{N_2O_4}}, \quad \mathrm{Da}_1 b' = \frac{k_{-1}\delta^2}{cD_{N_2O_4}} \tag{4.141}$$

$$c = \frac{C^0_{N_2O_4}}{K{C^0_{NO_2}}^2} \tag{4.142}$$

where c shows the degree of the deviation from the equilibrium relationship (In the case of equilibrium, c=1). The boundary conditions at the end of the liquid film are still the same [Eq. (4.35) and (4.36)]. At the interface with the PDMS membrane, Eq. (4.133), (4.134), (4.137), and (4.138) are boundary conditions coupled with the membrane ones. Due to the breakdown of the local equilibrium at the interface between the PDMS membrane and the liquid, it is impossible to apply the QEA to the liquid film in the combined case.

4.8.1 Limiting Form of Combined Model for Very Low Total Nitrogen Concentration

For very low total nitrogen concentrations, it is possible to obtain an analytical solution for the combined model, as with the aqueous model. By the same reasoning as the limiting aqueous form in this limit, the NO_2 conservation equation in the membrane is

$$\tilde{D}_{NO_2}\frac{d^2\tilde{C}_{NO_2}}{dx^2}=0 \tag{4.143}$$

The corresponding boundary conditions for NO_2 are Eq. (4.101), Eq. (4.131), and Eq. (4.135). By using the liquid solution [Eq. (4.82)], the PDMS NO_2 concentration is

$$\tilde{C}_{NO_2}(x)=\tilde{C}^0_{NO_2}\left(\frac{1}{1+\dfrac{D_{NO_2}LA_c}{\tilde{D}_{NO_2}Q_A(V+A_c\delta)}}-1\right)\left(1+\frac{x}{L}\right)+\tilde{C}^0_{NO_2} \tag{4.144}$$

$$\tilde{M}=\left(\frac{1}{1+\dfrac{D_{NO_2}LA_c}{\tilde{D}_{NO_2}Q_A(V+A_c\delta)}}-1\right)\frac{\tilde{C}^0_{NO_2}}{L} \tag{4.145}$$

The liquid NO_2 concentration and the NO_2 flux at PDMS-liquid interface can be expressed as

$$C^0_{NO_2}=\tilde{C}^0_{NO_2}\left(\frac{1}{Q_A+\dfrac{D_{NO_2}LA_c}{\tilde{D}_{NO_2}(V+A_c\delta)}}\right)\cong\left[1-\frac{D_{NO_2}LA_c}{\tilde{D}_{NO_2}Q_A(V+A_c\delta)}\right]\frac{\tilde{C}^0_{NO_2}}{Q_A} \tag{4.146}$$

$$-\tilde{D}_{NO_2}\frac{d\tilde{C}_{NO_2}(0)}{dx}=-\frac{\tilde{D}_{NO_2}\tilde{C}^0_{NO_2}}{L}\left(\frac{1}{1+\dfrac{D_{NO_2}LA_c}{\tilde{D}_{NO_2}Q_A(V+A_c\delta)}}-1\right)\cong\frac{D_{NO_2}A_c\tilde{C}^0_{NO_2}}{Q_A+(V+A_c\delta)} \tag{4.147}$$

By the same reasoning as the limiting aqueous form, the N_2O_4 conservation equation in the membrane is the same as Eq. (4.100). With the boundary condition (4.136), using the same reasoning, the PDMS N_2O_4 concentration is

$$\tilde{C}_{N_2O_4}(x) = \tilde{K}\tilde{C}_{NO_2}(x+L)^2 + \frac{2\tilde{K}\tilde{M}^2}{\tilde{\lambda}^2}(1-e^{-\tilde{\lambda}(x+L)}) \tag{4.148}$$

$$\tilde{\lambda} = \sqrt{\frac{\tilde{k}_{-1}}{\tilde{D}_{N_2O_4}}} = \frac{\sqrt{Da_m \tilde{b}}}{L} \tag{4.149}$$

By using Eqs. (4.78) and (4.148) together with boundary conditions Eqs. (4.132) and (4.136), it is possible to obtain the liquid N_2O_4 concentration and flux at the PDMS-liquid interface. It should be noted that at very low total nitrogen concentrations, almost all nitrogen is in the form of NO_2.

4.9 Experimental Method

Preliminary experiments were performed using an NO_2 delivery device based on PDMS gas-permeable tubing. This was the same as the NO delivery system of Wang and Deen (2003), except that the tubing loop for O_2 delivery was omitted. The NO_2 tubing length was 7.5cm; otherwise, all other dimensions were the same. The surrounding temperature was 23 C. The concentration of NO_2 cannot be directly measured because there are no available instruments for measuring dissolved NO_2 in the solution. Hence, the formation rates of nitrite (NO_2^-), which is a stable end product of NO_2 in the aqueous solution, were measured by using a Griess reagent. For NO_2 delivery by direct gas-liquid contacting, a more extensive set of experiments were performed by Brian Skinn in the Deen group. Only the results with PDMS tubing are presented here.

4.10 Results

4.10.1 Equilibrium Properties of NO_2 and N_2O_4 at Gas-Liquid Interface

Figure.4.3 shows how the liquid NO_2 and N_2O_4 concentrations [Eq. (4.8)] at the gas-liquid interface change with the gas composition. In this plot, the % of NO_2 is varied from 0.001% to 1%. Relatively low NO_2 concentrations are preferable, as will be discussed later. Over the entire range, the NO2 and N2O4 concentrations differ by no more than one order of magnitude. The liquid NO_2 concentration varies linearly throughout, but the N_2O_4 concentration falls very quickly as the % NO_2 in the gas is decreased from 1 to 0.1%.

Figure.4.4 shows the effect of gas composition on the fraction of total nitrogen in the gas and liquid as NO_2. The concentrations, calculated using Eq. (4.18) and (4.19), again are at the gas-liquid interface. The dimerization reaction causes the NO_2 fraction in both phases to decline with increasing NO_2 concentrations in the gas. At a given % NO_2 in the gas, the liquid fraction is much smaller than the gas fraction because of the 100-fold greater solubility of N_2O_4.

4.10.2 Concentrations in the Liquid Film

Figure.4.5 shows dimensionless concentrations in the liquid film for two different gas compositions. As mentioned in the model development, the estimated liquid film thickness (δ) is about $80\mu m$. Concentrations are shown here for only 40% of the film, from 0 to $32\mu m$, from the interface. At the same gas composition, the N_2O_4 concentration (ϕ) decreases more quickly because the N_2O_4 concentration is proportional to the square of the NO_2 concentration (θ). As the gas concentration is decreased, the NO_2 and N_2O_4 concentrations decline more gradually with distance from the interface.

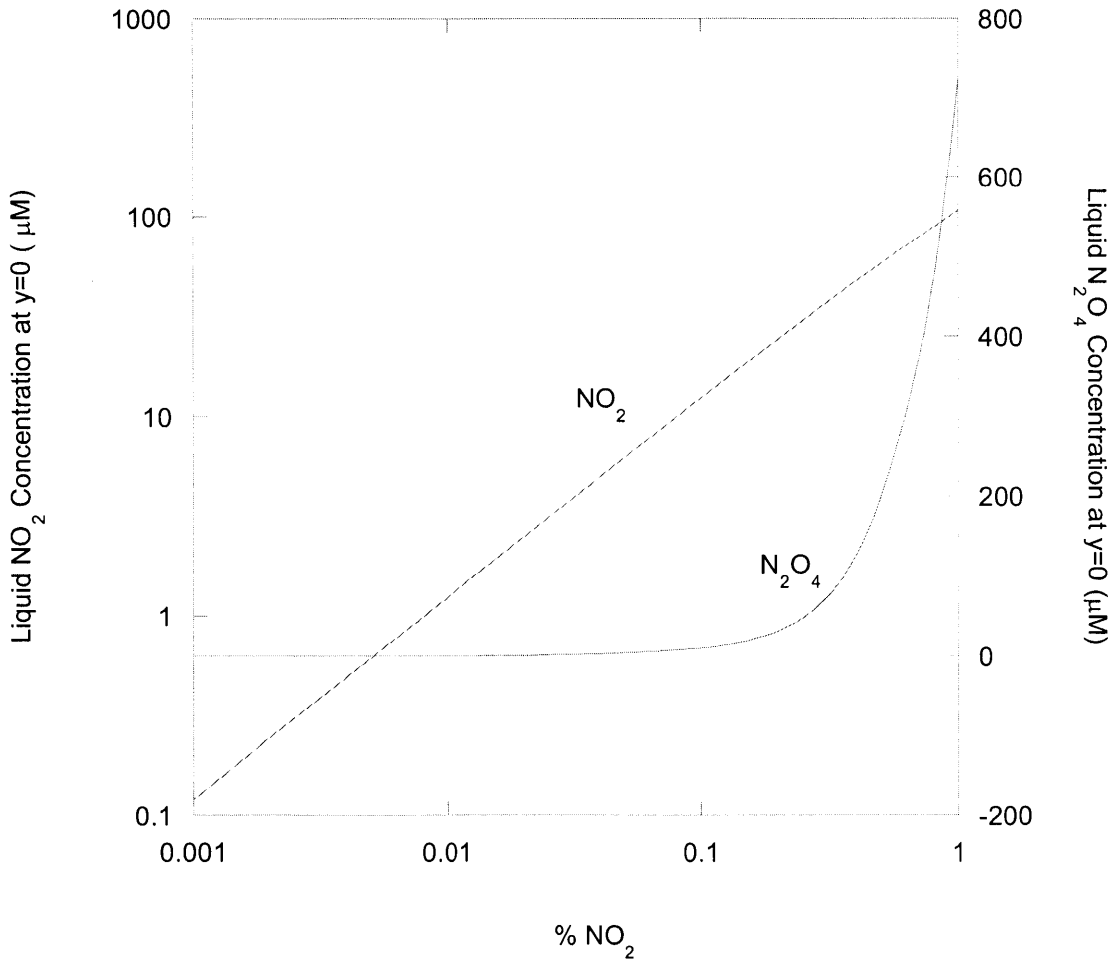

Figure 4.3. Effect of gas compositions on the liquid concentrations of NO_2 and N_2O_4 at the gas-liquid interface.

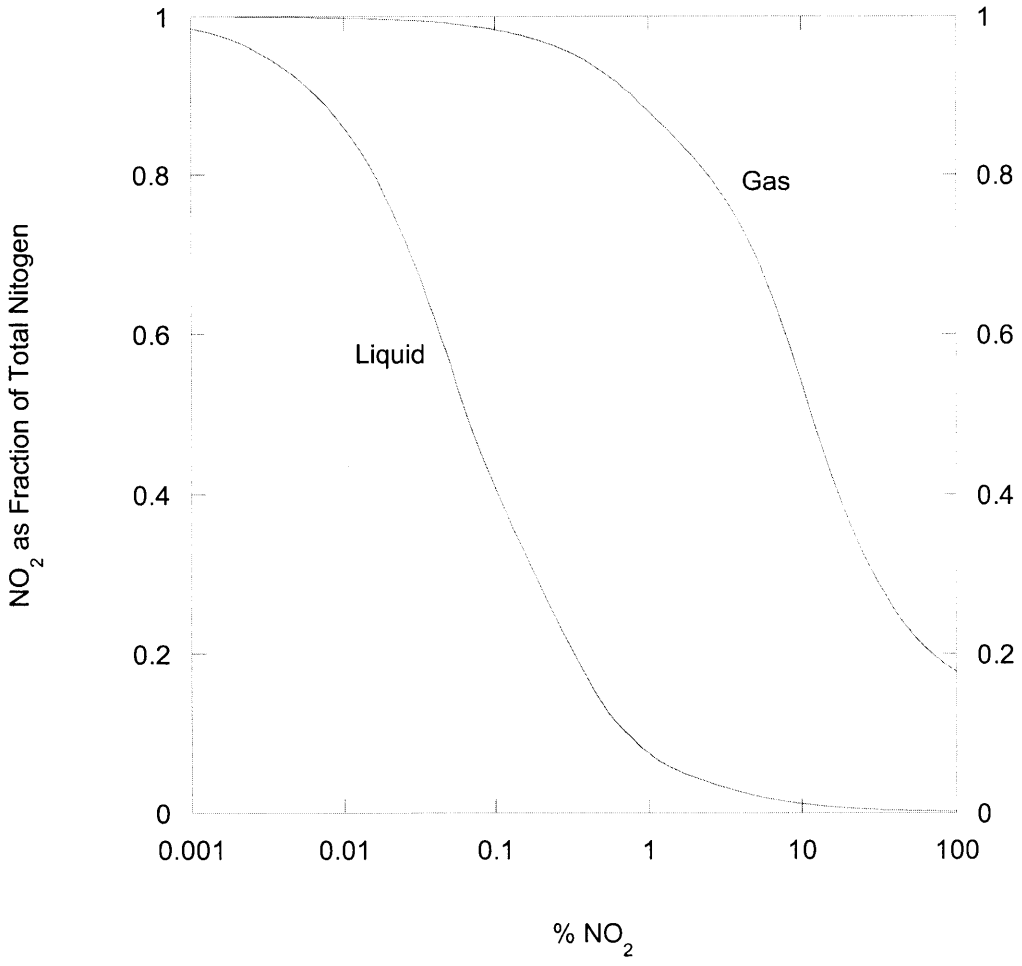

Figure 4.4. Effect of gas composition on the fractions of total nitrogen in the gas and liquid as NO_2. The liquid and gas are assumed to be in equilibrium.

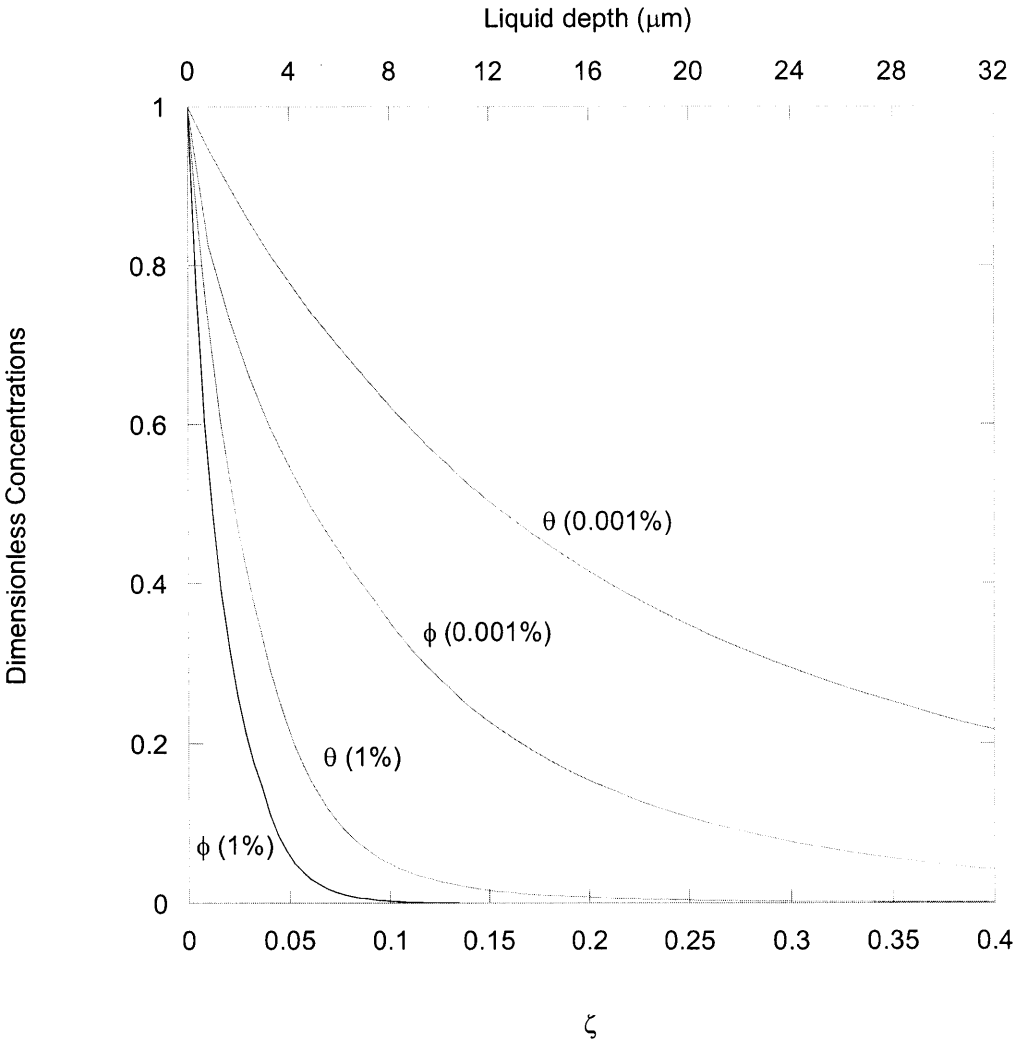

Figure 4.5. Dimensionless concentrations in the liquid film for different gas compositions, assuming a liquid film thickness of 80μm . The concentrations are scaled using the values at the gas-liquid interface.

The effect of the liquid film thickness on the NO_2 flux ratio at various % NO_2 is shown in Figure.4.6. The NO_2 flux ratio is the NO_2 flux at a given film thickness divided by that at 80μm, which is the standard liquid film thickness. In this plot the liquid film thickness (δ) is changed from 10 to 100μm .Overall, the flux ratio approaches one as δ increases. However, the liquid film thickness at which the flux ratio becomes one depends on the gas composition. For 0.001% and 0.01% NO_2 gas, the flux ratio becomes one at 75 and 24μm, respectively. Above 0.1%, the flux ratio is one even at 10μm. Overall, these results show that the NO_2 flux into the liquid is not very sensitive to the assumed film thickness (80μm), for the probable range of δ.

Figure.4.7 shows the dimensional NO_2 concentration in the whole liquid film for various gas compositions. As the gas concentration is reduced by 10 times, the maximum NO_2 concentration ($x = 0$) is also reduced about 10 times. The interfacial NO_2 concentration in the liquid ranges from 107μM for 1% NO_2 gas to 0.12μM for 0.001% NO_2 gas. However, all the well-mixed concentrations of NO_2 [$C_{NO_2}(\delta)$] at the outer edge of the liquid film for various gas compositions converge to the sub-nanomolar level. There are rapid decreases in NO_2 concentration at both edges of the film, and slower declines in the middle.

The dimensional N_2O_4 concentrations for various gas compositions are shown in Figure. 4.8. Overall, the trends are the same as for NO_2, although the concentration levels differ. The N_2O_4 concentration range at the gas-liquid interface is from 749 μM for 1% NO_2 gas to 0.96 nM for 0.001% NO_2 gas. The well-mixed N_2O_4 concentrations [$C_{N_2O_4}(\delta)$] converge at levels of tens fM. The N_2O_4 concentrations decrease more rapidly than the NO_2 concentrations.

Figures.4.9-a to 4.9-d directly compare the NO_2 and N_2O_4 concentrations for specific gas compositions. These figures clearly demonstrate that the N_2O_4 concentration diminishes more

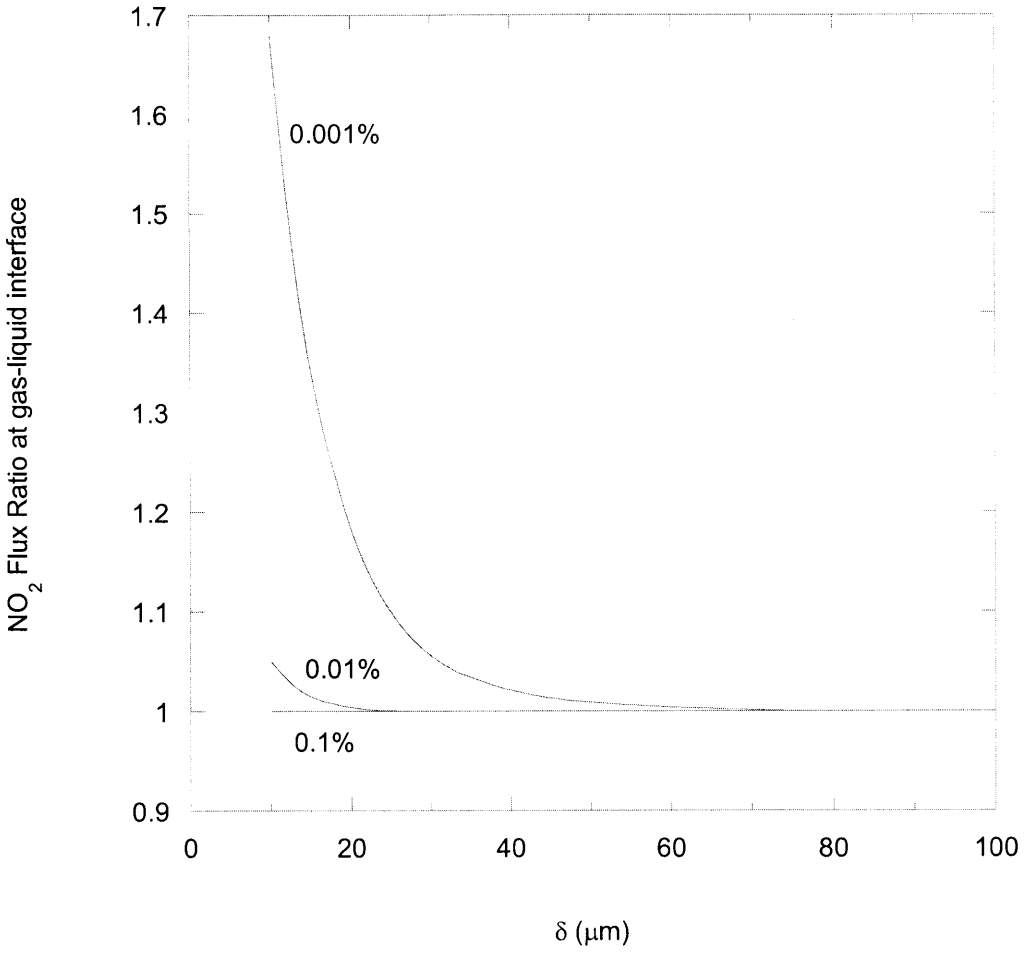

Figure 4.6. Effect of the liquid film thickness on the NO_2 flux ratio at the gas-liquid interface for various % NO_2. The NO_2 flux ratio is the flux at the given film thickness divided by that $\delta = 80\mu m$, which is the standard liquid film thickness.

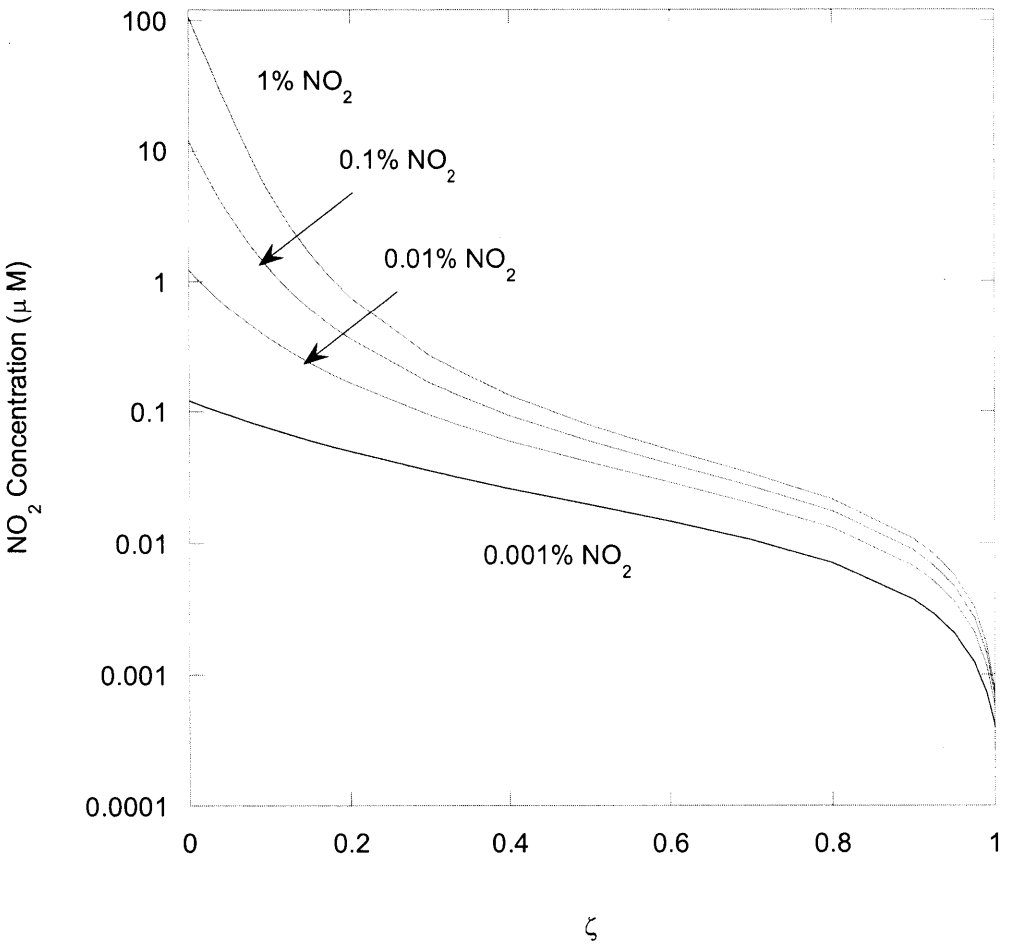

Figure 4.7. NO_2 concentration as a function of position in the liquid film, for various % NO_2.

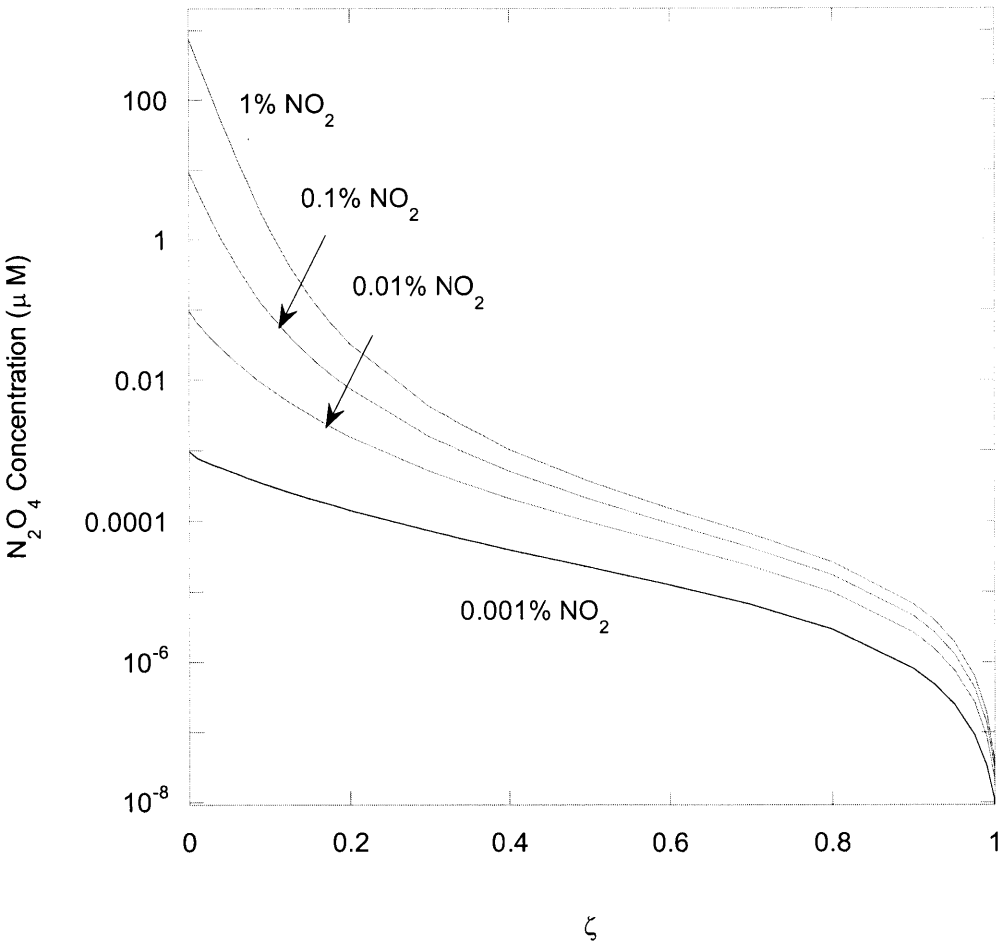

Figure 4.8. N_2O_4 concentration as a function of position in the liquid film, for various % NO_2.

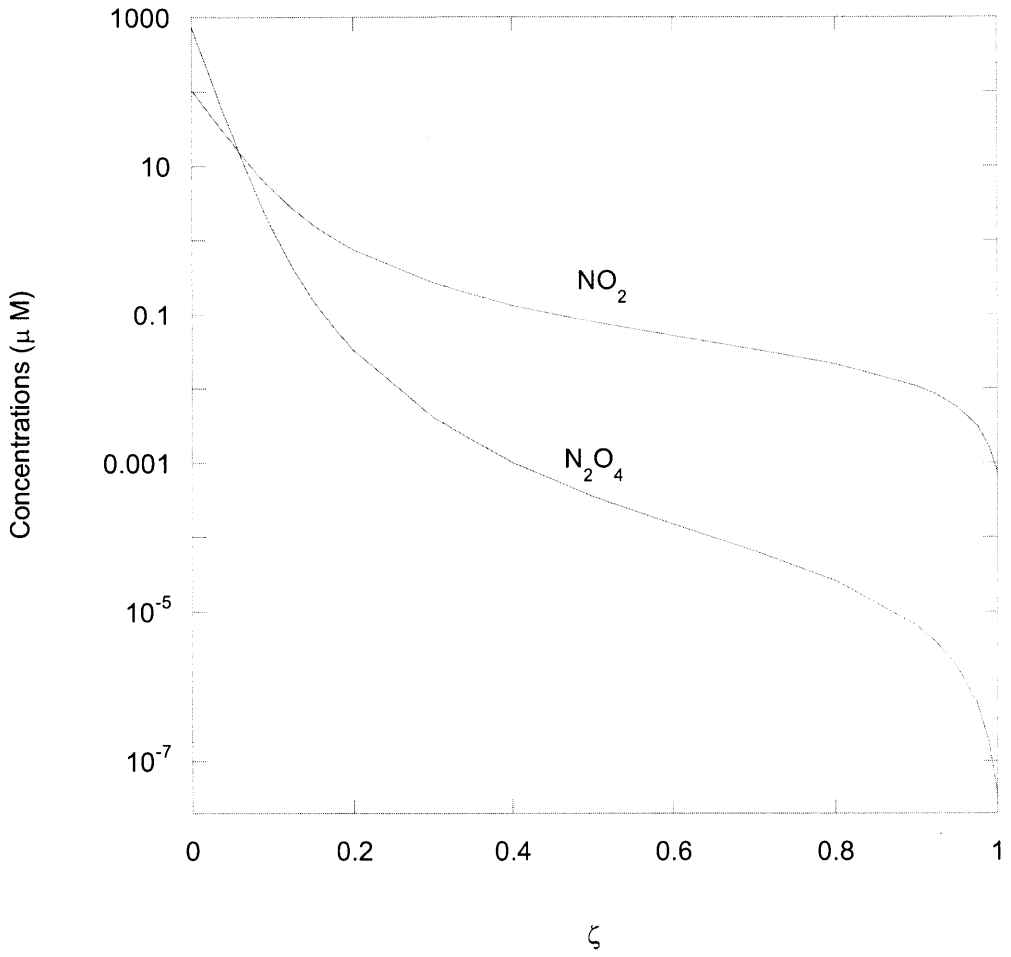

Figure 4.9-a. NO_2 and N_2O_4 concentration profiles for 1% NO_2 gas.

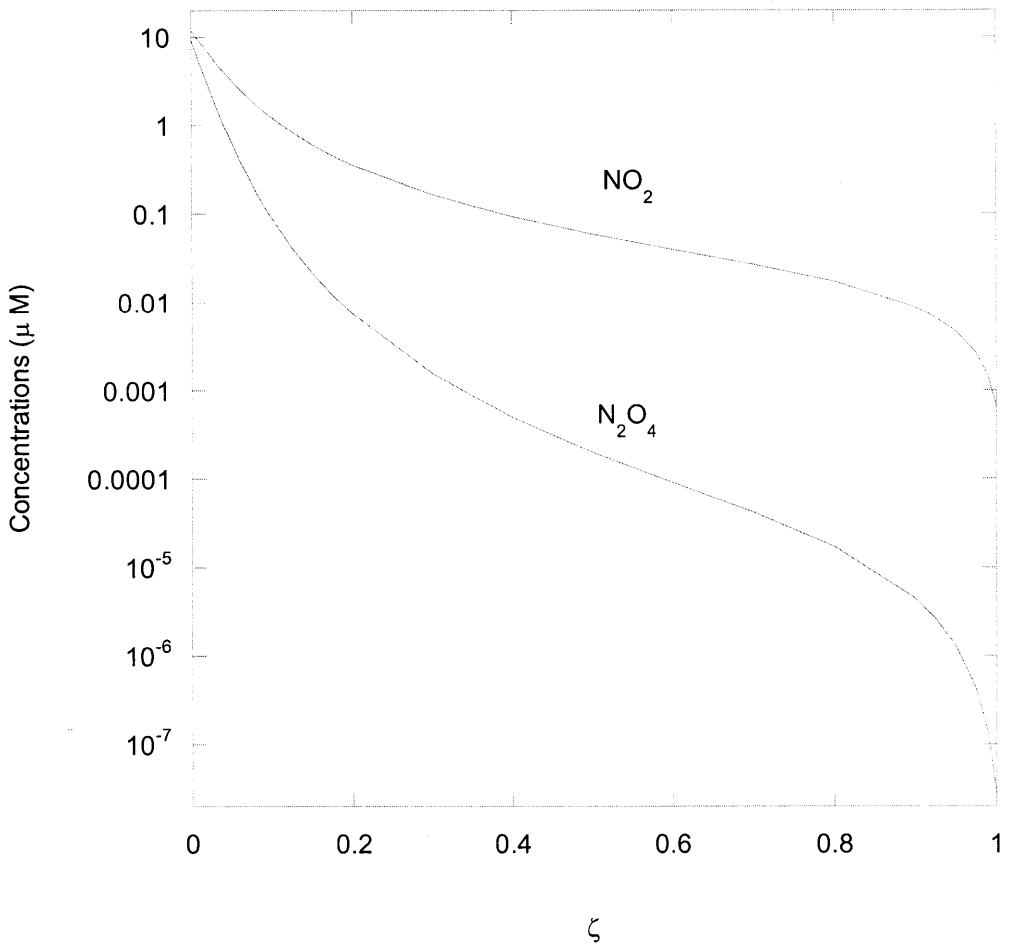

Figure 4.9-b. NO_2 and N_2O_4 concentration profiles for 0.1% NO_2 gas.

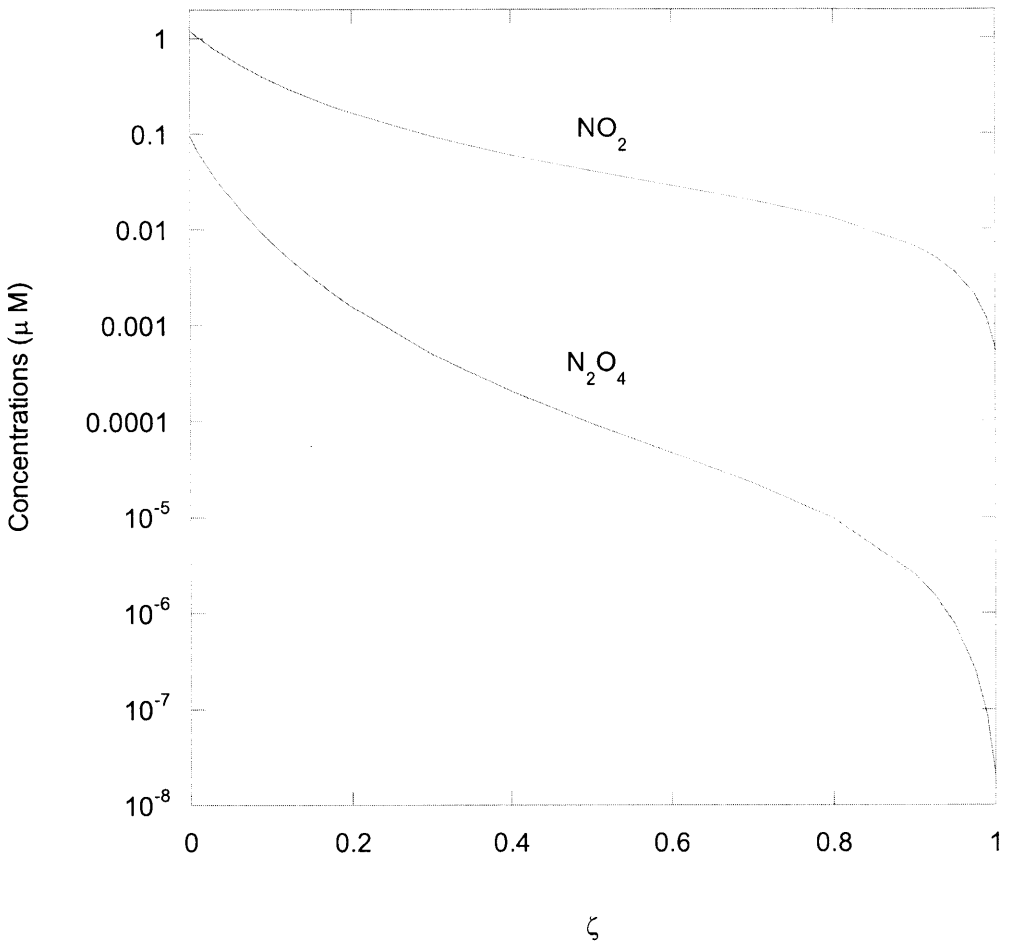

Figure 4.9-c. NO_2 and N_2O_4 concentration profiles for 0.01% NO_2 gas.

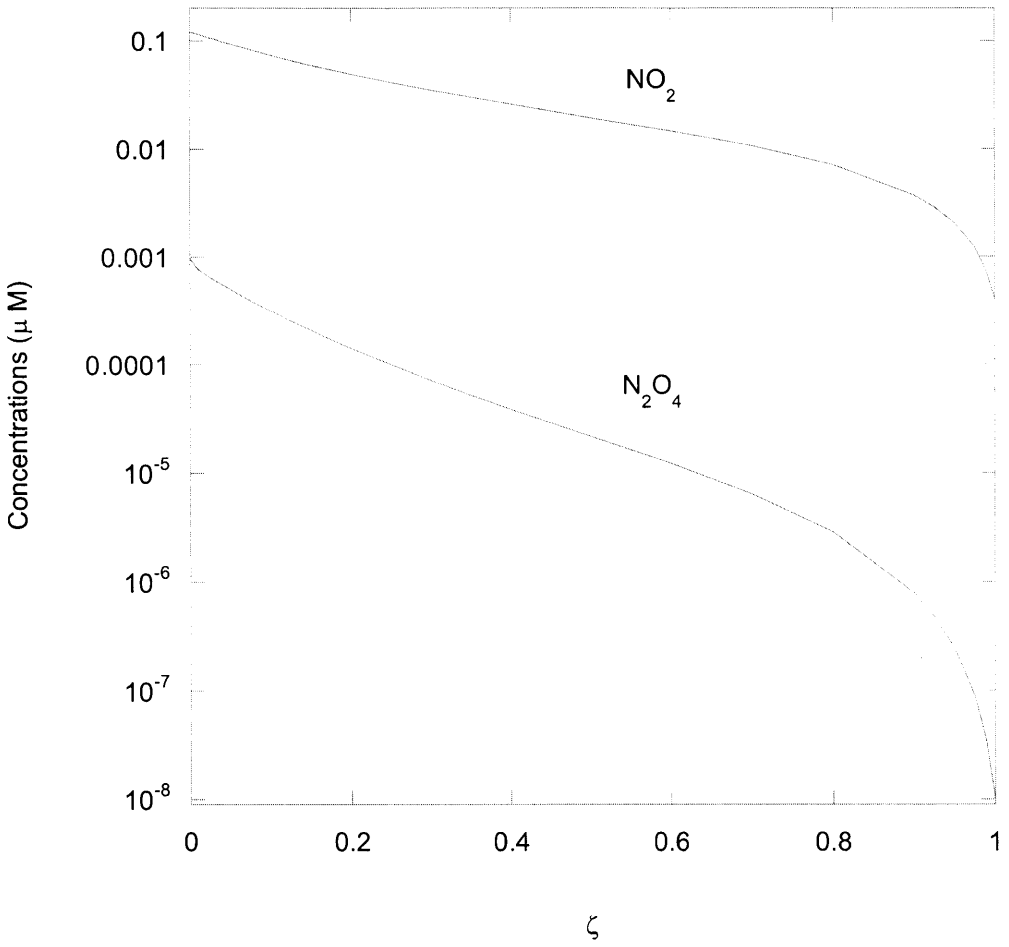

Figure 4.9-d. NO_2 and N_2O_4 concentration profiles for 0.001% NO_2 gas.

rapidly than the NO_2 concentration. When the NO_2 concentration at the gas-liquid interface is reduced by 10 times, the corresponding N_2O_4 concentration is reduced approximately by 100 times. Also, these figures compare the well-mixed concentrations of NO_2 and N_2O_4.

4.10.3 Fractional Flux as NO_2 at Gas-Liquid interface

Figure.4.10 shows the effect of gas composition on the fraction of the nitrogen flux at the gas-liquid interface ($x = 0$) that is in the form of NO_2. The fractional flux as NO_2 (F_{NO_2}) is

$$F_{NO_2} = \frac{D_{NO_2}\dfrac{dC_{NO_2}(0)}{dx}}{D_{NO_2}\dfrac{dC_{NO_2}(0)}{dx} + 2D_{N_2O_4}\dfrac{dC_{N_2O_4}(0)}{dx}} \tag{4.150}$$

The overall shape and trend of the graph are similar to that of the liquid fraction as NO_2 (Figure.4.4). The minor difference is that the fraction of the nitrogen flux as N_2O_4 remains noticeable (6.6%) even at 0.001% NO_2 gas.

4.10.4 Comparisons of Various Liquid Microscopic Models for Direct Contacting

Figure. 4.11 compares NO_2 concentrations from the exact model with that of the QEA model. For both models, the dimensionless NO_2 concentrations are plotted for three different gas compositions. The very similar concentration profiles show that the QEA is generally quite satisfactory. As shown, the NO_2 concentrations for both models are indistinguishable at 10% NO_2 gas. At lower gas concentrations, the gap between the two models becomes broader, although it is never large.

Figure.4.12-a shows percent errors in the total flux at the gas-liquid interface for various liquid microscopic models, over a wide range of gas compositions. "Low Nitrogen" and "High Nitrogen" represent limiting forms of the QEA for low and high nitrogen concentrations, respectively. All percent errors are based on the total flux obtained from the exact equations.

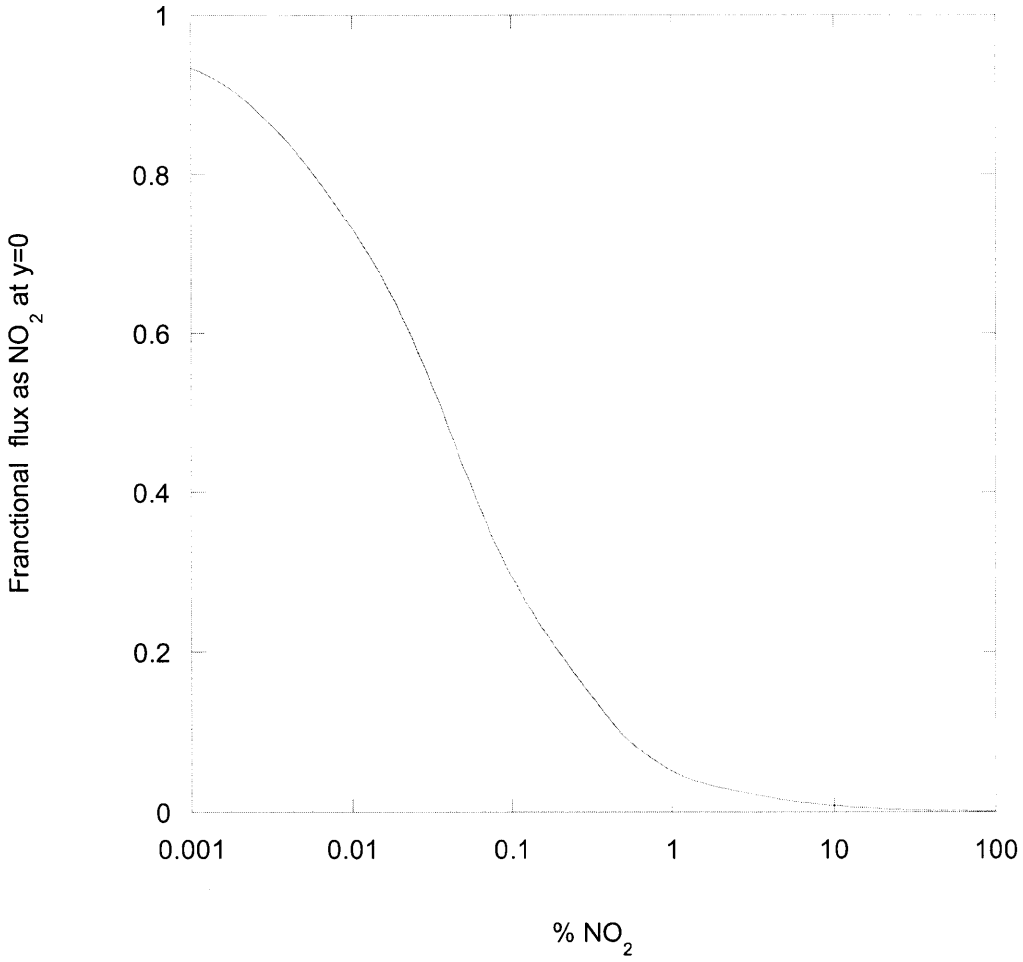

Figure 4.10. Effect of gas composition on the fraction of the total nitrogen flux as NO_2. The flux is evaluated at the gas-liquid interface.

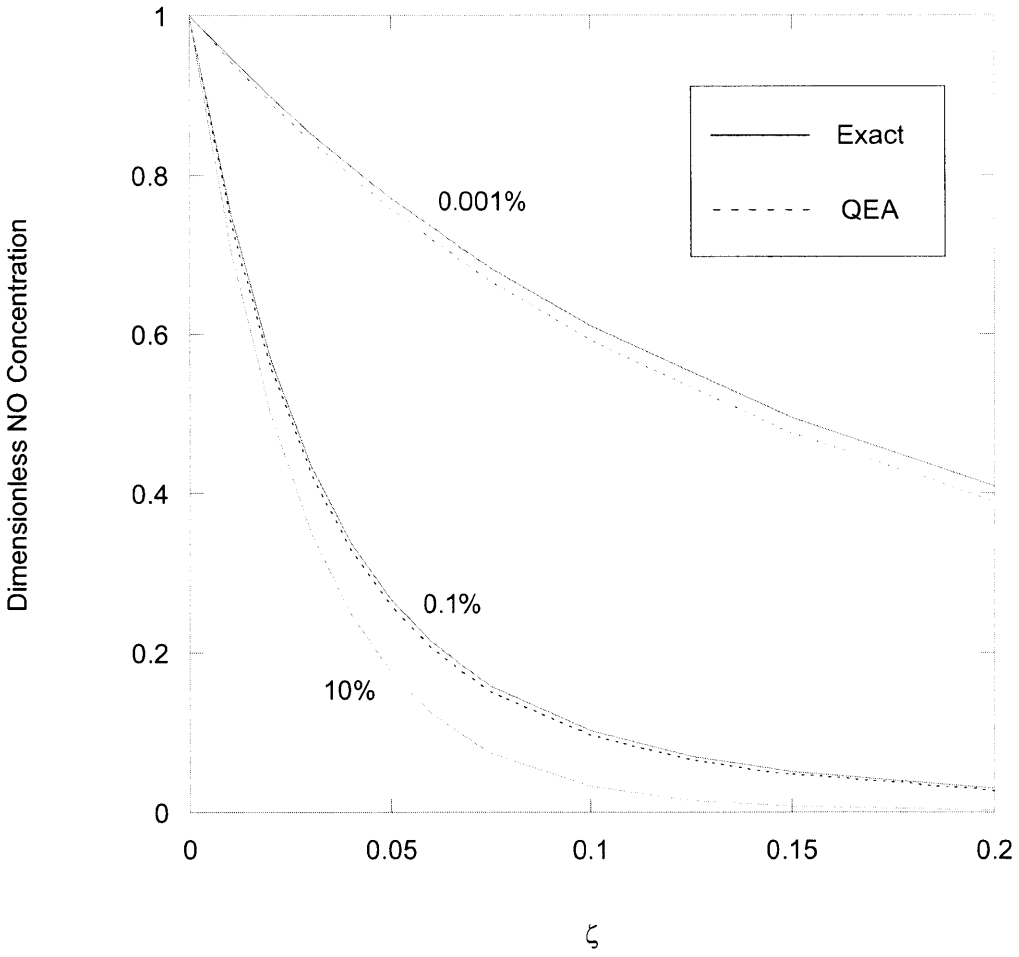

Figure 4.11. Dimensionless NO_2 concentration as a function of position in the liquid film, for various $\%NO_2$. Results from the exact equations are compared with those using the QEA.

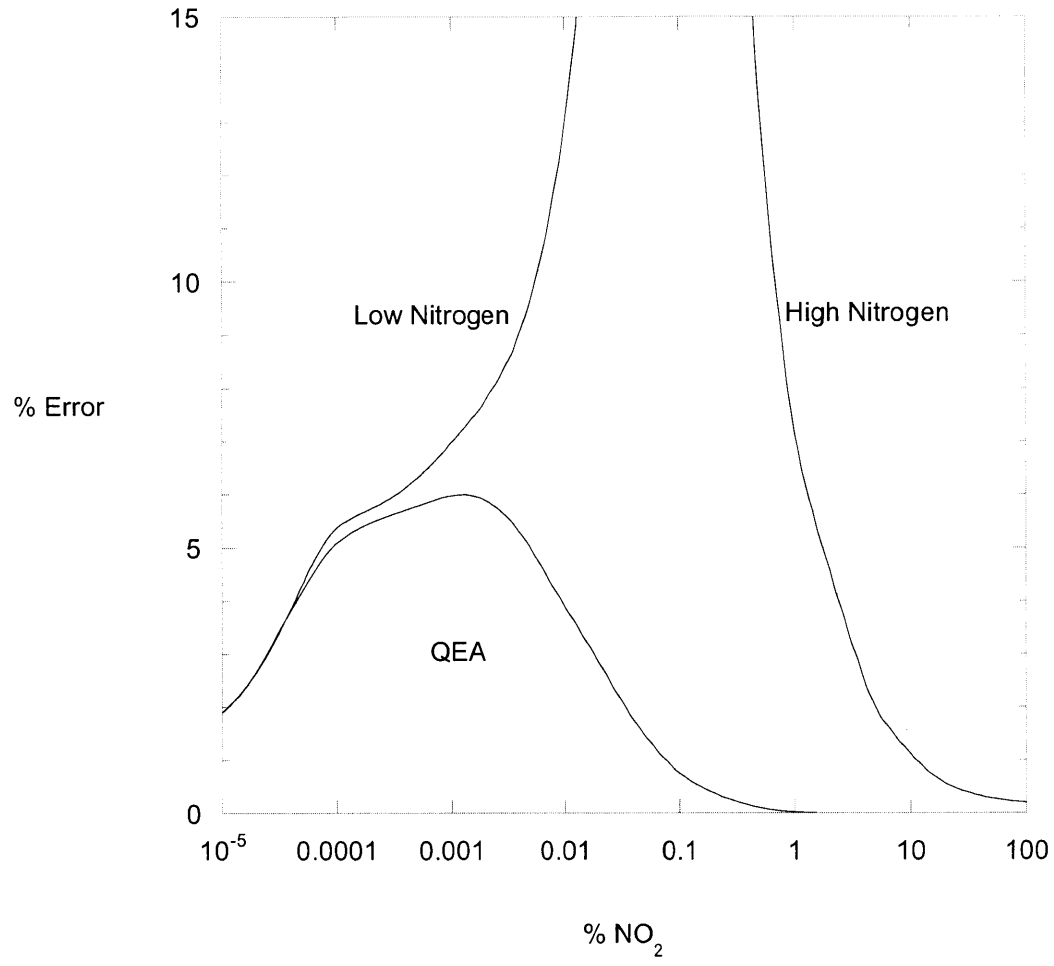

Figure 4.12-a. Percent errors in the total nitrogen flux at the gas-liquid interface for various liquid microscopic models. Results are shown for the QEA and its limiting forms for low and high nitrogen concentrations.

positive and negative values indicate that the approximation is an overestimate or an underestimate, respectively. As shown in Figure.4.12-a, the QEA and the high nitrogen limit converge for the hypothetical case of pure NO_2 gas. Above 1% NO_2 gas, the percent errors of the total flux for QEA are zero. As the gas concentration lowers, the percent error of the total flux for QEA reaches a maximum (6.1% error at 0.001% NO_2 gas) and then decreases towards zero. As expected, the QEA and the low nitrogen limit converge as the gas concentration approaches zero. At 10^{-5} % NO_2 gas, the percent errors of the total flux for the QEA and the low nitrogen limit are about 2%. Figure.4.12-b shows the percent errors of the NO_2 flux. Overall, the trends are the same as for the total flux. The percent error of the NO_2 flux has a maximum value of 15.7% at 0.01% NO_2 gas.

Figure.4.13 shows percent errors of the N_2O_4 flux at the gas-liquid interface for various liquid microscopic models, over a wide range of gas compositions. As shown, the QEA and the high nitrogen limit converge for pure NO_2 gas. This convergence is much better than that of NO_2. Even at 10% NO_2 gas, both errors are almost zero. As shown in Figure.4.8, the fractional flux as N_2O_4 is almost one in this high nitrogen range. Due to this high fractional flux of N_2O_4, the percent errors of the total flux for the QEA are nearly zero, even though the percent errors of the NO_2 flux for the QEA are not zero above 1% NO_2 gas. Unlike the NO_2 case, the percent error for the QEA becomes increasingly negative as the gas concentration falls. Once again, the QEA and the low nitrogen limit converge as the gas concentration approaches zero, but the absolute value of the error in both grow. At 0.001% NO_2 gas, the percent errors for the QEA and the low nitrogen limit are about -65%. However, the absolute error for N_2O_4 becomes smaller because the fractional flux as NO_2 is almost one in this low nitrogen range (Figure.4.10). Overall, the QEA works well in the high nitrogen limit for both NO_2 and N_2O_4. However, the QEA becomes

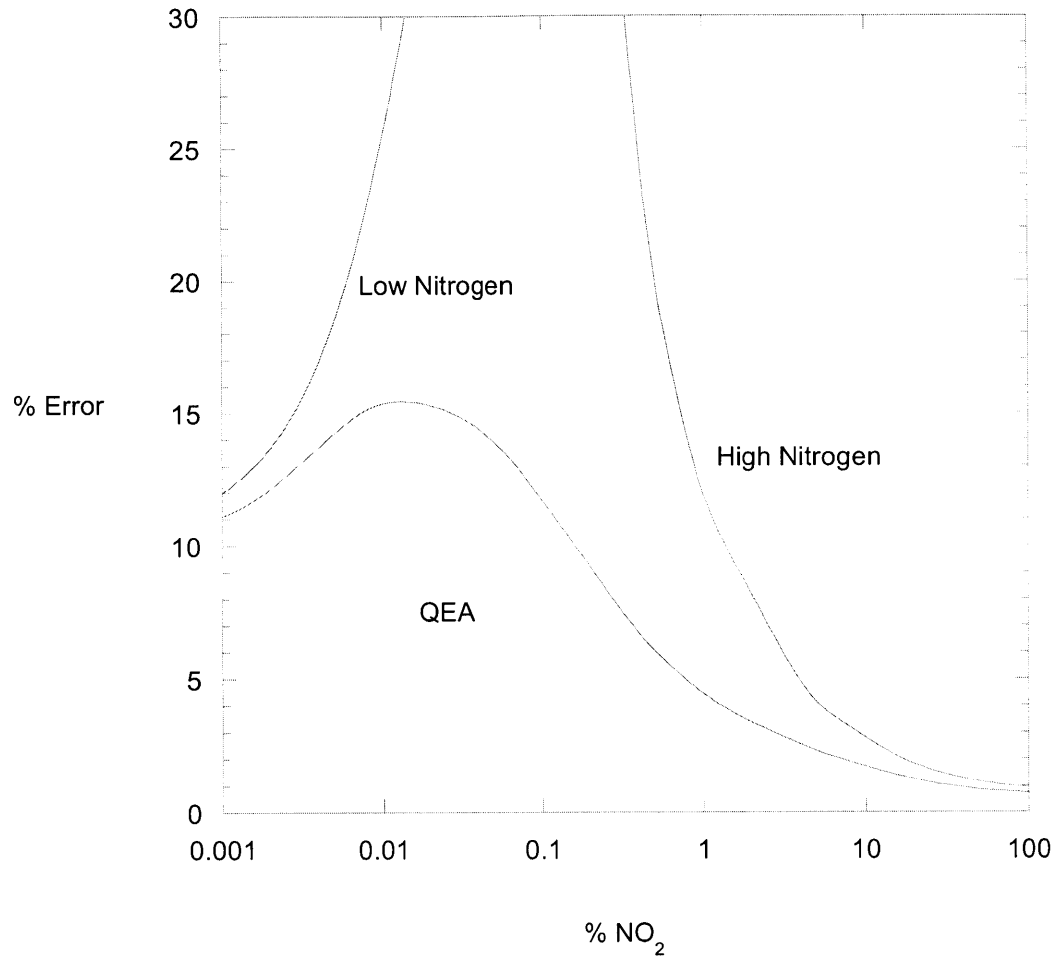

Figure 4.12-b. Percent errors in the NO_2 flux at the gas-liquid interface for various liquid microscopic models. Results are shown for the QEA and its limiting forms for low and high nitrogen concentrations.

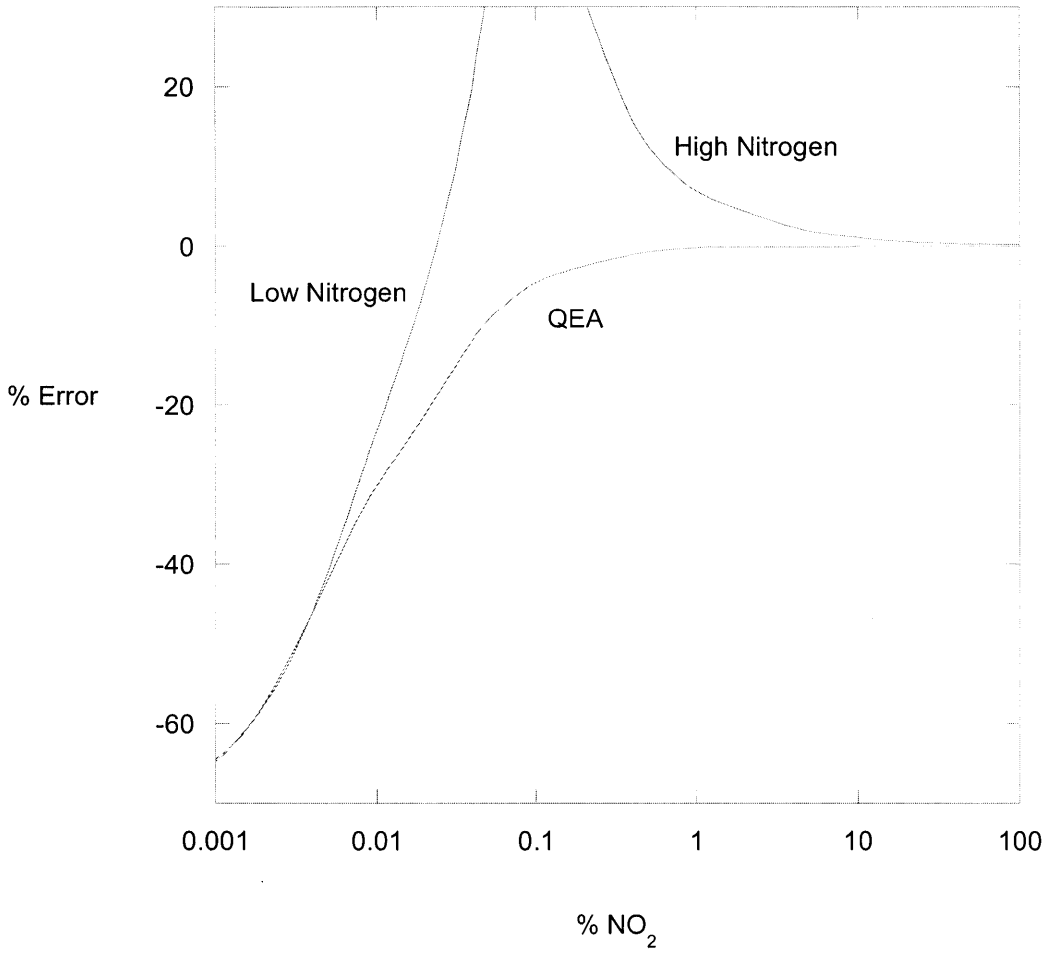

Figure 4.13. Percent errors in the N_2O_4 flux at the gas-liquid interface for various liquid microscopic models. Results are shown for the QEA and its limiting forms for low and high nitrogen concentrations.

worse at low concentrations. The reason for this will be discussed in detail later.

As defined in Eq. (4.38), κ_{NO_2} is the volume averaged (bulk) NO_2 concentration divided by that in the well-mixed region. Figure.4.14 shows κ_{NO_2} values for the exact equation, the QEA, and the low nitrogen limit. Here, the gas concentration spans low (0.001%) to moderate (1%) values. Accordingly, the high nitrogen limit was not considered at all. As shown in Figure.4.14, the range of κ_{NO_2} values for the exact equation is 1.1 at 0.001% to 10.2 at 1%. The κ_{NO_2} values from the QEA are in good agreement with those from the exact equations over the entire range of gas concentrations, although a small gap develops above 0.05% NO_2 gas. The low nitrogen limit κ_{NO_2} values become inaccurate above 0.1%. However, as expected, the low nitrogen limit κ_{NO_2} values converge with the QEA as the gas concentration becomes small. All three κ_{NO_2} values are indistinguishable at 0.001% NO_2 gas.

Figure.4.15 shows $\kappa_{N_2O_4}$ values for the exact equation, the QEA, and the low nitrogen limit. Overall, the trends are the same as those for κ_{NO_2} in Figure.4.14. However, the range of $\kappa_{N_2O_4}$ is much larger than that of κ_{NO_2}. Its range for the exact equation is 21 (0.001%) to 7.6×10^5 (1%). Whereas the value of κ_{NO_2} at 0.001% (1.1) is almost unity, the value of $\kappa_{N_2O_4}$ at 0.001% (21) is much higher than that.

As defined in Eq. (4.39), γ indicates the degree of the concentration non-uniformity. Figure.4.16 shows γ values for the exact equation, the QEA, and the low nitrogen limit. Overall, the trends are the same as for κ_{NO_2} and $\kappa_{N_2O_4}$ (Figures.4.15 and 4.16). The range of γ values for the exact equation is 16 (0.001%) to 6400 (1%). Like $\kappa_{N_2O_4}$, all three models converge as the gas concentration approaches zero, but to a value (16) that is much higher than unity.

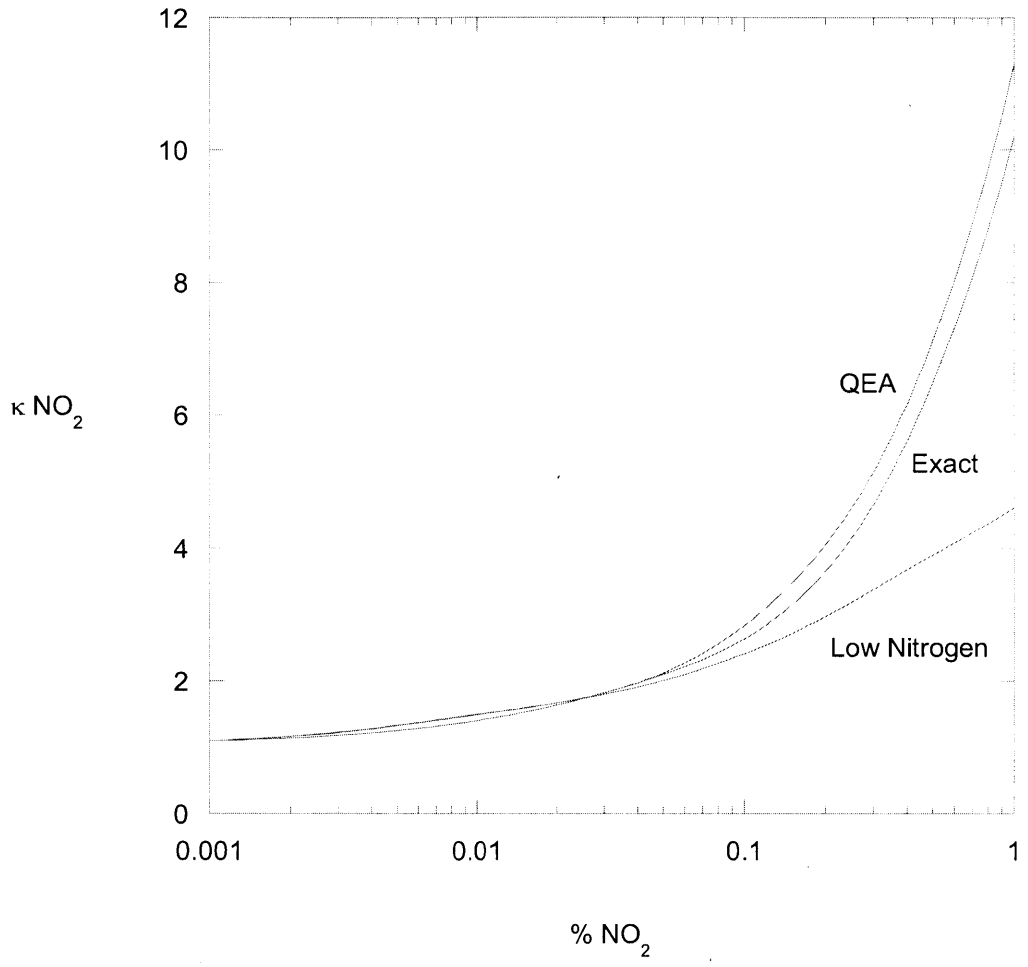

Figure 4.14. Effect of gas composition on κ_{NO_2} for various liquid microscopic models.

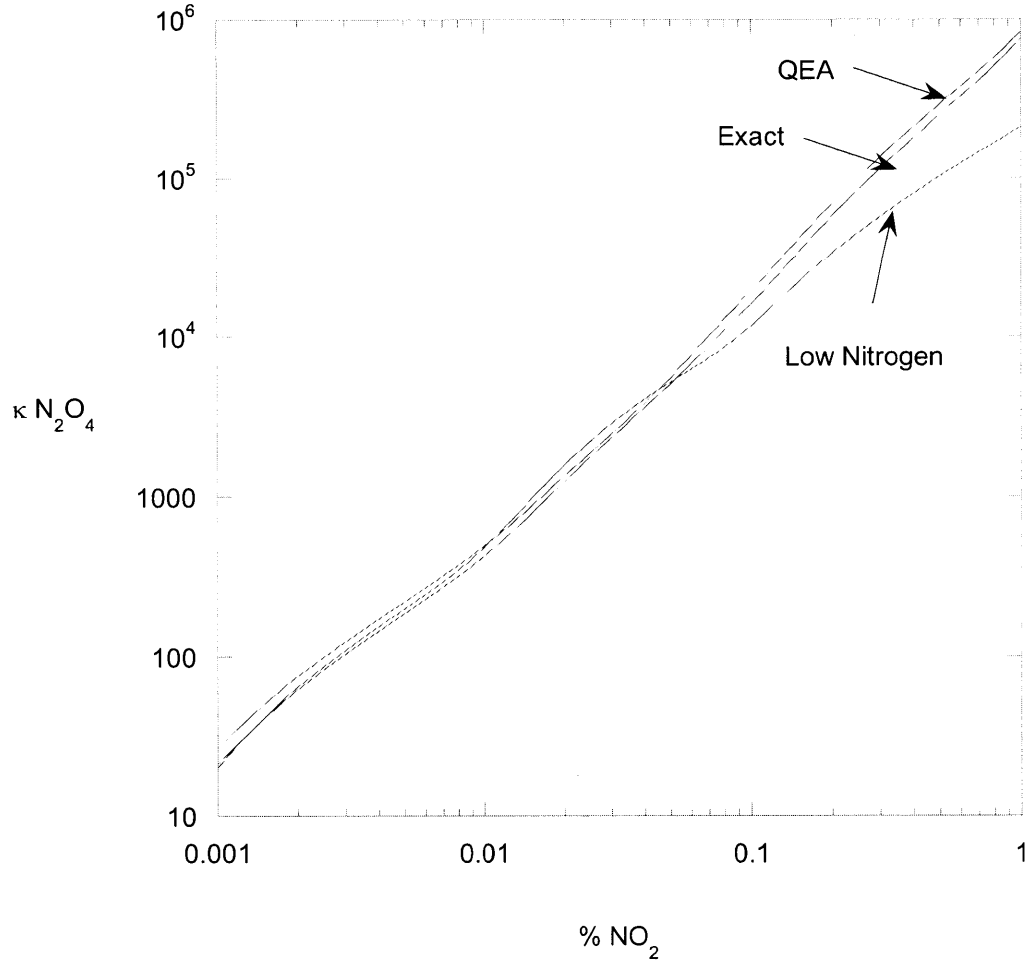

Figure 4.15. Effect of gas composition on $\kappa_{N_2O_4}$ for various liquid microscopic models.

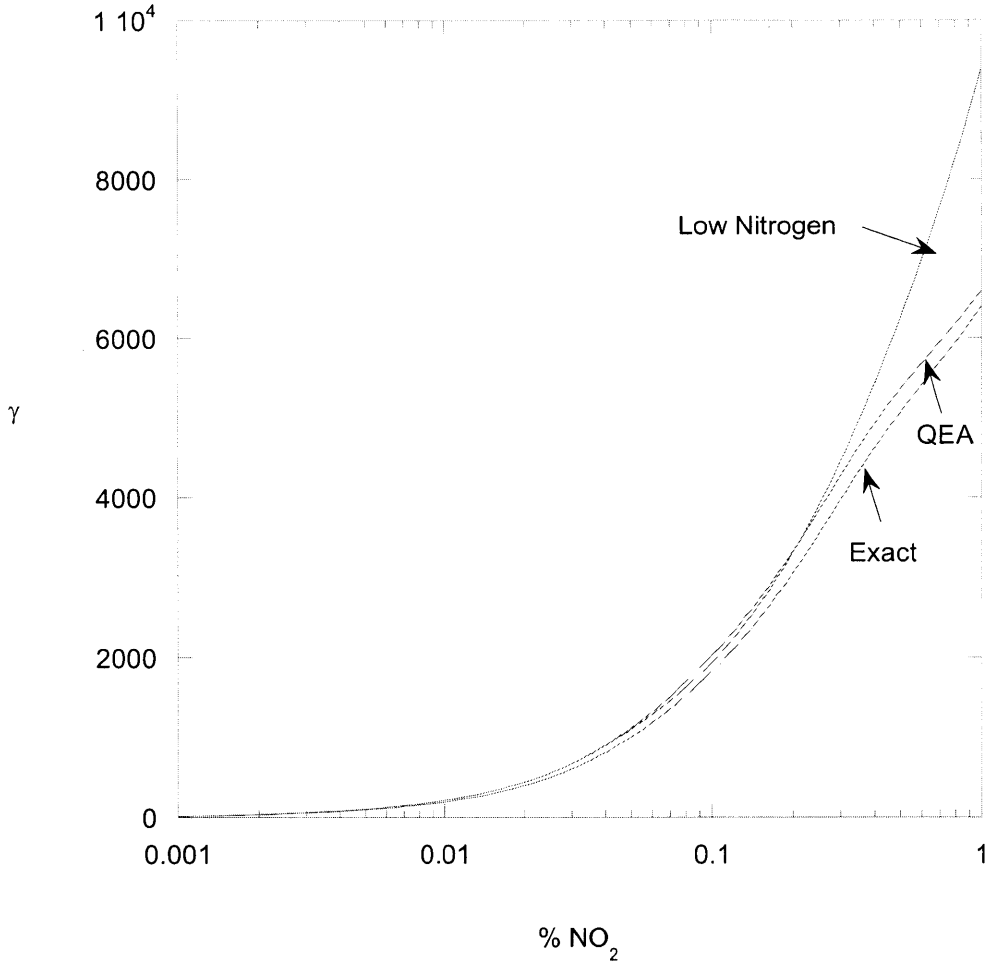

Figure 4.16. Effect of gas composition on γ for various liquid microscopic models.

4.10.5 Macroscopic Models for Direct Gas-Liquid Contact

Figure.4.17 shows the time to reach the steady-state concentration (τ) [Eq. (4.94)] for the gas-liquid case for 0.001% to 1% NO_2 gas. At 0.001%, τ is about 1 second. As the gas concentration is increased, τ decreases because both the dimerization and its reverse reaction becomes faster. At 1% NO_2 gas, τ reaches about 1 ms. Overall, the time to reach the steady-state is quite fast and the time-dependence in the macroscopic balance can be ignored. So, the aqueous volume-averaged (bulk) concentrations can be obtained from Eq. (4.95) and (4.96).

Figures.4.18-a to 4.18-d show the NO_2 and N_2O_4 bulk concentrations as functions of time for various gas compositions. As already shown in Figure.4.17, the time to reach steady-state is about 1 ms at 1% NO_2 gas (Figure.4.18-a). The bulk concentrations of NO_2 and N_2O_4 at 1% are 7.1 and 21 nM respectively. As the gas concentration is decreased by 10 times, τ is increased by 10 times. The range of bulk concentrations of NO_2 is from 0.45 to 7.1 nM. The bulk concentration range for N_2O_4 is from 0.19 pM to 21nM. Once again, it is verified that the N_2O_4 concentration changes more widely, because of its quadratic relationship with NO_2. All microscopic parameters and bulk concentrations for the direct contacting case are summarized in Table 4.4. In addition to quantities already discussed, predictions are shown for the mass transfer coefficients of NO_2 and N_2O_4 (k_{NO_2} and $k_{N_2O_4}$, respectively). Both decline gradually with decreases in the % NO_2. For the range of concentrations shown, there is a 6-fold variation in k_{NO_2} and a 2-fold variation in $k_{N_2O_4}$.

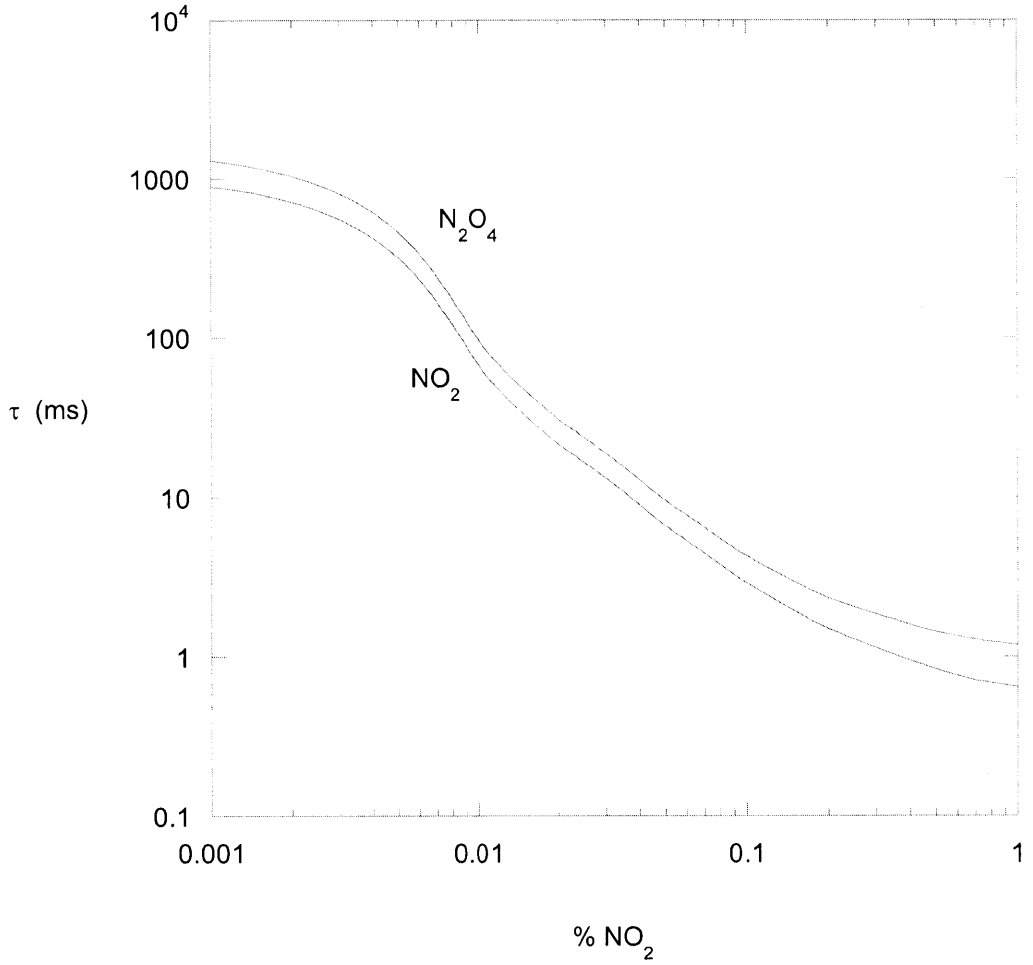

Figure 4.17. Time to reach the steady-state concentrations in the macroscopic model for direct gas-liquid contacting.

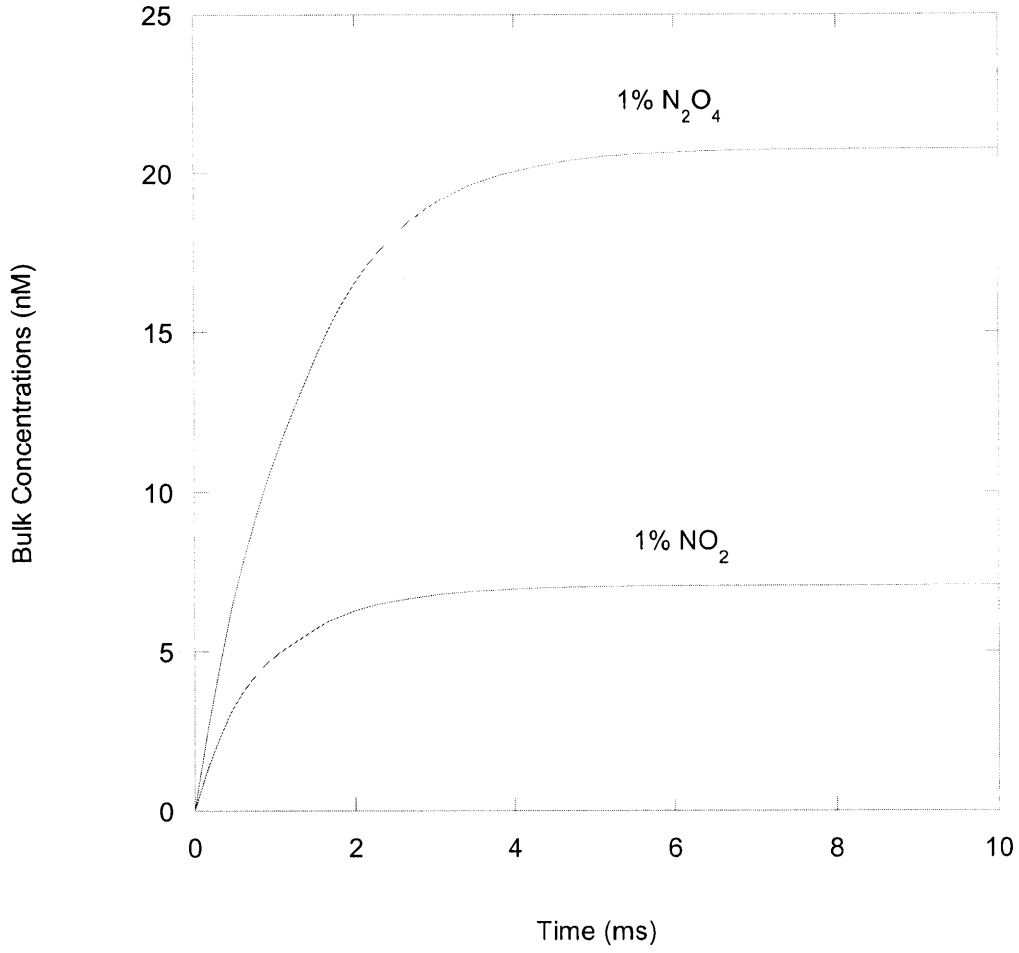

Figure 4.18-a. Bulk NO_2 and N_2O_4 concentrations as functions of time for 1 % NO_2.

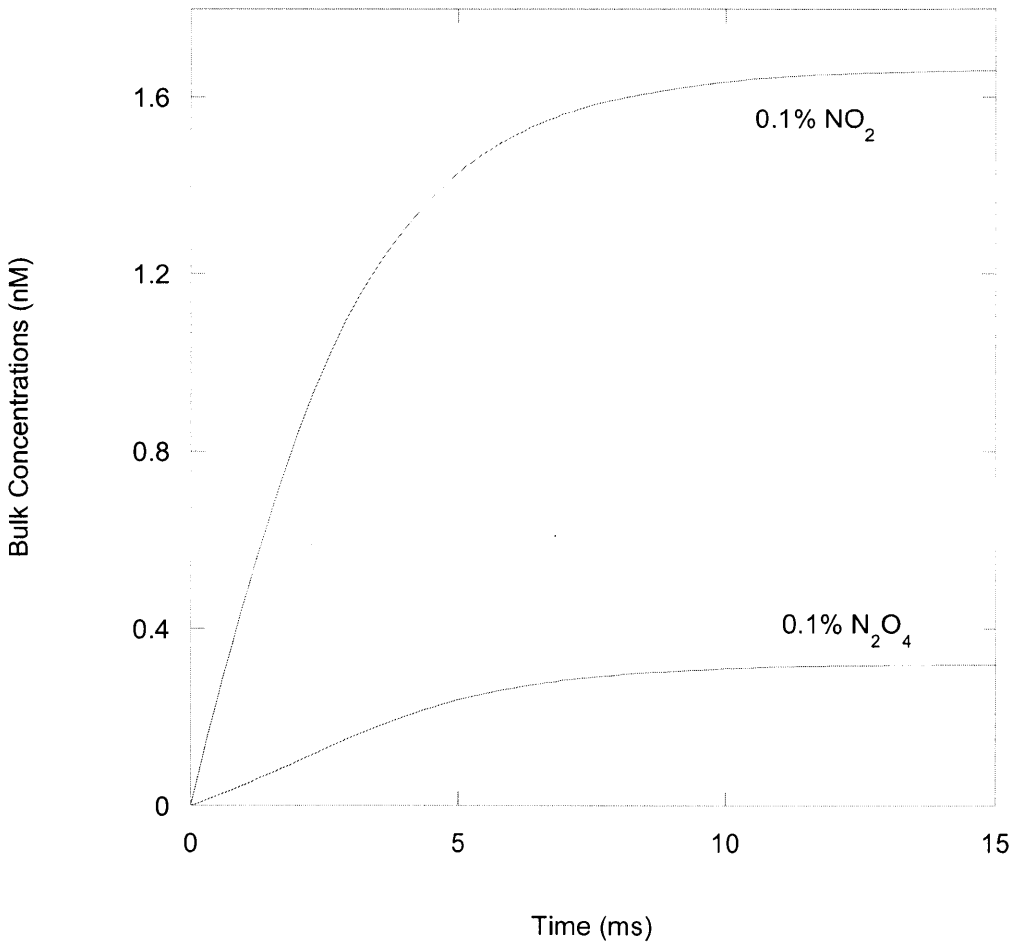

Figure 4.18-b. Bulk NO_2 and N_2O_4 concentrations as functions of time for 0.1 % NO_2.

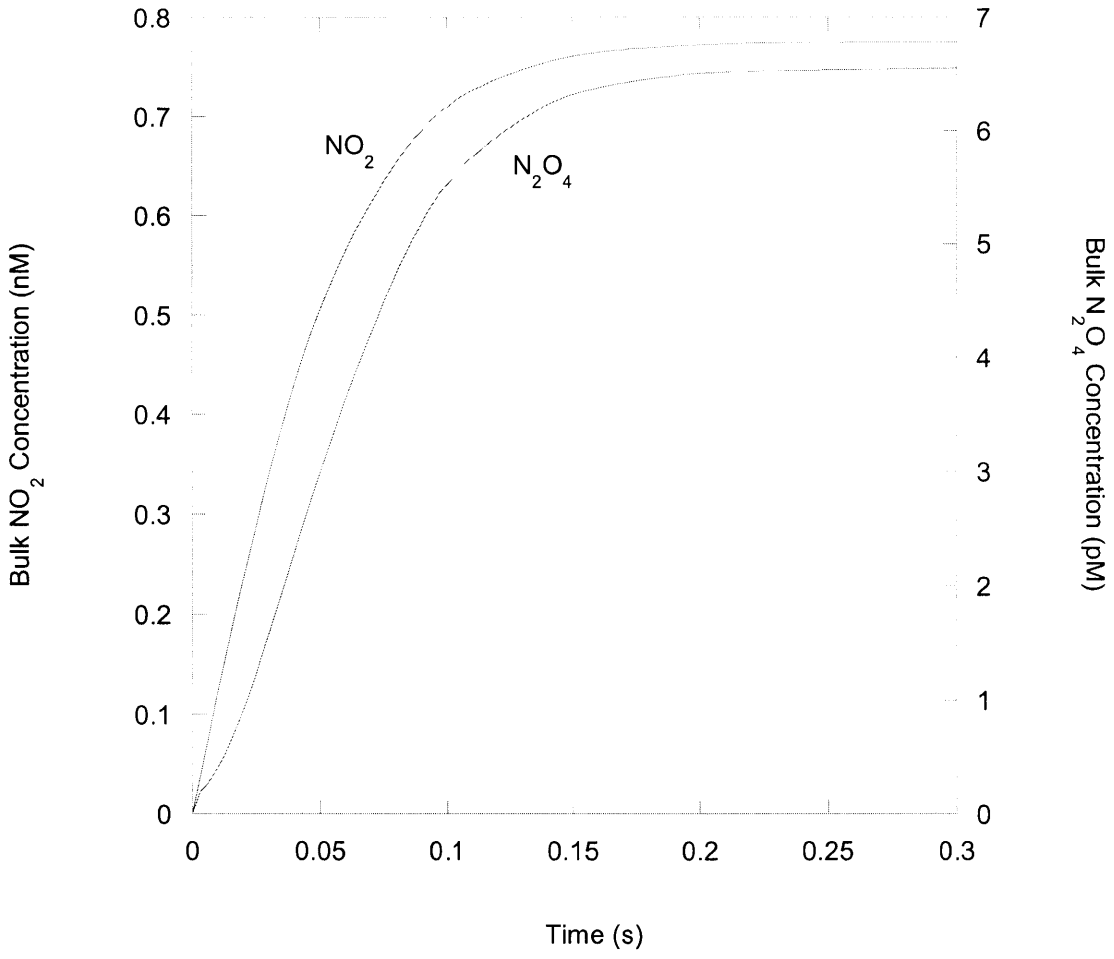

Figure 4.18-c. Bulk NO_2 and N_2O_4 concentrations as functions of time for 0.01 % NO_2.

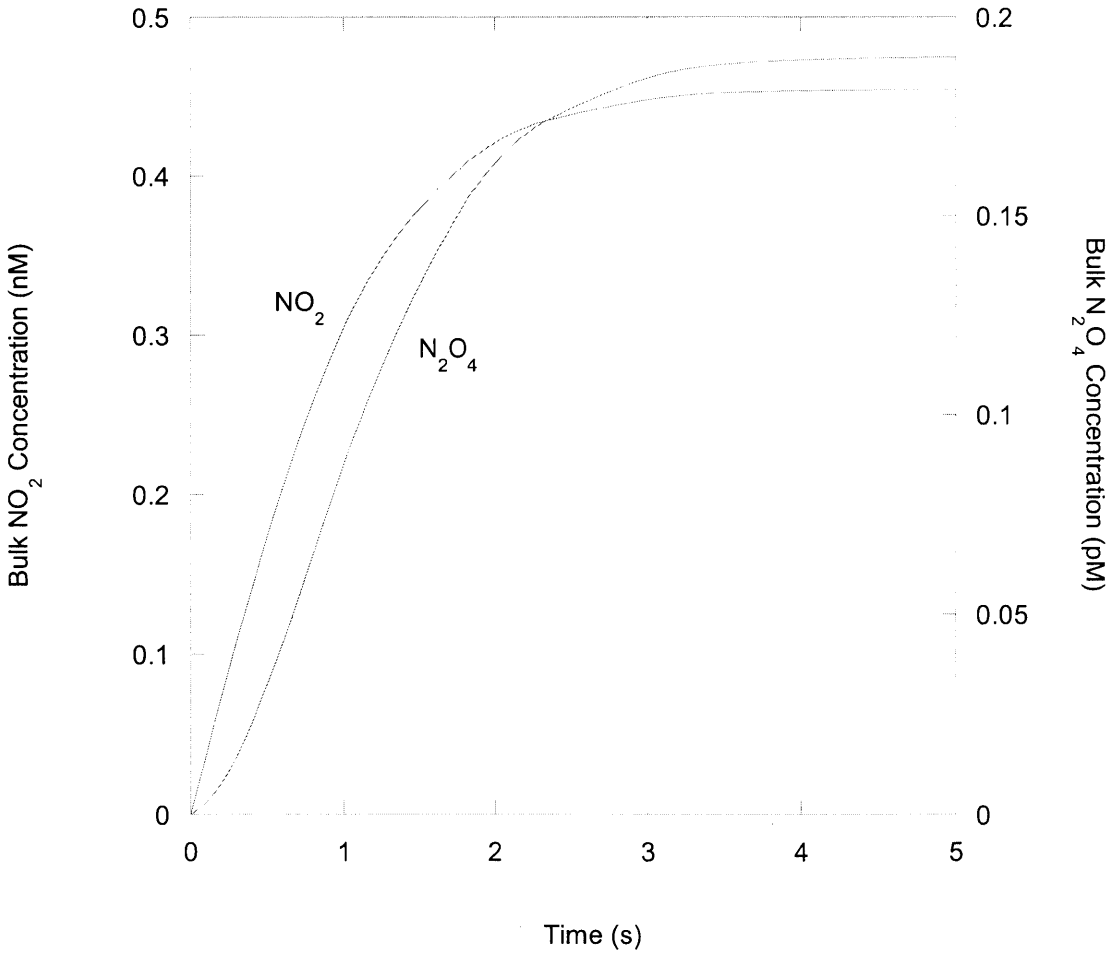

Figure 4.18-d. Bulk NO_2 and N_2O_4 concentrations as functions of time for 0.001 % NO_2.

Table 4.4. Microscopic and macroscopic parameters calculated from the microscopic model in gas-liquid direct contacting case

Total Gas %	$C_{NO_2}(\delta)$ (nM)	κ_{NO_2}	$\overline{C}_{NO_2}$ (nM)	k_{NO_2} (m/s)	γ	$C_{N_2O_4}(\delta)$ (fM)	$\kappa_{N_2O_4}$	$k_{N_2O_4}$ (m/s)	$\overline{C}_{N_2O_4}$ (nM)
1	0.69	10.2	7.1	7.65×10^{-4}	6400	27	7.6×10^{5}	1.16×10^{-3}	21
0.5	0.67	6.4	4.3	7.42×10^{-4}	5100	26	2.3×10^{5}	1.15×10^{-3}	6
0.1	0.63	2.6	1.7	6.33×10^{-4}	1800	22	1.4×10^{4}	1.07×10^{-3}	0.32
0.05	0.60	2.1	1.2	5.54×10^{-4}	990	21	4500	1.00×10^{-3}	0.094
0.01	0.54	1.4	0.78	3.38×10^{-4}	190	17	390	7.98×10^{-4}	0.0066
0.001	0.40	1.1	0.45	1.25×10^{-4}	16	9.0	21	5.69×10^{-4}	1.9×10^{-4}

4.10.6 Equilibrium Properties of NO_2 and N_2O_4 at PDMS-Water Interface

Figure.4.19 shows the effect of gas composition on the fraction of total nitrogen in PDMS as NO_2 at the gas-PDMS interface. Results are shown for various assumed values of the ratio of the dimerization equilibrium constant in PDMS to that in water [ε, Eq. (4.12)], ranging from 1 to 10^{-5}. The reason for choosing the range shown is discussed later. As evident in Eq. (4.12), $Q_{N_2O_4}$ is proportional to ε. So, as ε becomes smaller, the fraction of N_2O_4 in PDMS also becomes smaller. In other words, the fraction of NO_2 in PDMS is increased with decreasing ε. For $\varepsilon = 10^{-5}$, the NO_2 fraction in PDMS is one with 10% NO_2 gas and 0.926 at 100% NO_2 gas.

4.10.7 Concentrations in PDMS and Liquid at PDMS-Water Interface in Combined Microscopic Model

Figure.4.20 shows PDMS NO_2 concentrations at the PDMS-liquid interface for various ε values and concentrations from 0.001% to 1% NO_2 gas. For fixed ε, the NO_2 concentration decreases, of course, as the gas concentration decreases. At 1% NO_2 gas, the NO_2 concentration range is from 1.16 mM ($\varepsilon = 1$) to 118μM ($\varepsilon = 10^{-3}$). Although not shown in Figure.4.20, the concentrations for $\varepsilon = 10^{-5}$ are indistinguishable from those for $\varepsilon = 10^{-3}$. In other words, as ε decreases, the PDMS NO_2 concentrations converge. As the gas concentration decreases, the NO_2 concentrations for different ε are all about 1μM at 0.001% NO_2 gas. Thus, the PDMS NO_2 concentration at low gas concentrations is independent of ε.

Figure.4.21 shows PDMS N_2O_4 concentrations at the PDMS-liquid interface for various ε and for 0.001% to 1% NO_2 gas. Unlike that for NO_2, the PDMS N_2O_4 concentration does not converge either for both low ε or low gas concentration.

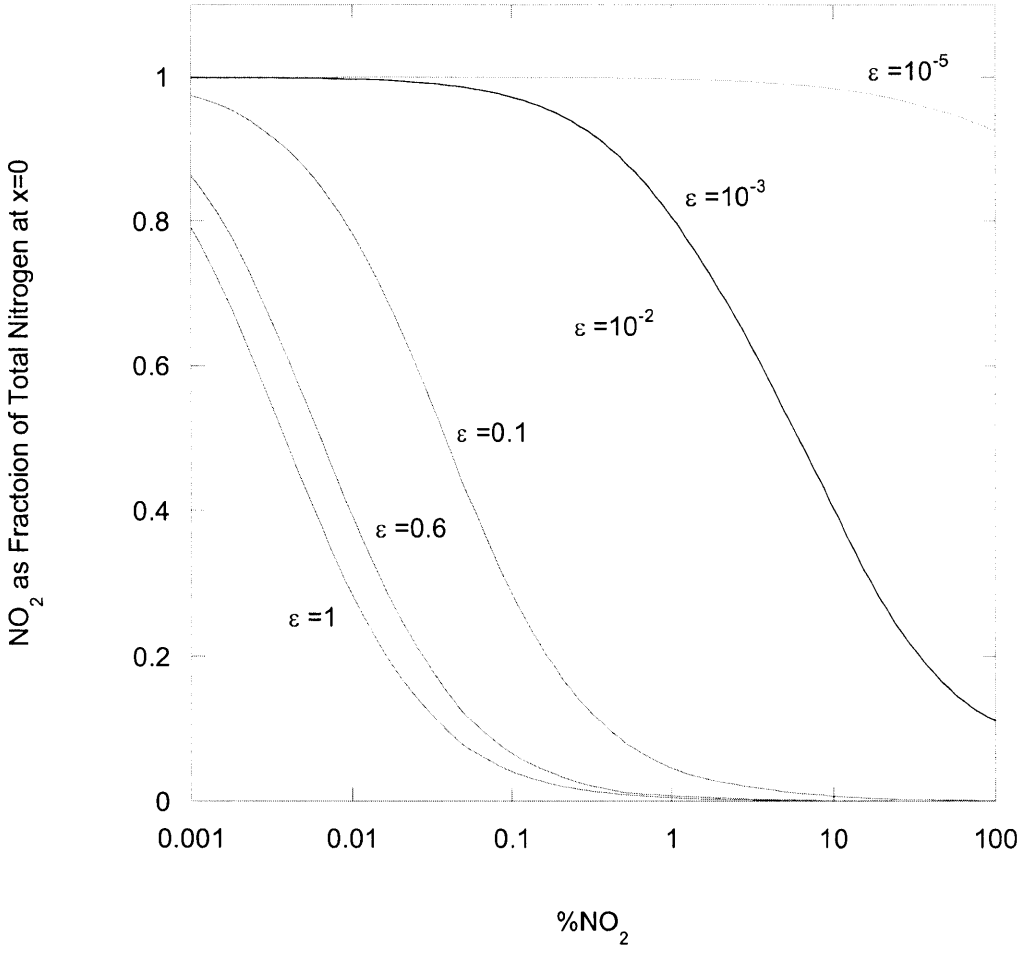

Figure 4.19. Effect of gas composition on the fraction of total nitrogen in PDMS as NO_2 at the gas-PDMS interface. Results are shown for various assumed values of the ratio of the dimerization equilibrium constant in PDMS to that in water [ε , Eq. (4.12)].

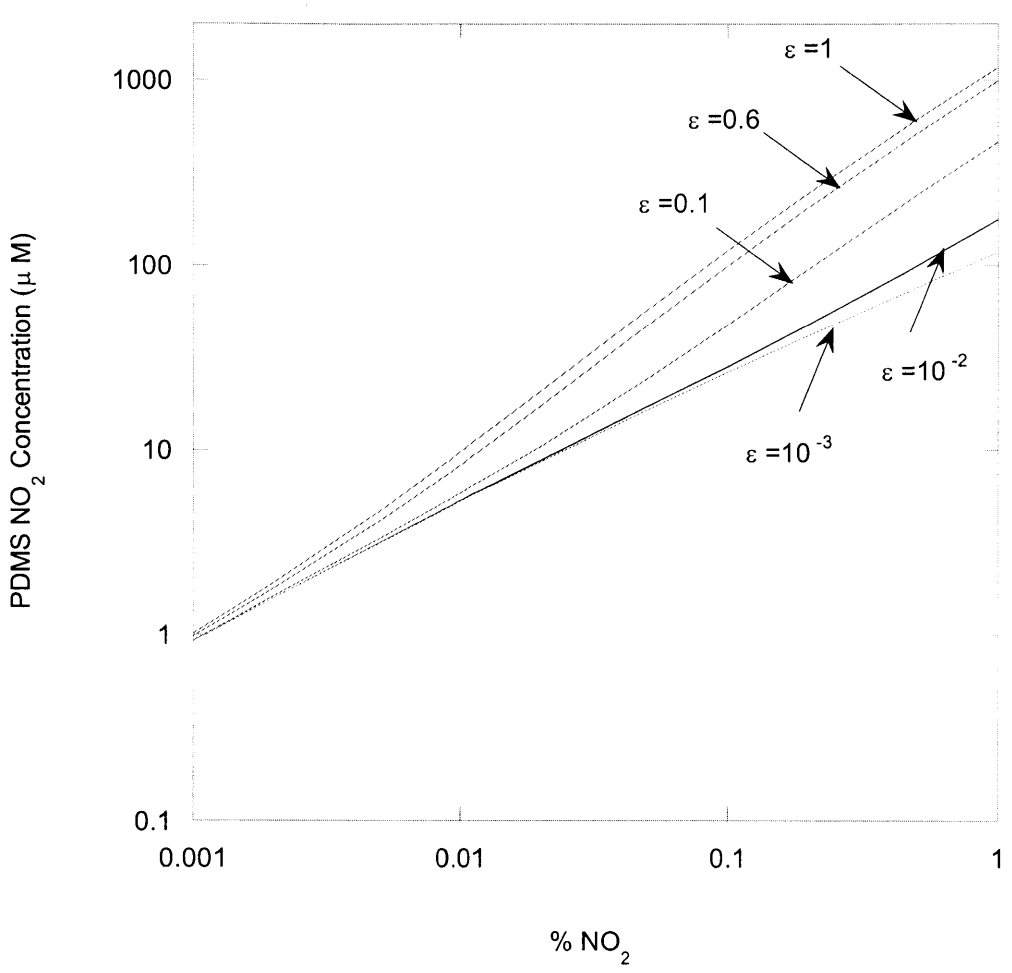

Figure 4.20. Effect of gas composition on the PDMS NO_2 concentration at the PDMS-liquid interface. Results are shown for various equilibrium constant ratios between PDMS and water.

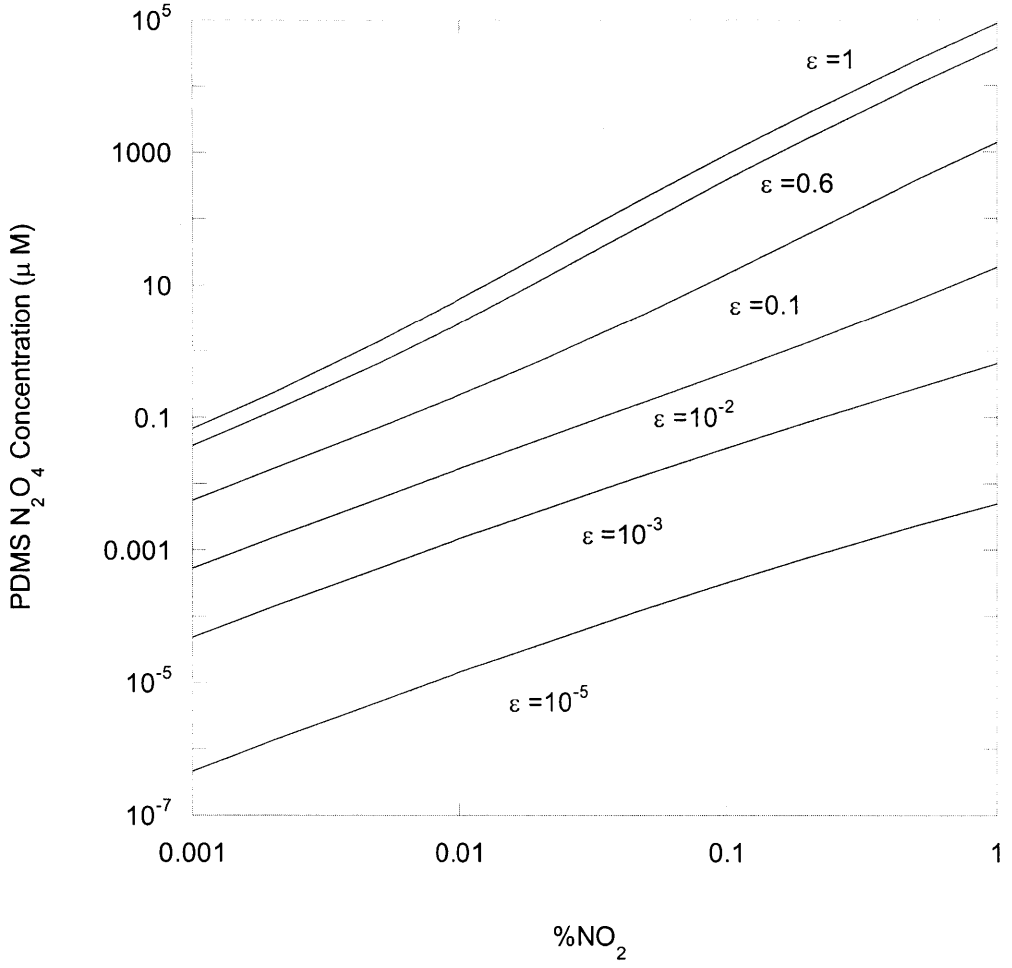

Figure 4.21. Effect of gas composition on the PDMS N_2O_4 concentration at the PDMS-liquid interface. Results are shown for various equilibrium constant ratios between PDMS and water.

Figure.4.22 shows liquid NO_2 concentrations at the PDMS-liquid interface for various ε values and concentrations from 0.001% to 1% NO_2 gas. The overall trends are similar to those for NO_2 in PDMS. As in Figure.4.20, the concentrations for $\varepsilon = 10^{-5}$ (not shown) are indistinguishable from those for $\varepsilon = 10^{-3}$. The liquid values in each case are those in PDMS divided by $Q_{NO_2} = 16.7$ (Table 4.2).

Figure.4.23 shows liquid N_2O_4 concentrations at the PDMS-liquid interface for various ε values and concentrations. Unlike that in PDMS, the liquid N_2O_4 concentration shows similar trends as that of NO_2. The N_2O_4 concentrations for $\varepsilon = 10^{-3}$ and $\varepsilon = 10^{-5}$ (not shown) are almost indistinguishable, although they are slightly separated above 0.1% NO_2 gas. At 0.001% NO_2 gas, the N_2O_4 concentrations are still slightly separated, converging less rapidly at low concentrations than those for NO_2.

4.10.8 Fractional Flux as NO_2 at PDMS-Water Interface

Figure.4.24 shows the effect of gas composition on the fractional flux as NO_2 at the PDMS-liquid interface. The fractional flux was defined in Eq. (4.150). As ε decreases, the fractional flux as NO_2 increases. In the case of $\varepsilon = 10^{-5}$, the NO_2 fractional flux is one over the entire range of gas concentrations. As the gas concentration decreases, the NO_2 fractional flux converges to one for all ε.

4.10.9 Microscopic Parameters in Combined PDMS-Water Model

Figure.4.25 shows κ_{NO_2} values for various ε and for concentrations from 0.001% to 1% NO_2 gas. At a fixed gas composition, κ_{NO_2} decreases as ε decreases. For 1% NO_2 gas, the range of κ_{NO_2} is from 3.55 ($\varepsilon = 1$) to 1.45 ($\varepsilon = 10^{-3}$). Although not shown in Figure.4.25, the

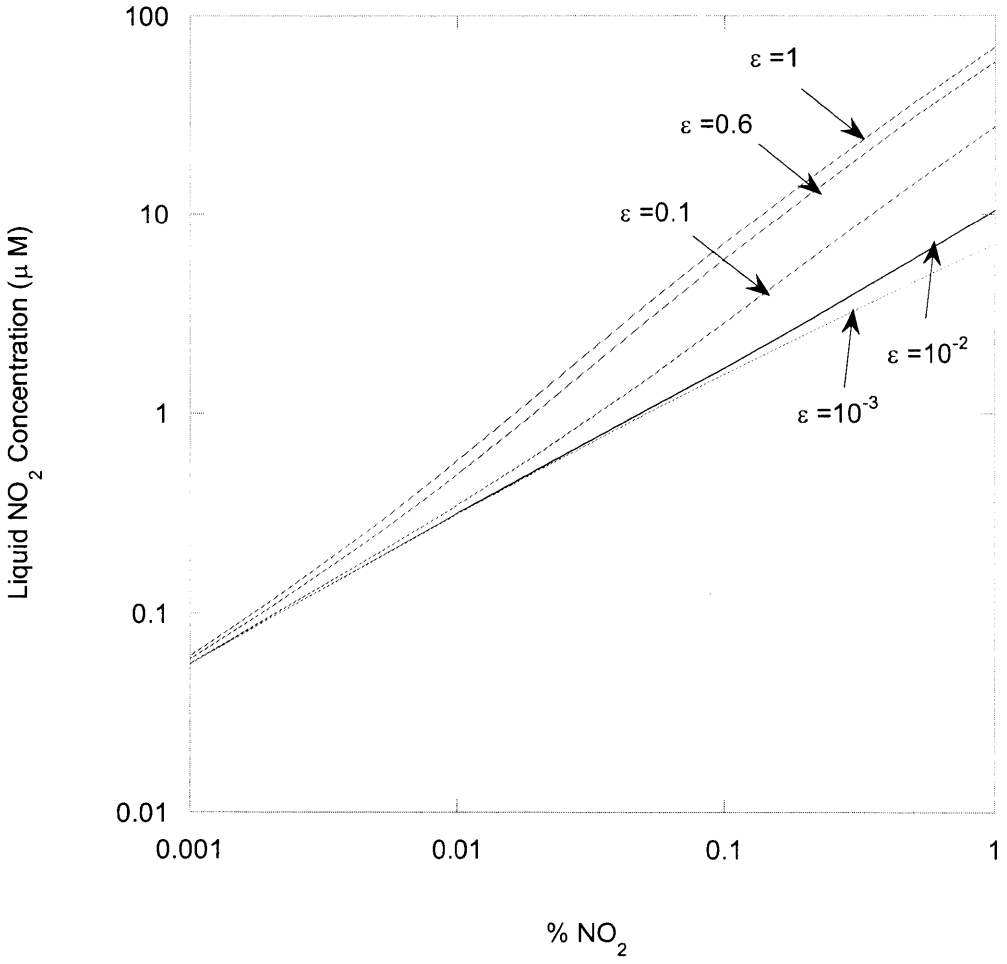

Figure 4.22. Effect of gas composition on the liquid NO_2 concentration at the PDMS-liquid interface. Results are shown for various equilibrium constant ratios between PDMS and water.

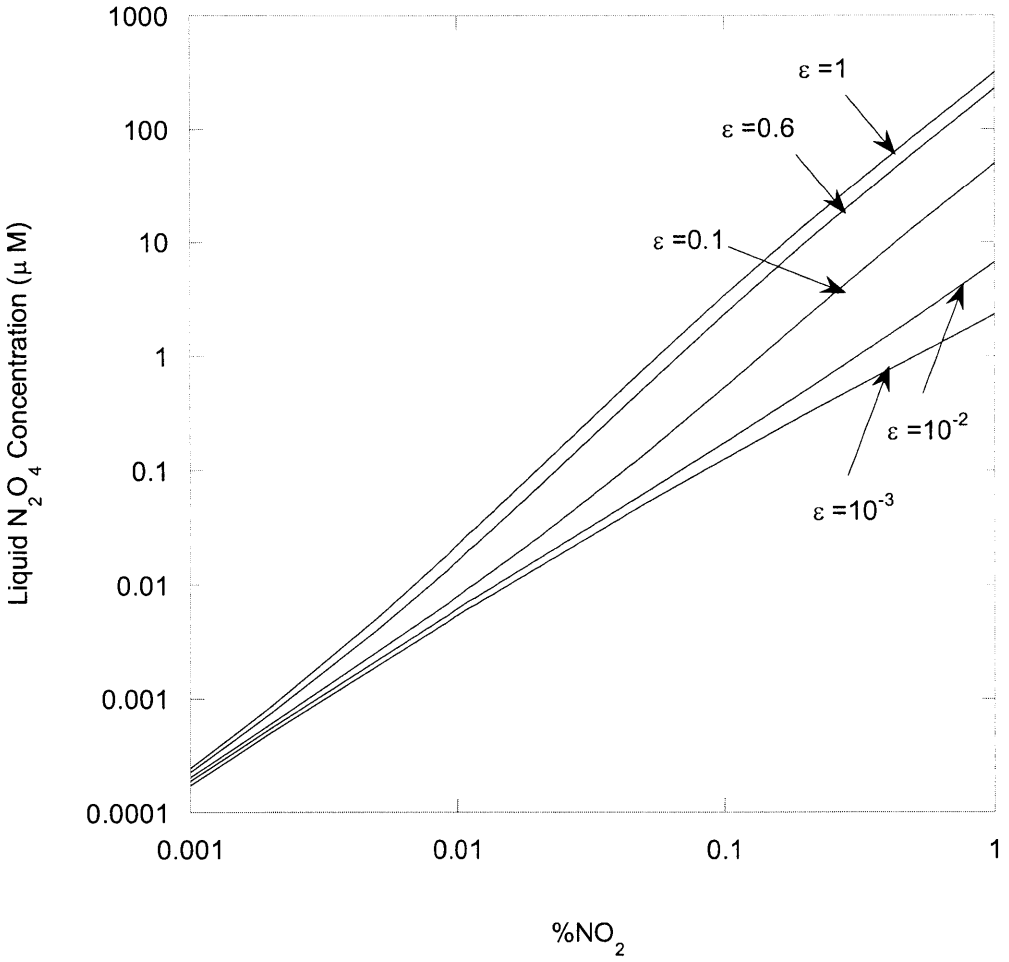

Figure 4.23. Effect of gas composition on the liquid N_2O_4 concentration at the PDMS-liquid interface. Results are shown for various equilibrium constant ratios between PDMS and water.

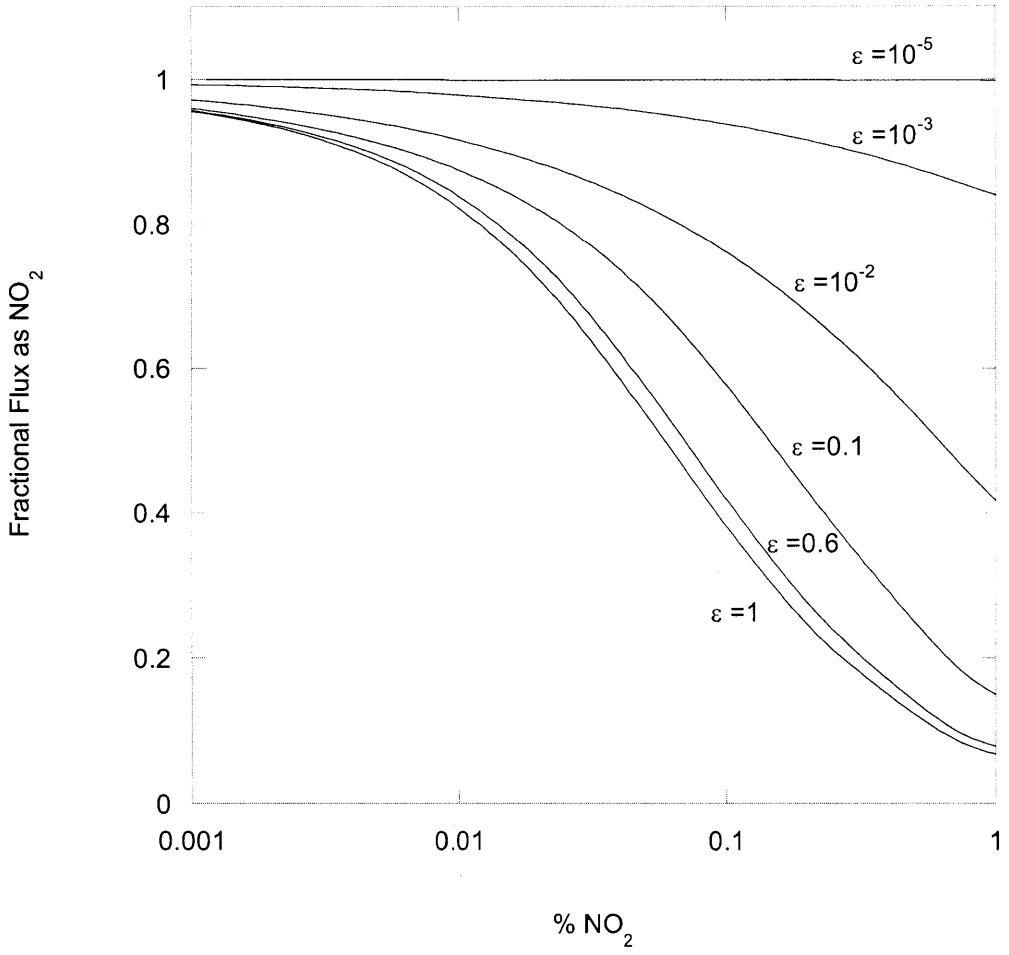

Figure 4.24. Effect of gas composition on the fraction of the total nitrogen flux as NO_2 at the PDMS-liquid interface. Results are shown for various equilibrium constant ratios between PDMS and water.

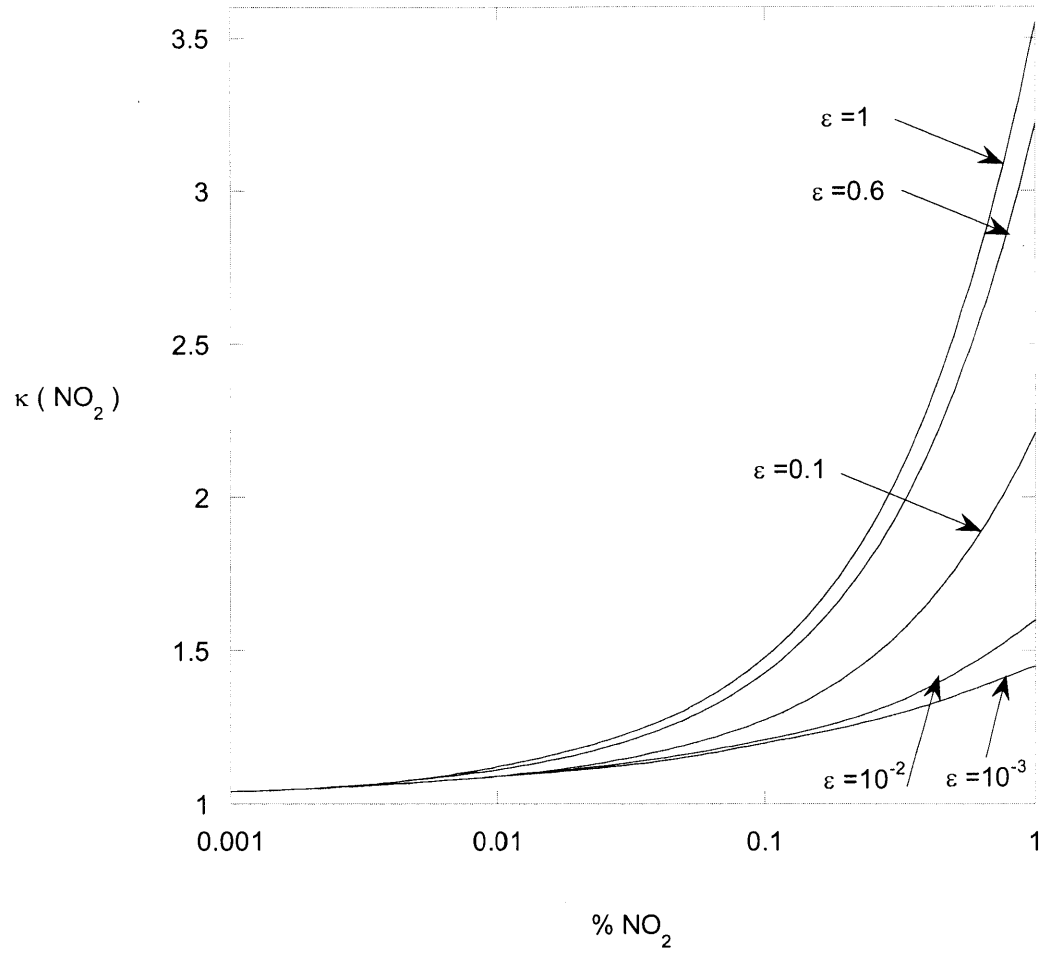

Figure 4.25. Effect of gas composition on κ_{NO_2} for the combined PDMS and aqueous microscopic model. Results are shown for various equilibrium constant ratios between PDMS and water.

κ_{NO_2} graph for $\varepsilon = 10^{-5}$ is indistinguishable from that for $\varepsilon = 10^{-3}$. As the gas concentration decreases, the κ_{NO_2} values for different ε converge to about 1.04 at 0.001% NO_2 gas. In other words, the κ_{NO_2} value at low gas concentration is independent of ε.

Figure.4.26 shows $\kappa_{N_2O_4}$ values for the combined model. The overall trends are the same as for NO_2 in Figure.4.25. However, the range of $\kappa_{N_2O_4}$ is much larger than that of κ_{NO_2}. Its range is 9.1 (0.001%) to 3.35×10^5 (1%, $\varepsilon = 1$). As already pointed out, the value of κ_{NO_2} at 0.001% (1.04) almost reaches unity, but the value of $\kappa_{N_2O_4}$ at 0.001% (9.1) is still much higher than that.

Figure.4.27 shows γ for various ε values and gas concentrations. The overall trends are the same as for κ_{NO_2} and $\kappa_{N_2O_4}$ (Figures.4.25 and 4.26). The range of γ is 9 (0.001%) to 23,400 (1%, $\varepsilon = 1$). Like $\kappa_{N_2O_4}$, the γ values for various ε at low gas concentrations, but remain much higher than unity (about 9).

4.10.10 Macroscopic Results for Delivery Using PDMS Tubing

Figure.4.28 shows the time to reach steady state concentrations (τ) [Eq. (4.94)] for NO_2 and N_2O_4. Results are shown for various gas concentrations and two ε values. At 0.001% NO_2 gas, τ is about 5 to 8 seconds. As the gas concentration is increased, τ decreases because both the dimerization and its reverse reaction are faster. At 1% NO_2 gas, τ reaches about 1 ms for $\varepsilon = 1$ and 10 ms for $\varepsilon = 10^{-3}$. As the gas concentration is decreased by 10 times, τ is increased by roughly 10 times. Although not shown in Figure.4.28, τ for $\varepsilon = 10^{-5}$ is indistinguishable from that for $\varepsilon = 10^{-3}$. As the gas concentration decreases, τ converges.

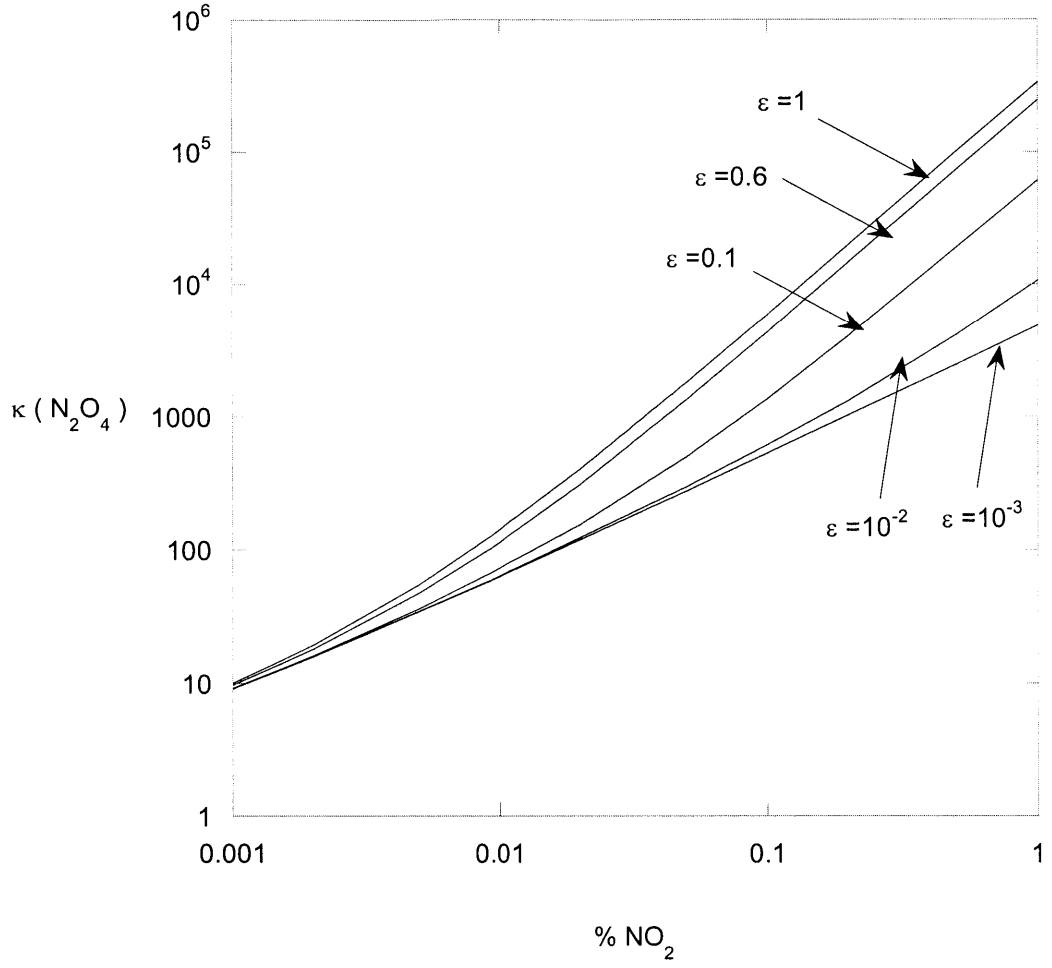

Figure 4.26. Effect of gas composition on $\kappa_{N_2O_4}$ for the combined PDMS and aqueous microscopic model. Results are shown for various equilibrium constant ratios between PDMS and water.

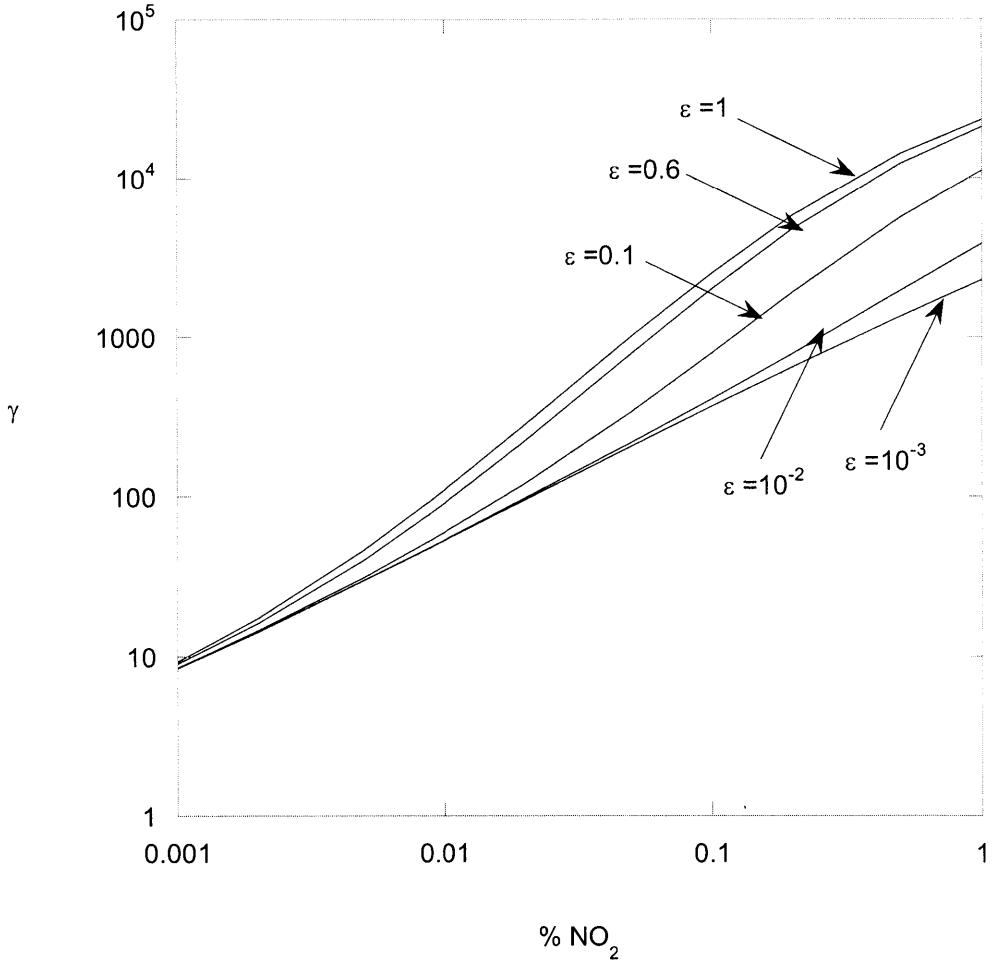

Figure 4.27. Effect of gas composition on γ for the combined PDMS and aqueous microscopic model. Results are shown for various equilibrium constant ratios between PDMS and water.

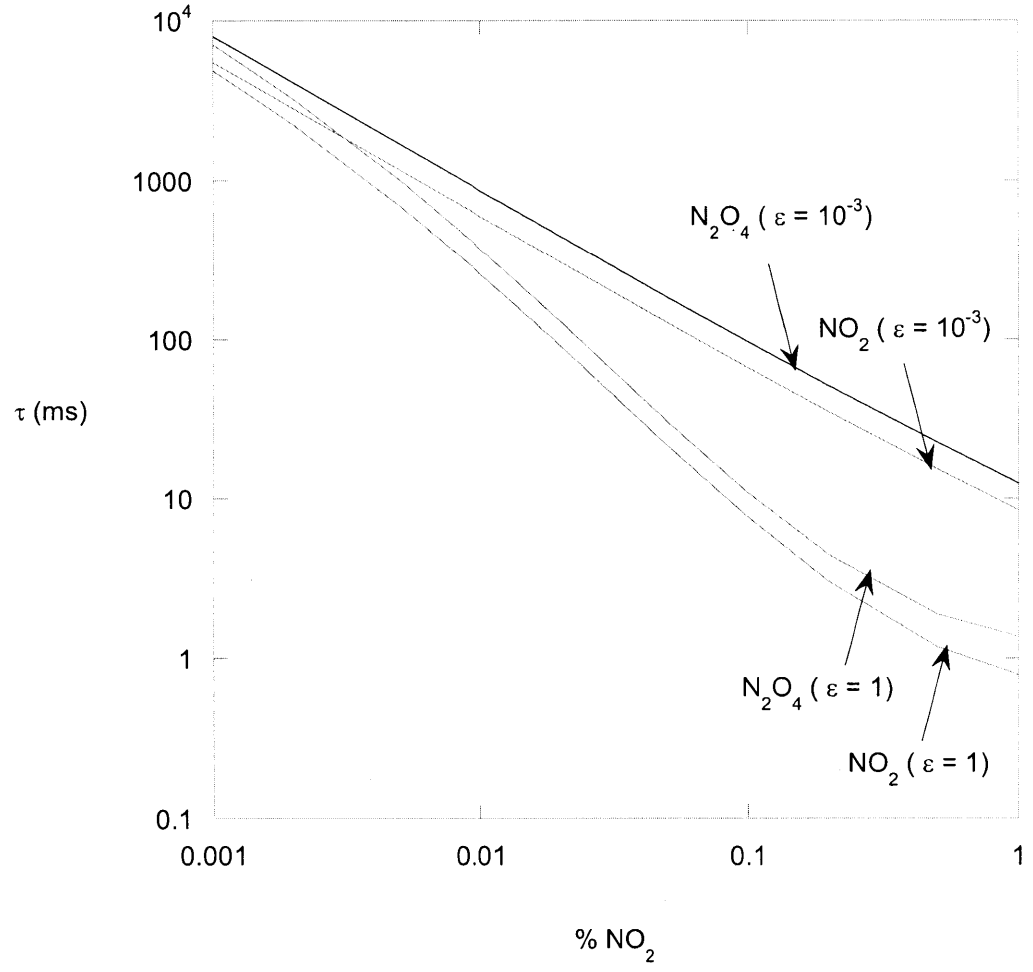

Figure 4.28. Time to reach steady-state concentrations in the macroscopic model for delivery via PDMS tubing. Results are shown for NO_2 and N_2O_4 at two assumed value of ε.

Overall, the time to reach steady state is quite fast (at most 8 seconds) and the time-dependence in the macroscopic balances can be ignored, as with direct gas-liquid contacting. Thus, the aqueous volume-averaged (bulk) concentrations in the PDMS-aqueous model are obtained again from Eqs. (4.95) and (4.96).

Figures.4.29-a through 4.29-g show NO_2 and N_2O_4 bulk concentrations as functions of time for specific gas compositions and selected ε values. As already shown in Figure.4.28, the time to reach steady-state for 1% NO_2 gas ranges from about 1 ms ($\varepsilon = 1$) to 10 ms ($\varepsilon = 10^{-3}$) (Figure.4.29-a). The bulk concentration of NO_2 at 1% varies from 0.98 nM ($\varepsilon = 1$) to 0.36 nM ($\varepsilon = 10^{-3}$) (Figure.4.29-a). As ε is decreased, the steady state concentrations converge. The bulk concentrations of N_2O_4 at 1% NO_2 gas are shown in Figure.4.29-b for various ε values. The overall trends are the same as for NO_2, and the bulk concentration ranges in this case from 1.5 nM ($\varepsilon = 1$) to 17 pM ($\varepsilon = 10^{-3}$). As mentioned before, the N_2O_4 concentration changes more widely because of its quadratic relationship with NO_2.

Figure.4.29-c shows the bulk NO_2 concentrations for 0.1% NO_2 gas with various ε values, the steady state values ranging from 0.37 nM ($\varepsilon = 1$) to 0.27 nM ($\varepsilon = 10^{-3}$). Compared to Figure.4.29-a, the convergence speed as is ε decreased is somewhat increased for 0.1% NO_2 gas. Figure.4.29-d shows the corresponding bulk concentrations of N_2O_4 for 0.1% NO_2 gas, the steady values ranging from 21 pM ($\varepsilon = 1$) to 1.5 pM ($\varepsilon = 10^{-3}$).

For 0.01% NO_2 gas, bulk NO_2 and N_2O_4 concentrations are shown in Figure.4.29-e and Figure.4.29-f, respectively. In these plots the results for $\varepsilon = 10^{-3}$ are not shown because they are indistinguishable from those for $\varepsilon = 10^{-2}$. The range of NO_2 is from 0.23 nM ($\varepsilon = 1$) to 0.21 nM ($\varepsilon = 10^{-2}$), and the range of N_2O_4 is from 0.34 pM ($\varepsilon = 1$) to 0.13 pM ($\varepsilon = 10^{-2}$).

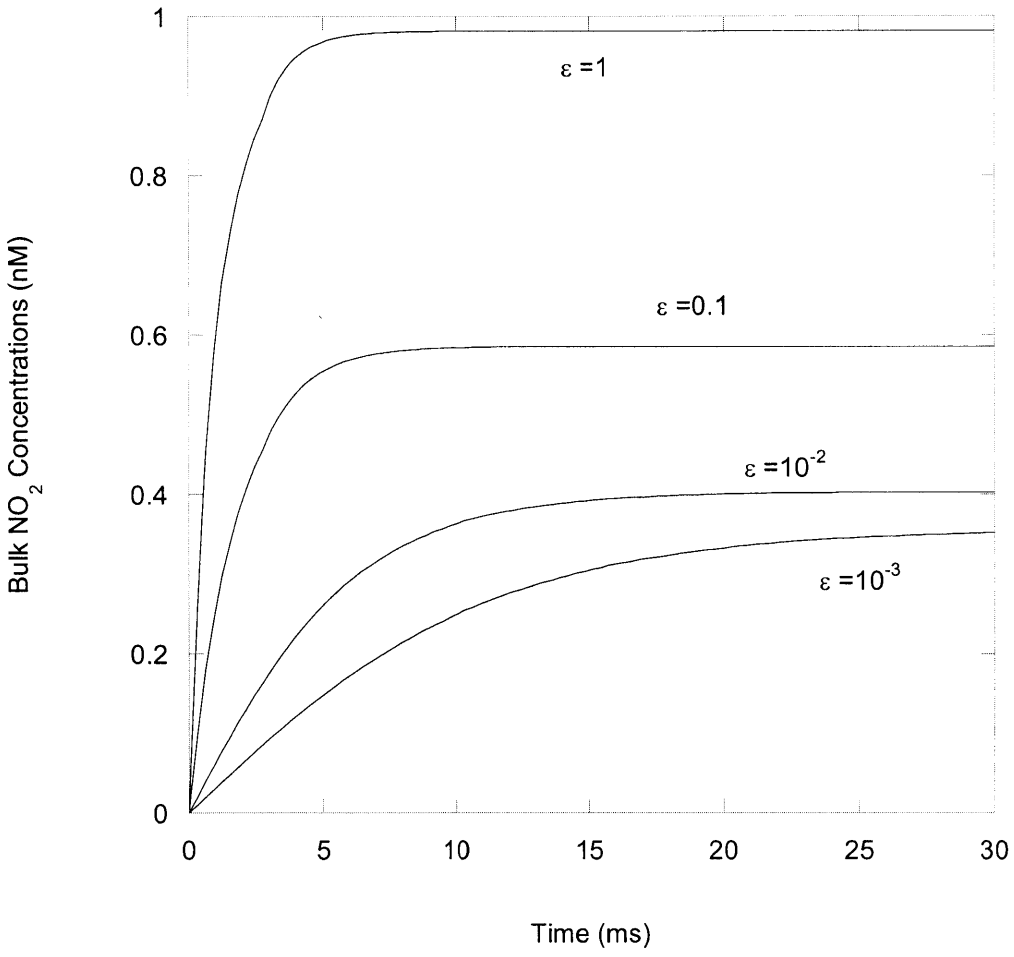

Figure 4.29-a. Bulk NO_2 concentrations for 1 % NO_2 gas with different equilibrium ratios.

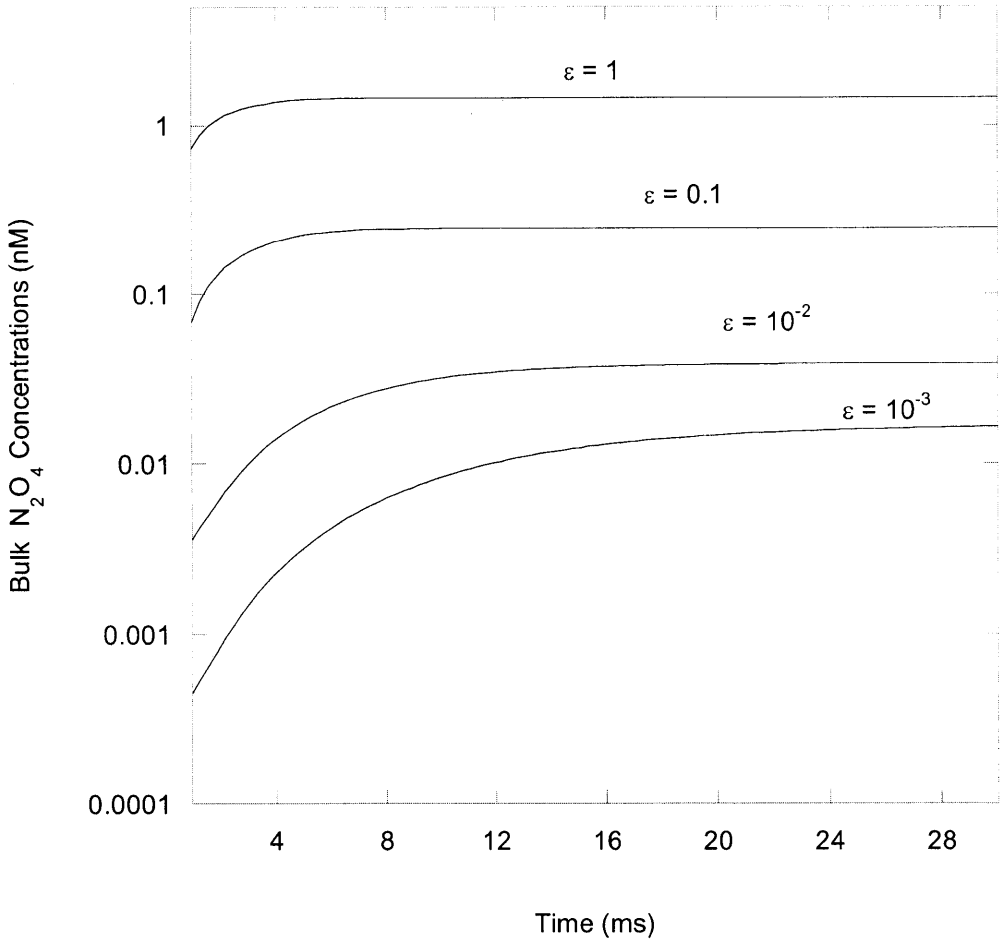

Figure 4.29-b. Bulk N_2O_4 concentrations for 1 % NO_2 gas with different equilibrium ratios.

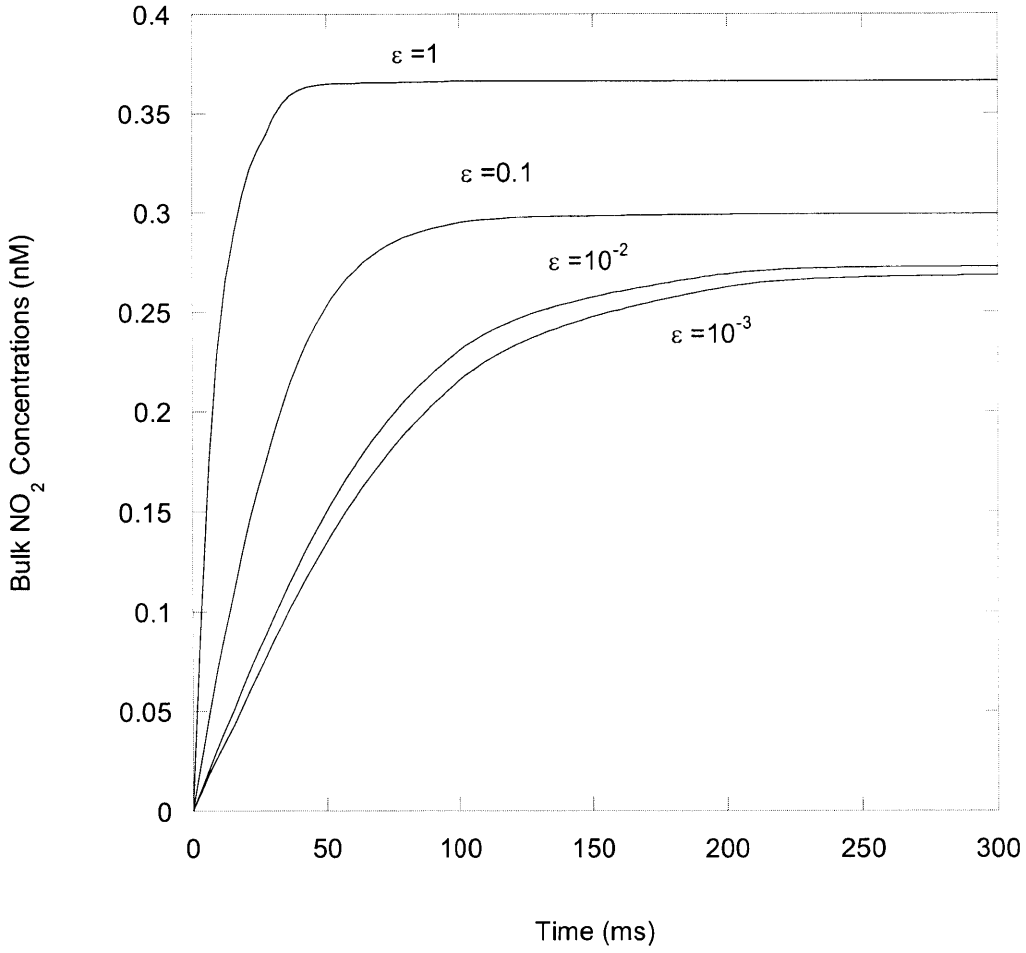

Figure 4.29-c. Bulk NO_2 concentrations for 0.1 % NO_2 gas with different equilibrium ratios.

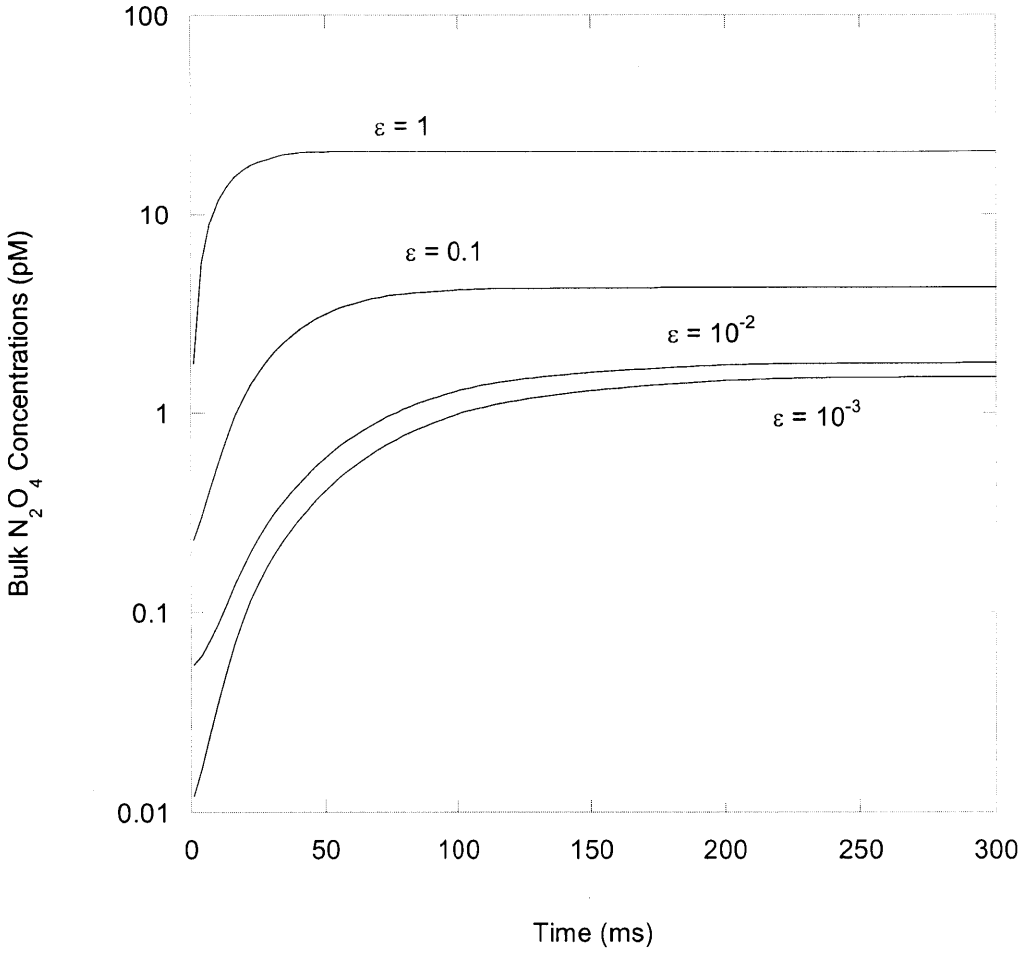

Figure 4.29-d. Bulk N_2O_4 concentrations for 0.1 % NO_2 gas with different equilibrium ratios.

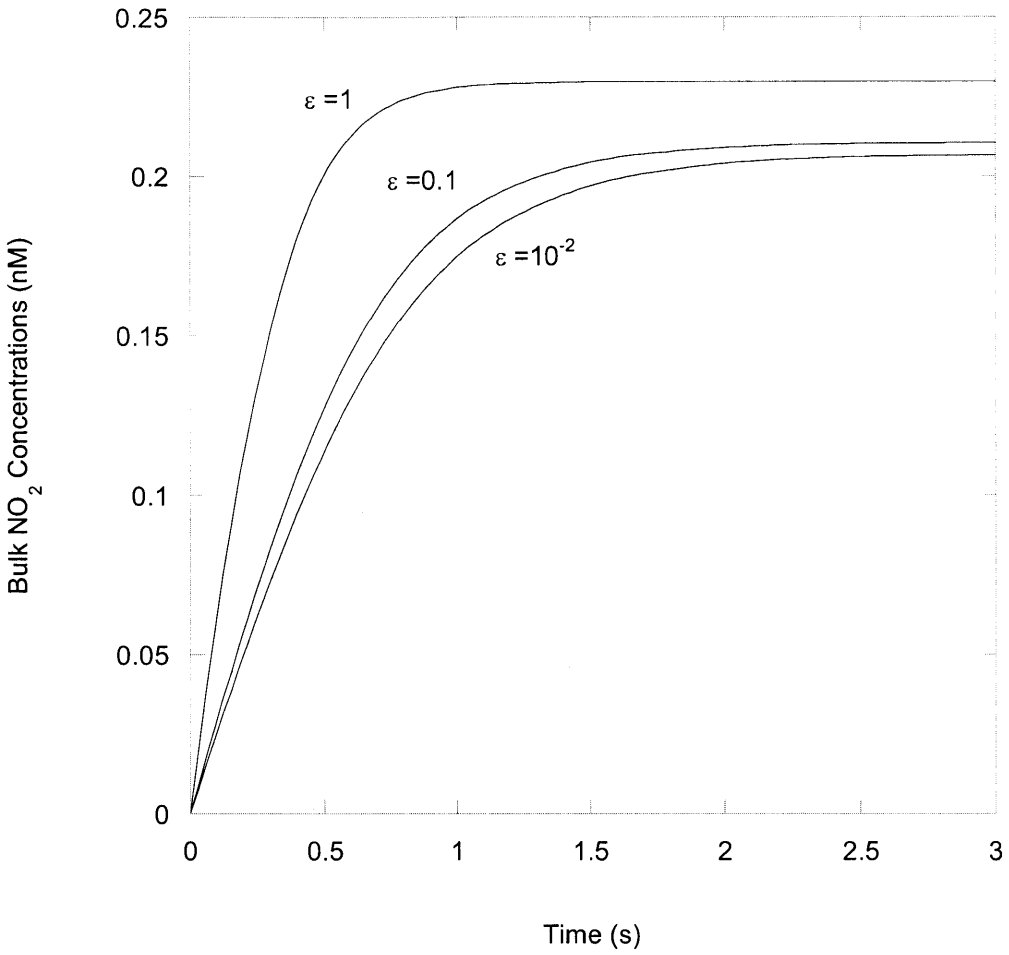

Figure 4.29-e. Bulk NO_2 concentrations for 0.01 % NO_2 gas with different equilibrium ratios.

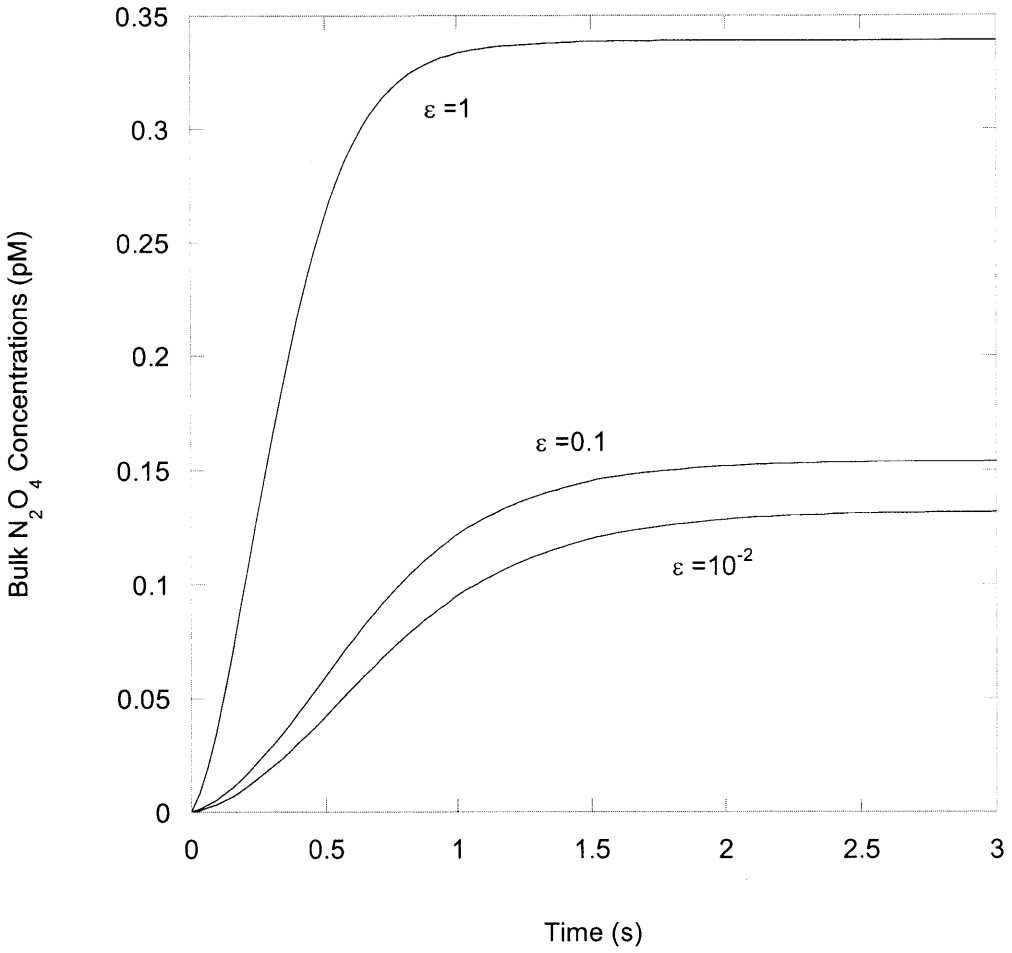

Figure 4.29-f. Bulk N_2O_4 concentrations for 0.01 % NO_2 gas with different equilibrium ratios.

Finally, Figure.4.29-g shows bulk NO_2 and N_2O_4 concentrations for 0.001% NO_2 gas. Now, the concentrations for $\varepsilon = 10^{-2}$ are indistinguishable from those for $\varepsilon = 0.1$. At this composition, the steady concentrations are relatively insensitive to ε. The range for NO_2 is from 0.145 nM ($\varepsilon = 1$) to 0.141 nM ($\varepsilon = 0.1$), and the range for N_2O_4 is from 11 fM ($\varepsilon = 1$) to 9.5 fM ($\varepsilon = 0.1$). Here, the NO_2 level is 4 orders of magnitude higher than that of N_2O_4.

Table 4.5 shows the well-mixed concentrations, bulk concentrations, κ values, γ values, and values for the mass transfer coefficients for NO_2 and N_2O_4. These results are all based on $\varepsilon = 10^{-5}$. As will be discussed, this small value for ε appears to be the most realistic. As for direct gas-liquid contacting, k_{NO_2} was found to decrease with decreasing NO_2 concentration. However, $k_{N_2O_4}$ was found to increase with decreasing NO_2 concentration.

4.10.11 Nitrite Concentrations

Figure.4.30 shows the measured NO_2^- concentrations for 0.5% and 1% NO_2 gas in the chamber which uses the PDMS tubing loop for NO_2 delivery. The rates of NO_2^- formation obtained from the slopes are 7.14 and 14.9 nM/s, respectively, for 0.5% and 1% NO_2 gas.

Dividing the rates of NO_2^- formation by k_2 gives an experimental value for the bulk N_2O_4 concentration [Eq. (4.5)]. The measured bulk N_2O_4 concentrations obtained in this manner are 7.14 pM (0.5%) and 0.0149 nM (1%). Figure.4.31 shows the rates of NO_2^- formation (R) as functions of ε, ranging from 10^{-3} to 10^{-5}. For 1% R=14.9 nM/s, the corresponding $\varepsilon = 2.2 \times 10^{-5}$. And for 0.5% nitrite data, the corresponding $\varepsilon = 6.7 \times 10^{-7}$ can be obtained using extrapolation. Based on these results, ε ranges from 6.7×10^{-7} to 2.2×10^{-5}. In this case, the value of $Q_{N_2O_4}$ ranges from 0.0002 to 0.006.

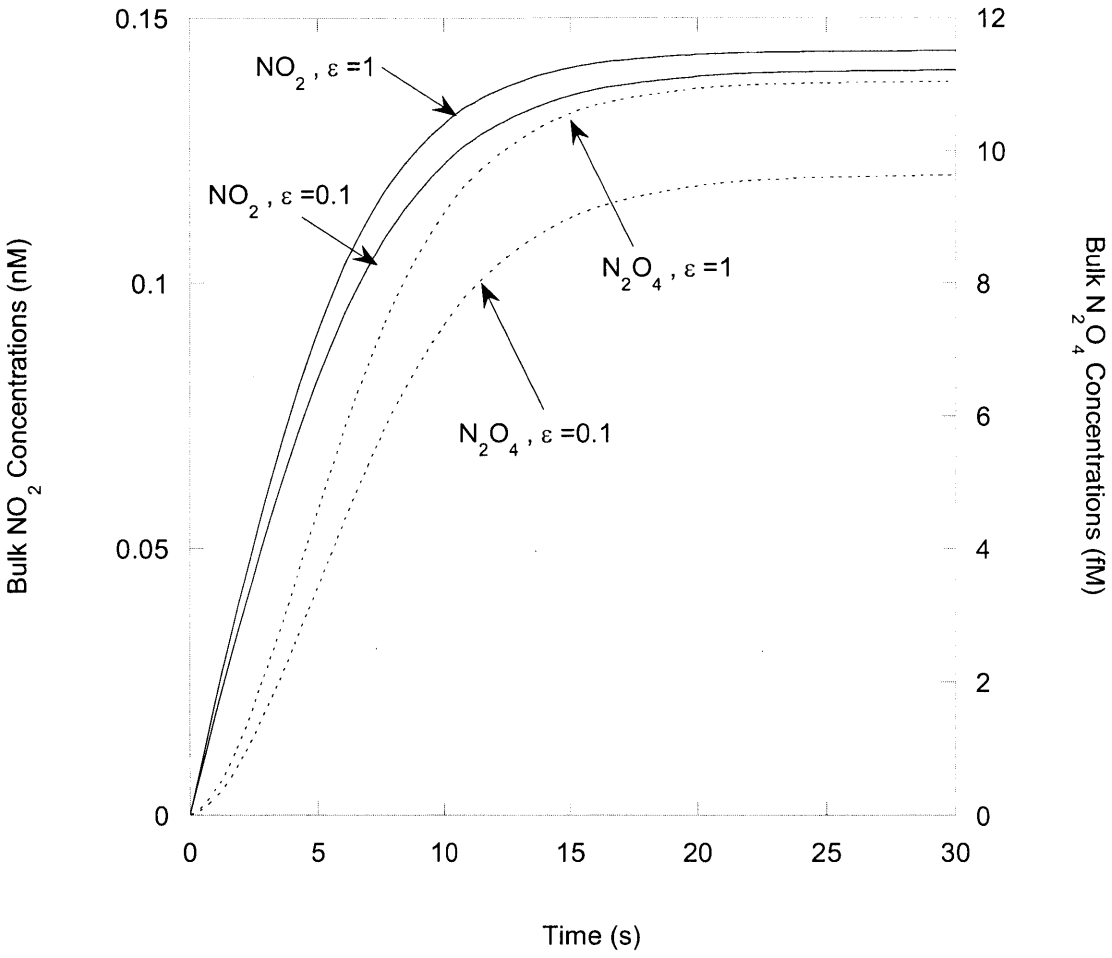

Figure 4.29-g. Bulk NO_2 and N_2O_4 concentrations for 0.001 % NO_2 gas with different equilibrium ratios.

Table 4.5. Microscopic and macroscopic parameters calculated from the combined microscopic model in the case of $\varepsilon = 10^{-5}$

Total Gas %	$C_{NO_2}(\delta)$ (nM)	κ_{NO_2}	$\overline{C}_{NO_2}$ (nM)	k_{NO_2} (m/s)	γ	$C_{N_2O_4}(\delta)$ (fM)	$\kappa_{N_2O_4}$	$k_{N_2O_4}$ (m/s)	$\overline{C}_{N_2O_4}$ (nM)
1	0.246	1.43	0.350	7.02×10^{-5}	2070	3.44	4220	1.01×10^{-8}	0.0145
0.5	0.240	1.34	0.322	6.90×10^{-5}	1280	3.29	2290	1.43×10^{-8}	7.54 pM
0.2	0.232	1.25	0.290	6.69×10^{-5}	636	3.07	991	2.26×10^{-8}	3.04 pM
0.1	0.225	1.20	0.269	6.50×10^{-5}	364	2.88	521	3.15×10^{-8}	1.50 pM
0.05	0.216	1.15	0.250	6.26×10^{-5}	205	2.66	273	4.37×10^{-8}	0.728 pM
0.01	0.190	1.09	0.207	5.54×10^{-5}	53.1	2.06	62.8	8.89×10^{-8}	0.129 pM
0.002	0.154	1.05	0.162	4.56×10^{-5}	14.4	1.35	15.7	1.69×10^{-7}	0.0213 pM
0.001	0.136	1.04	0.141	4.07×10^{-5}	8.48	1.05	9.08	2.16×10^{-7}	9.51 fM

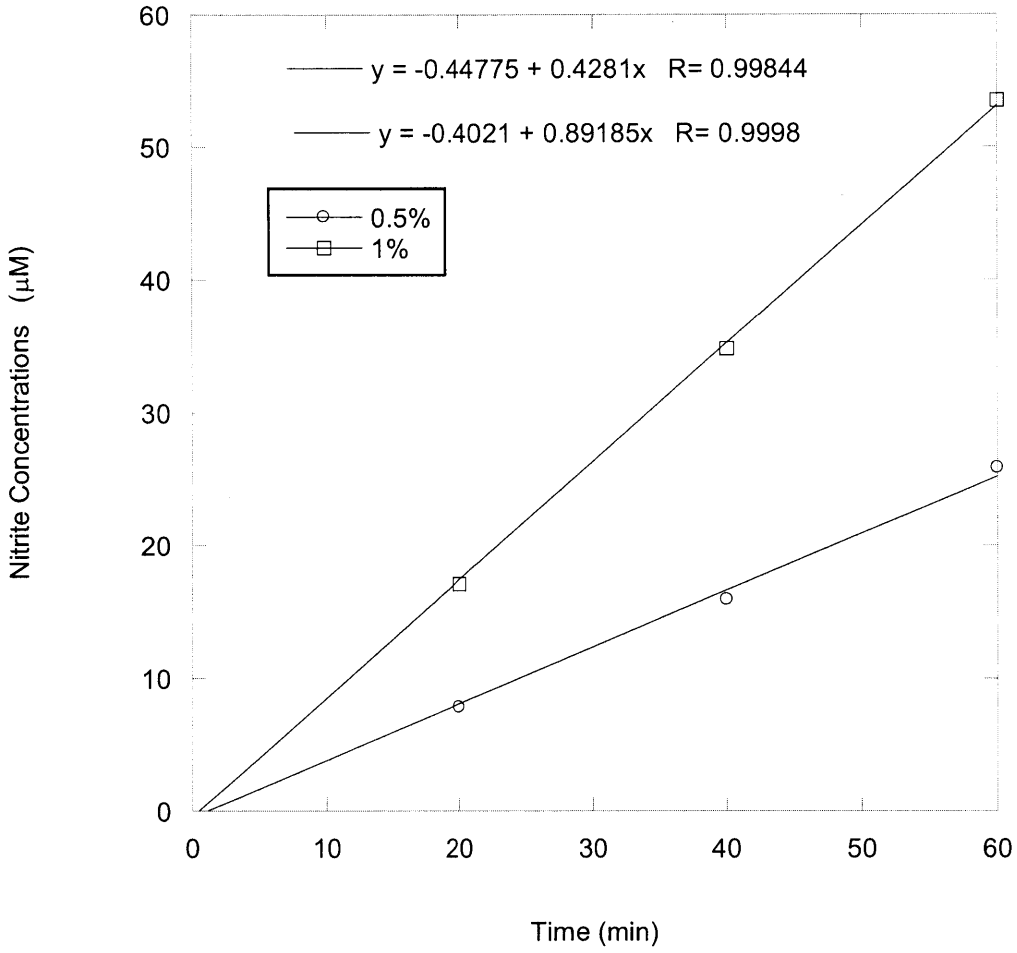

Figure 4.30. Experimental nitrite concentrations for 1% and 0.5% NO_2 gas delivery using PDMS tubing.

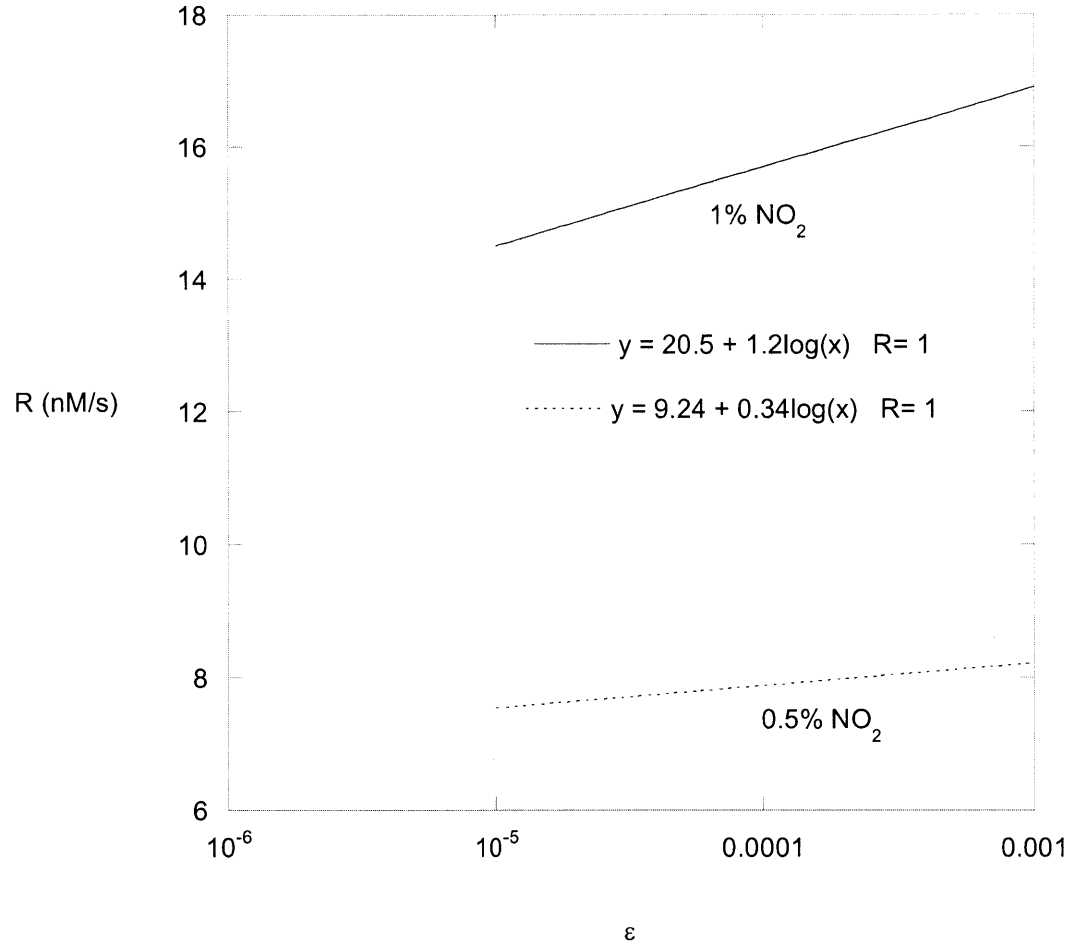

Figure 4.31. The nitrite formation rates (R) as functions of ε for 0.5 and 1% NO_2 gas.

4.11 Discussion

The steady-state NO_2 level (bulk concentration) in simple aqueous solutions with $\overline{C}_{NO} = 1.0\mu M$ (representative level of inflamed tissues) and $\overline{C}_{O_2} = 200\mu M$ (ambient level) was calculated to be 40pM (Lim et al., 2008). The estimated steady-state NO_2 concentrations from the NO_2 delivery models are from 0.45 to 7.1 nM in the gas-liquid case (Table 4.4) and 0.14 to 0.35nM in the PDMS for $\varepsilon = 10^{-5}$ for the combined model (Table 4.5). These NO_2 levels are from 3.5 times to 180 times the value predicted for NO delivery under the conditions stated (40pM). However, it might be possible to obtain pM levels with NO_2 delivery reactors by manipulating antioxidant concentrations. As pointed out in the introduction, the greatest advantage of these NO_2 reactors is the isolation of the biological effects of NO_2 from those of the other main effectors, such as N_2O_3 and peroxynitrite, which come from NO. Furthermore, together with the NO delivery reactor, it is possible to obtain a wide range of RNS mixtures.

As shown in Figure.4.11, the QEA results in almost the same concentration profiles as the exact equations. It is especially accurate at the high gas concentrations, as shown in Figures.4.12 and 4.13. At gas concentrations above 10%, the errors in the NO_2 and N_2O_4 concentrations and in the total flux are nearly zero. The reason why the QEA works perfectly at high gas concentrations is that the diffusion term in NO_2 conservation equation [Eq. (4.23)] can be ignored. This is because the Da_1 [Eq. (4.32)] values are then very large ($Da_1 = 1.1\times10^7$ for 100% NO_2 gas). When the diffusion term is negligible, Eq. (4.23) reduces to the definition of the QEA [Eq. (4.43)]! In other words, the exact equations are virtually the same as the QEA at high gas concentrations. As shown in Figure.4.13, the percent error in the N_2O_4 flux becomes increasingly large and negative as the gas concentration is decreased. This corresponds to the

NO_2 diffusion term becoming more important. Eventually, at very low concentrations, the NO_2 concentration becomes independent of the N_2O_4 concentration. When the dimerization is too slow to affect the NO_2 concentration, the equilibrium relationship in the QEA fails. This reasoning was already discussed in connection with the limiting form of the aqueous model for very low total nitrogen concentrations.

In the low concentration regime (< 1% NO_2 gas), the QEA becomes increasingly inaccurate for the N_2O_4 and N_2O_4 flux as the concentrations are decreased. While the percent error in the N_2O_4 flux becomes larger and larger, the percent error for the NO_2 flux reaches a maximum and then decreases as the gas concentration is lowered further. The reason for this NO_2 behavior is that a competition between QEA and independent behavior occurs. That is, the NO_2 governing equation is in a transition from Eq. (4.23) to (4.70). Below 10^{-6} % NO_2 gas, Eq. (4.23) is virtually reduced to Eq. (4.70). Because at low concentrations most nitrogen is transported as NO_2, the growing N_2O_4 error becomes unimportant. Overall, the total flux error of the QEA is at most 6% (Figure.4.12-a), so it is a good approximation. As shown in Figures.4.14 to 4.16, all microscopic parameters (κ_{NO_2} , $\kappa_{N_2O_4}$, and γ) for the QEA are almost the same as those for the exact equations.

For experimental applications with the delivery of NO_2 gas directly into a liquid solution, it is recommended that 0.001% NO_2 gas be used. As summarized in Table 4.4, $\overline{C}_{NO_2}$ is then 3 orders of magnitude higher than $\overline{C}_{N_2O_4}$, thereby minimizing the effects of N_2O_4. This gas composition is also good because the well-mixed NO_2 concentration [$C_{NO_2}(\delta)$] is almost the same as the bulk NO_2 concentration ($\overline{C}_{NO_2}$). The time constant τ is just one second at this composition, as shown in Figure.4.17. As already mentioned, there are no available instruments

for measuring the dissolved NO_2 in the solution. However, it is possible to measure the NO_2^- concentration, and obtain $\overline{C}_{N_2O_4}$ [Eq. (4.5)] as described earlier. By using Eq. (4.95) and the measured $\overline{C}_{N_2O_4}$, it is possible to find the actual mass-transfer coefficients by minimizing the sum of the squared differences between the measured and the predicted values. With these mass-transfer coefficients and Eq. (4.96), it is possible to obtain $\overline{C}_{NO_2}$ .The time to reach the usual detection limit ($0.5\mu M$) of the Griess reagent based on the predicted $\overline{C}_{N_2O_4}(=0.19\text{pM})$ is about 44 min. Although several hours of experiment would be needed, this should be practical.

In the combined model of PDMS and the liquid, the range of the main unknown parameter ε was assumed to be $0 < \varepsilon \leq 1$. In the case of $\varepsilon = 1$, the value of $Q_{N_2O_4}$ is 279 by using Eq. (4.12) and the known value of Q_{NO_2} . This value seems unrealistically large, and would be even larger if $\varepsilon > 1$. If it is assumed that the forward rate constant of the reaction (4.1) is proportional to NO_2 diffusivity, it would be true for an encounter-limited reaction, then $\tilde{k}_1/k_1 = \tilde{D}_{NO_2}/D_{NO_2}$ and $\varepsilon = 0.6$. From the results of Figure.4.31, the value of ε is really small (ε ranges from 6.7×10^{-7} to 2.2×10^{-5}). Although there is uncertainty in ε, it is okay because all parameters converge in these small values of ε.

As shown in Figures.4.22 and 4.23, the liquid NO_2 and N_2O_4 concentrations at the PDMS-liquid interface both become independent of ε at low gas concentrations, such as 0.001%. This is true also for the fractional flux as NO_2 and the quantities κ_{NO_2} , $\kappa_{N_2O_4}$, and γ . Thus, a major advantage of operating at low concentrations is that ε (and thus $Q_{N_2O_4}$) need not be known.

For experimental applications of the PDMS method, using 0.001 % NO_2 gas is strongly recommended because we have no information about $Q_{N_2O_4}$. As summarized in Table 4.5, $\overline{C}_{NO_2}$ is 4 orders of magnitude higher than $\overline{C}_{N_2O_4}$ which shows the greater selectivity toward NO_2 compared to the gas-liquid model. Likewise, $C_{NO_2}(\delta)$ is almost the same as $\overline{C}_{NO_2}$. The time constant τ is still less than ten seconds at this composition, as shown in Figure.4.26. However, for the combined model, the time to reach the usual detection limit (0.5μM) of the Griess reagent based on the predicted $\overline{C}_{N_2O_4}$ (9.5 fM) is about 15 hrs. This means that at least 2-3 days are required. Thus, 0.01% NO_2 gas might be a better choice if PDMS tubing is used. All parameters are still independent of ε at this gas concentration if $\varepsilon < 10^{-2}$ and τ is less than a second (Figures.4.22-4.28). In addition, $C_{NO_2}(\delta)$ is still almost the same as $\overline{C}_{NO_2}$ for 0.01% NO_2 gas (Table 4.5). Finally, the required experimental time is only a few hours because the predicted $\overline{C}_{N_2O_4}$ of the combined model at 0.01% is similar to that of the gas-liquid model at 0.001%. Overall, both methods for NO_2 delivery might be quite satisfactory.

Bibliography

Alvarez, B., and Radi, R. (2003) Peroxynitrite reactivity with amino acids and proteins. *Amino Acids.* 25: 295-311

Atkinson, R., Baulch, D.L., Cox, R.A., Crowley, J.N., Hampson, R.F., Hynes, R.G., Jenkin, M.E., Rossi, M.J., and Troe, J. (2004) Evaluated kinetic and photochemical data for atmospheric chemistry: Volume I - gas phase reactions of O_x, HO_x, NO_x and SO_x species. *Atmos.Chem.Phys.* 4, 1461-1738.

Bartesaghi, S., Ferrer-Sueta, G., Peluffo, G., Valez, V., Zhang, H., Kalyanaraman, B., and Radi, R. (2007) Protein tyrosine nitration in hydrophilic and hydrophobic environments. Amino acids, 32, 501-515.

Behar, D., Czapski, G., and Duchovny, I. (1970) Carbonate radical in flash photolysis and pulse radiolysis of aqueous carbonate solutions. *J. Phys. Chem.* 74: 2206-2210.

Bergstrom, J., Furst, P., Noree, L.O., and Vinnars, E. (1974) Intracellular free amino acid concentration in human muscle tissue. *J. Appl. Physiol.* 36: 693-697.

Bonini, M.G and Augusto, O. (2001) Carbon dioxide stimulates the production of thiyl, sulfinyl and disulfide radical anion from thiol oxidation by peroxynitrite. *J. Biol. Chem.* 276: 9749-9754.

Broszkiewicz, R.K. (1976) The pulse radiolysis study of $NaNO_2$ and $NaNO_3$ solutions.*Bull. Acad. Pol. Sci. Sedr. Sci. Chim.* 24: 221-229.

Burner, U., Furtmüller, P.G., Kettle, A.J., Koppenol, W.H. and Obinger., C. (2000) Mechanism of reaction of myeloperoxidase with nitrite. *J. Biol. Chem.* 275: 20597 – 20601.

Buxton, G.V and Elliot, A.J. (1986) Rate-constant for the reaction of hydroxyl radical with bicarbonate ions. *Radiat. Phys. Chem.* 27: 241-243.

Chen, S.N. and Hoffman, M.Z. (1973) Rate constants for the reaction of the carbonate radical with compounds of biochemical interest in neutral aqueous solution. *Radiat. Res.* 56: 40-47.

Conner, E.M. and Grisham, M.B. (1995) NO: biochemistry, physiology, and pathophysiology. *Methods*, 7:3-13.

Cross, C.E, Eiserich, J.P, and Halliwell, B. (1997) General biological consequences of inhaled environmental toxicants. In: Crystal, R.G; West, J.B; Barnes, P.J., eds. *The lung*: scientific foundations. Philadelphia: Lippincott-Raven Publishers: 2431-2437

Czapski, G., Holcman, J., and Bielski, B.H. (1994) Reactivity of nitric oxide with simple short-lived radicals in aqueous solutions. . *J. Am. Chem. Soc.* 116: 11465-11469.

Deen, W.M. (1998) Analysis of transport phenomena, Oxford University Press.

deRojas-Walker, T., Tamir, S., Ji, H., Wishnok, J.S., and Tannenbaum, S.R. (1995) Nitric oxide induces oxidative damage in addition to deamination in macrophage DNA. *Chem.Res.Toxicol.* 8: 473-477.

Dong, M., Wang, C., Deen, W.M., and Dedon, P.C. (2003) Absence of 2-deoxyoxanosine and presence of abasic sites in DNA exposed to nitric oxide at controlled physiological concentrations. *Chem. Res. Toxicol.* 16: 1044-1055.

Dong, M. and Dedon, P.C. (2006) Relatively small increases in the steady-state levels of nucleobase deamination products in DNA from human TK6 cells exposed to toxic levels of nitric oxide. *Chem. Res. Toxicol.* 19: 50-57.

Eiserich, J.P., Hristova, M., Cross, C.E., Jones, A.D., Freeman, B.A., Halliwell, B., and van der Vliet, A. (1998) Formation of nitric oxide-derived inflammatory oxidants by myeloperoxidase in neutrophils. Nature. 391:293-396.

England, C. and Corcoran, W.H. (1974) Kinetics and mechanism of the gas-phase reaction of water vapor and nitrogen dioxide. *Ind.Eng.Chem.Fundam.* 13, 373-381.

Estevez, A. G., N. Spear, H. Pelluffo., A. Kamaid, L. Barbeito, and J. S. Beckman. (1999) Examining apoptosis in cultured cells after exposure to nitric oxide and peroxynitrite. *Methods Enzymol.* 301: 393-402.

Ford, E., Hughes, M.N., and Wardman, P. (2002) Kinetics of the reactions of nitrogen dioxide with glutathione, cysteine, and uric acid at physiological pH. *Free Radic. Biol. Med* 32: 1314-1323.

Fritsche, E., Schäfer, C., Calles, C., Bernsmann, T., Bernshausen, T., Wurm, M., Hübenthal, U., Cline, J.E., Hajimiragha, H., Schroeder, P., Klotz, L.O., Rannug, A., Fürst, P., Hanenberg, H., Abel, J., and Krutmann, J.(2007) Lightening up the UV response by identification of the arylhydrocarbon receptor as a cytoplasmatic target for ultraviolet B radiation. *Proc. Natl. Acad. Sci. USA* 104: 8851-8856.

Garcia-Ruiz, C., Morales, A., Ballesta, A., Rodes, J., Kaplowitz, N., and Fernandez-Checa, J.C. (1994) Effect of chronic ethanol feeding on glutathione and functional integrity of mitochondria in periportal and perivenous rat hepatocytes. *J. Clin. Invest.* 94: 193-201.

Gasco, A., R. Fruttero, and G. Sorba. (1996) NO donors: An emerging class of compounds in medicinal chemistry. *Farmacognosia* 51: 617-635.

Gaston, B., Reilly, J., Drazen, J.M., Fackler, J., Ramdev, P., Arnelle, D., Mullins, M.E., Sugarbaker, D.J., Chee, C., Singel, D.J., Loscalzo, J. and Stamler, J.S. (1993) Endogenous nitrogen oxides and bronchiolar S-nitrosothiols in human airways. *Proc. Natl. Acad. Sci. USA* 90: 10957-10961.

Goldstein, S. and Czapski, G. (1995) The reaction of NO with O_2^- and HO_2: a pulse radiolysis study. *Free Radic. Biol. Med.* 19: 505-510.

Goldstein, S., and Czapski, G. (1996) Mechanism of the nitrosation of thiols and amines by oxygenated NO solutions: the nature of the nitrosating intermediates. *J. Am. Chem. Soc.* 118: 3419-3425.

Goldstein, S., and Czapski, G. (1998) Formation of peroxynitrate from the reaction of peroxynitrite with CO_2: Evidence for carbonated radical production. *J. Am. Chem. Soc.* 120: 3458-3463.

Goldstein, S., Czapski, G. (2000) Reactivity of peroxynitrite versus simultaneous generation of NO and O_2^- toward NADH. *Chem. Res. Toxicol.* 13: 736-741.

Goldstein, S., Czapski, G., Lind, J., Merenyi, G. (2000) Tyrosine nitration by simultaneous generation of NO and O_2^- under physiological conditions. How the radicals do the job. *J. Biol. Chem.* 275: 3031-3036.

Goldstein, S., Lind, J., Merenyi, G. (2004) Reaction of organic peroxyl radicals with NO_2 and NO in aqueous solution: Intermediacy of organicperoxynitrate and peroxynitrite species. *J. Phys. Chem.* 108: 1719-1725.

Goldstick, T. K., and Fatt, I. (1970) Diffusion of oxygen in solutions of blood proteins. *Chem. Eng. Prog. Symposium Ser. 99.* 66:101-107.

Gratzel, M, Henglein, A, Lilie, J, and Beck, G. (1969) Pulsradiolytische untersuchung

einigerelementarprozesse der oxidation und reduction des nitritions. *Ber. Bunsenges. Phys. Chem.* 73:646-653.

Halliwell, B., and Gutteridge, J.M.C., eds. (1998) *Free Radicals in Biology and Medicine.* Oxford, Oxford University Press.

Hansen, J.M., Go, Y.M., and Jones, D.P. (2006) Nuclear and mitochondrial compartmentation of oxidative stress and redox signaling. *Annu. Rev. Pharmacol. Toxicol.* 46: 215-234.

Hodges, G.R. and Ingold, K.U. (1999) Cage-escape of germinate radical pairs can produce peroxynitrate from peroxynitrite under a wide variety of experimental conditions. *J.Am.Chem.Soc.* 121:10695-10701.

Hodges, G.R., Marwaha, J., Paul, T., and Ingold, K.U. (2000) A novel procedure for generating both nitric oxide and superoxide in situ from chemical sources at any chosen mole ratio. First application: tyrosine oxidation and a comparison with performed peroxynitrite. *Chem. Res. Toxicol.* 13: 1287-1293.

Hoffman, M., Hayon, E. (1973) Pulse radiolysis study of sulfhydryl compounds in aqueous solution. *J. Phys. Chem.* 77: 990-996.

Hollenbach, S., Dhenaut, A., Eckert, I., Radicella, J. P., and Epe, B. (1999) Overexpression of Ogg1 in mammalian cells: effects on induced and spontaneous oxidative DNA damage and Mutagenesis. *Carcinogenesis* 20: 1863-1868.

Hunter, E.P.L., Desrosiers, M.F., and Simic, M.G. (1989) The effect of oxygen, antioxidants, and superoxide radical on tyrosine phenoxyl radical dimerization. *Free Radic. Biol. Med.* 6: 581-585.

Ischiropoulos, H. (1998) Biological tyrosine nitration: a pathophysiological function of nitric oxide and reactive oxygen species. *Arch.Biochem.Biophys* 356:1-11.

Jones, C.M., Lawrence, A., Wardman, P., and Burkitt, M.J. (2003) Kinetics of superoxide scavenging by glutathione: an evaluation of its role in the removal of mitochondrial superoxide. *Biochem. Soc. Trans.* 31: 1337-1339.

Jourd'heuil, D., Mai, C.T., Laroux, F.S., Wink, D.A., and Grisham, M.B. (1998) The reaction of S-nitrosoglutathione with superoxide. *Biochem. Biophys. Res. Commun.* 246: 525-530.

Jourd'heuil, D., Jourd'heuil, F.L, Kutchukian, P.S., Musah, R.A., Wink, D.A., and Grisham, M.B. (2001) Reaction of superoxide and nitric oxide with peroxynitrite. Implications for peroxynitrite-mediated oxidation reactions in vivo. *J. Biol. Chem.* 276: 28799-28805.

Jourd'heuil, D., Jourd'heuil, F.L., and Feelisch, M. (2003) Oxidation and nitrosation of thiols at low micromolar exposure to nitric oxide. *J. Biol. Chem.* 278: 15720-15726.

Kameoka, Y., and Pigford, R.L. (1977) Absorption of nitrogen dioxide into water, sulfuric acid, sodium hydroxide, and alkaline sodium sulfite aqueous solutions. *Ind. Eng. Chem.*

Fundamen. 16, 163-169.

Karunakaran, C., Zhang, H., Joseph J., Antholine W.E., and Kalyanaraman, B. (2005) Thiol oxidase activity of copper, zinc superoxide dismutase stimulates bicarbonate-dependent peroxidase activity via formation of a carbonate radical. *Chem. Res. Toxicol.* 18: 494-500.

Keshive, M., Singh, S., Wishnok, J.S., Tannenbaum, S.R., and Deen, W.M. (1996) Kinetics of S-nitrosation of thiols in nitric oxide solutions. *Chem. Res. Toxicol.* 9: 988-993.

Kikugawa, K., Kato, T., and Okamoto, Y. (1994) Damage of amino acids and proteins induced by nitrogen dioxide, a free radical toxin, in air. *Free Radic. Biol. Med.* 16: 373-382.

Kirsch, M., Lehnig, M., Korth, H-G., Sustmann, R., and de Groot, H. (2001) Inhibition of peroxynitrite-induced nitration of tyrosine by glutathione in the presence of carbon dioxide through both radical repair and peroxynitrite formation. *Chem. Eur. J.*15: 3313-3320.

Kluge, I., Gutteck-Amsier, U., Zollinger, M. and Quang Do, K. (1997) S-nitrosoglutathione in rat cerebellum: identification and quantification by liquid chromatography-mass spectrometry. *J. Neurochem.* 69: 2599-2607.

Lai, C. S., Hopwood, L. E., Hyde, J. S., and Lukiewicz, S. (1982) ESR studies of O_2 uptake by

Chinese hamster ovary cells during the cell cycle. *Proc. Natl. Acad. Sci. USA* 79: 1166-1170.

Lancaster, J.R., Jr. (2006) Nitroxidative, nitrosative, and nitrative stress: kinetic predictions of reactive nitrogen species chemistry under biological conditions. *Chem. Res. Toxicol.* 19: 1160-1174.

Leo, Albert, Hoekman, D.H, Hansch, Corwin. (1995) *Exploring QSAR*, Washington, DC: American Chemical Society.

Lewis, R. S., and Deen, W. M. (1994) Kinetics of the reaction of nitric oxide with oxygen in aqueous solutions. *Chem. Res. Toxicol.* 7: 568-574.

Lewis, R.S., Tamir, S., and Deen, W.M. (1995a) Kinetic analysis of the fate of nitric oxide synthesized by macrophages in vitro. *J.Biol.Chem.* 270:29350-29355.

Lewis, R.S., Tannenbaum, S.R, and W. M. Deen. (1995b) Kinetics of N-nitrosation in oxygenated nitric oxide solutions at physiological pH: Role of nitrous anhydride and effects of phosphate and chloride. *J. Am. Chem. Soc.* 117: 3933-3939.

Li, C.Q., Wright T.L., Dong M., Dommels Y.E., Trudel L.J., Dedon P.C., Tannenbaum S.R., and Wogan, G.N. (2005) Biological role of glutathione in nitric oxide-induced toxicity in cell culture and animal models. *Free Radic. Biol. Med.* 39: 1489-1498.

Lim, C.H., Dedon, P.C., and Deen, W. M. (2008) Kinetic analysis of intracellular concentrations

of reactive nitrogen species. *Chem.Res.Toxicol.* 21, 2134-2147.

Liu, X., M.J.S. Miller, M.S.Joshi, D.D. Thomas, and J.R. Lancaster. (1998) Accelerated reaction of nitric oxide with O_2 within the hydrophobic interior of biological membranes. *Proc. Natl. Acad. Sci. U.S.A.* 95:2175-2179, 1998

Luo, D., Smith, S.W., and Anderson, B.D. (2005) Kinetics and mechanism of the reaction of cysteine and hydrogen peroxide in aqueous solution. *J. Pharm. Sci.* 94: 304-316.

Lymar, S.V. and Hurst, J.K. (1995) Rapid reaction between peroxonitrite ion and carbon dioxide: Implications for biological activity. *J. Am. Chem. Soc.* 117: 8867-8868.

Mertes, S., and A. Wahner (1995) Uptake of nitrogen dioxides and nitrous acid on aqueous surfaces. *J. Phys. Chem.* 99, 14000–14006.

Meylan, W.M. and Howard, P.H. (1995) Atom/fragment contribution method for estimating octanol-water partition coefficients. *J. Pharm. Sci.* 84: 83-92.

Moller, M.N., Li, Q., Vitturi, D.A., Robinson, J.M., Lancaster, J.R., and Denicola, A. (2007) Membrane "lens effect": focusing the formation of reactive nitrogen oxides from the NO/O_2 reaction. *Chem. Res. Toxicol.* 20: 709-714.

Moncada, S., Palmer, R.M.J., and Higgs, E.A. (1989) Biosynthesis of NO from L-arginine: A pathway for the regulation of cell function and communication. *Biochem. Pharmacol.,*

38:1709-1715.

Moncada, S., R.M.J. Palmer, and E.A. Higgs. (1991) Nitric oxide: Physiology, pathophysiology and pharmacology. *Pharmacol. Rev.* 43: 109-142.

Nalwaya, N., and Deen, W. M. (2003) Analysis of cellular exposure to peroxynitrite in suspension cultures. *Chem. Res. Toxicol.* 16: 920-32.

Nalwaya, N., and Deen, W.M. (2005) Nitric oxide, oxygen, and superoxide formation and consumption in macrophage cultures. *Chem.Res.Toxicol.* 18: 486-493.

Nathan, C.F. and Hibbs, J.B., Jr. (1991) Role of No synthesis in macrophage antimicrobial activity. *Curr. Opin. Immunol.,* 3:65-70.

Nguyen, T., Brunson, D., Crespi, C.L., Penman, B., Wishnok, J.S., and Tannenbaum, S.R. (1992) DNA damage and mutation in human cells exposed to nitric oxide in vitro. *Proc. Natl. Acad. Sci. USA* 89: 3030-3034.

Pryor, W.A. and Lightsay, J.W. (1981) Mechanisms of nitrogen dioxide reactions: initiation of lipid-peroxidation and the production of nitrous acid. *Science* 214:435-437

Pryor, W.A., Lightsay, J.W., and Church, D.F. (1982) Reaction of nitrogen dioxide with alkenes and poly-unsaturated fatty-acids: addition and hydrogen abstraction mechanisms. *J.Am.Chem.Soc.* 104:6685-6692.

Prutz, W.A., Monig, H. Butler, J, and Land, E.J. (1985) Reactions of nitrogen dioxide in aqueous model systems: oxidation of tyrosine units in peptides and proteins.

Arch.Biochem.Biophys. 243:125-134.

Quijano, C., Romero, N., and Radi, R. (2005) Tyrosine nitration by superoxide and nitric oxide fluxes in biological systems: modeling the impact of superoxide dismutase and nitric oxide diffusion. *Free Radic. Biol. Med.* 39: 728-741.

Radi, R. (2004) Nitric oxide, oxidants, and protein tyrosine nitration. *Proc. Natl. Acad. Sci. USA* 101: 4003-4008.

Ramirez, D.C., Mejiba, S.E.C., and Mason, R.P. (2005) Mechanism of hydrogen peroxide-induced Cu, Zn-superoxide dismutase-centered radical formation as explored by immuno-spin trapping: the role of copper and carbonate radical anion-mediated oxidations. *Free Radic. Biol. Med.* 38: 201-214.

Robb, W. L. (1968) Thin silicone membranes —Their permeation properties and some applications. *Ann. N.Y. Acad. Sci.* 46, 119-137.

Roos, A. and Boron, W.F. (1981) Intracellular pH. *Physiol. Rev.* 61: 296-434.

Ross, A.B., Mallard, W.G.., Helman, W.P., Buxton, G.V., Hurie, R.E., Neta, P. (1998) *NDRL/NIST Solution Kinetics Database ver 3.* Notre Dame Radiation Laboratory, Gaithersburg, MD: Notre Dame, (http://www.rcdc.nd.edu/browse_compil.html)

Santos, C., Bonini, M.G and Augusto, O. (2000) Role of the carbonate anion in tyrosine nitration and hydroxylation by peroxynitrite. *Arch. Biochem. Biophys.* 377: 146-152.

Schrammel, A., Gorren, A., Schmidt, K., Pfeiffer, S., and Mayer, M. (2003) S-nitrosation of glutathione by nitric oxide, peroxynitrite, and NO/O_2^-. *Free Radic. Biol. Med.* 34: 1078-1088.

Schwartz, S.E. (1983) Trace atmospheric constituents: properties, transformations, and fates. In *Advances in Environmental Science and Technology*, Wiley, N.Y. 1-115

Schwartz, S.E and White, W.H. (1983) Kinetics of reactive dissolution of nitrogen oxide in aqueous solution. *Adv. Environ. Sci. Technol.* 12: 1-116.

Shin, H.W. and George, C. Steven. (2001) Microscopic modeling of NO and S-nitrosoglutathione kinetics and transport in human airways. *J. Appl. Physiol.* 90: 777-788.

Singh, R.J., Goss, S.P.A., Joseph, J., and Kalyanaraman, B. (1998) Nitration of γ -tocopherol and oxidation of α -tocopherol by copper-zinc superoxide dismutase/H_2O_2/ NO_2^-: role of the nitrogen dioxide free radical. *Proc. Natl. Acad. Sci. U.S.A.* 95:12912-12917.

Skinn, B.T, Lim, C.H., and Deen, W. M. (2011) Nitric oxide delivery system for biological media. *Free Radical.Biol.Med.* 50: 381-388.

Solar, S., Solar, W., and Getoff, N. (1984) Reactivity of OH with tyrosine in aqueous solution studied by pulse radiolysis. *J. Phys. Chem.*88: 2091-2095.

Sovitj, P., and Rose, G.M (1998) Generation of thiyl radical by nitric oxide: a spin trapping study. *J. Chem. Soc., Perkins Trans.* 2: 1507-1512.

Stamler, J.S., Jaraki, O., Osborne, J., Simon, D.I., Keaney, J., Vita, J., Singeli, D., Valeri, C.R. and Loscalzo, J. (1992) Nitric oxide circulates in mammalian plasma primarily as an S-nitroso adduct of serum albumin. *Proc. Natl. Acad. Sci. USA* 89: 7674-7677.

Tamir, S., Burney, S., and Tannenbaum, S.R. (1996) DNA damage by nitric oxide. *Chem. Res. Toxicol.* 9: 821-827.

Tamir, S., and Tannenbaum, S.R. (1996) The role of nitric oxide in the carcinogenic process. *Biochim.Biophys.Acta.* 1288:F31-F36.

Thomas, D. D., Liu. X, Kantrow, S.P., and Lancaster, J.R. (2001) The biological life of nitric oxide: Implications for the perivascular dynamics of NO and O_2. *Proc. Natl. Acad. Sci. USA* 95: 2175-2179.

Thomas, D. and Vanderschuren, J. (1999) Removal of tetravalent NO_x from flue gases using solutions containing hydrogen peroxide. Chem.Eng.Technol. 21, 975-981.

Traut, T.W. (1994) Physiological concentrations of purines and pyrimidines. *Mol. Cell. Biochem.* 140: 1-22.

van der Vliet, A., Eiserich, J.P., Halliwell, B., and Cross, C.E. (1997) Formation of reactive nitrogen species during peroxidase-catalyzed oxidation of nitrite. A potential additional mechanism of nitric oxide-dependent toxicity. *J.Biol.Chem.* 272:7617-7625.

Waldman, S.A., and Murad, F. (1988) Biochemical mechanisms underlying vascular smooth muscle relaxation. *J. Cardiovasc.Pharmacol.,* 12:115-118.

Wang, C., Deen, W.M. (2003) Nitric oxide delivery system for cell culture studies. *Ann. Biomed. Eng.* 31:65-79.

Wardman, P. and von Sonntag, C. (1995) Kinetic factors that control the fate of thiyl radicals in cells. *Methods Enzymol.* 251: 31-45.

Wardman, P. (1998) Evaluation of the 'radical sink' hypothesis from a chemical-kinetic viewpoint *J. Radioanal. Nucl. Chem.* 232: 23-27.

Washko, P., Rotrosen, D., and Levine, M. (1989) Ascorbic acid transport and accumulation in human neutrophils. *J. Biol. Chem.* 264: 18996 – 19002.

Wood, P.D., Mutus, B., and Redmond, R.W. (1996) The mechanism of photochemical release of nitric oxide from S-nitrosoglutathione. *Photochem. Photobiol.* 64: 518-524.

Zacharia, I. and Deen, W. M. (2005) Diffusivity and solubility of nitric oxide in water and saline. *Annals of Biomedical Engineering*, 33: 214-222.

Zhang, H., Joseph J., Felix, C., and Kalyanaraman, B. (2000) Bicarbonate enhances the hydroxylation, nitration and peroxidation reactions catalyzed by copper, zinc superoxide dismutase. *J. Biol. Chem.* 275: 14038 – 14045.

Zhuang, J. C., and Wogan, G. N. (1997) Growth and viability of macrophages continuously stimulated to produce nitric oxide. *Proc. Natl. Acad. Sci. USA. 94*: 11875-11880.